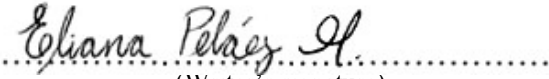




University of
Stavanger

Faculty of Science and Technology

MASTER'S THESIS

Study program/ Specialization: Offshore Technology- Marine and Subsea technology	Spring semester, 2018.. Open access
Writer: Eliana Pelaez Manrique	 (Writer's signature)
Faculty supervisor: Sudath Chaminda Siriwardane External supervisor(s): Gunnar Gjerde and Ivar Holta, Aker Solutions Stavanger	
Title of thesis: ANALYSES OF JACKET PLATFORMS UNDER SHIP COLLISIONS	
Credits (ECTS): 30	
Key words: Ship collision Jacket platform Grouted members Accidental Limit State Strain Capacity of dented tubes	Pages:104..... + enclosure:104..... Stavanger, 14-06-2018..... Date/year

Abstract

Ship collisions with jacket platforms constitute a risk to the facility integrity, the personnel and the environment. Visiting vessels are used in the Norwegian Continental Shelf to handle different goods and materials for offshore platforms. In general, platforms with four legs are highly common worldwide, and the study of the forces that arise from ship impacts have been studied since latest 80's. Thereby, jacket platforms were designed to support impact energies of 11 MJ and 14 MJ for head-on and side collision, respectively. With the increase in weights and more sophisticated navigations programs, the impact energies have enlarged considerably. Recent updates in guidelines as in Norsok Standard N-003 suggest impact energies of 28 MJ and 50 MJ for side and head-on collision correspondingly, when no detailed risk analysis is performed. In other words, this represents an increase in the demand of dissipation energy from the platform structure.

This report compiles parametric studies performed in USFOS, for steel and steel grouted tubes with different ratios D/t (diameter/thickness) and constant length. The tubes are fixed at the ends in all degrees of freedom, and impacted at mid-span. Strain fracture (0.15) is accounted for failure criteria. Moreover, the numerical results are compared to different sources of experimental data, as well as the force-deformation relationships provided by Veritas DNV-RP-C204 and Norsok Standard N-004, assigned in this study as the simplified method. Very satisfactory agreement is found in impact force predictions and overall absorption energies. Likewise, details of the membrane effects in the resistance to denting and bending are shown in non-dimensional graphs.

Furthermore, boat Impact analyses are conducted in two platforms, they are denominated as, Platform A and Platform B, the aim is to check their capacity to dissipate an impact energy of 50MJ. Correspondingly, different scenarios of impacts on leg/brace members are investigated. An approach of a quasi-static analysis and finite element computer program are used to simulate the impact loads. A summary of the energies absorbed, impact forces, global displacements and local dents in the members is presented for each platform. Failure criteria is taken according to Veritas DNV-RP-C204 and Norsok Standard N-004. The boat impact analyses include the absence or presence of concrete in the leg/brace under impact. The difference and gains from the use of concrete filled members are also reported.

Additionally, a dynamic analysis in Platform B is performed under different velocities 3.0m/s, 3.5m/s, and 4.0m/s with constant impact energy of 50MJ. The dynamic amplification ratios for the base shear force, and the over-turning moment are calculated as, the ratio between the dynamic response to the static response. An increase of 42% in the base shear force and 25% of the overturning moment is found when the ship impacts a hard point in the platform, for example a leg joint.

Finally, the axial capacity of dented tubes is numerically tested in USFOS. The parametric study consists in an axially-free steel tube, that is subjected to impact energy to produce a dent between 50%-60% of the diameter. Afterwards, the tubes are axially loaded in compression to investigate the remaining axial capacity of the dented tubes. The failure

is assumed when the member is incapable of taking more load or when the strain reaches the critical value of 0.15.

Acknowledgements

First of all, thanks to God for his mercy in my life and the gift of each new day.

This thesis is submitted as a requirement to complete my master degree in Offshore Technology - Marine and Subsea Technology at the University of Stavanger. The work presented has been done in cooperation with Aker Solutions in Stavanger.

Second, I would like to express my sincere gratitude to my faculty supervisor Mr. Sudath Siriwardane for his valuable assistance and motivation during these months. Third, my thanks to the supervisors in Aker Solutions Mr. Gunnar Gjerde and Mr. Ivar Holta for the opportunity to work close to the Analysis Group, their guidance and the helpful comments throughout the work. Also, I want to show my appreciation to Tore Holmås in the USFOS support for his advice.

Equally important, I would like to express my personal thanks to my family in Colombia, my husband and my children that gave me their support during these two years of study. Luis Carlos, you are an amazing man, and I love every minute we share as a family with Luciana and Simon.

Finally, allow me to extend my gratitude to my friends in the University of Stavanger for all the wonderful moments during the master.

Stavanger, June 2018

Eliana Pelaez

Contents

1	Introduction	1
1.1	Background	1
1.2	Objectives	1
1.3	Limitations	2
1.4	Thesis outline	2
2	Recent Research	4
3	Theoretical Background for Ship Impact Analysis	7
3.1	Energy absorption	7
3.2	Type of damage	7
3.3	Plastic theory	8
4	Guidelines for Ship Impact Analysis	12
4.1	Design principles	12
4.2	Force-deformation relationships for vessels	13
4.3	Forces-deformation relationship for legs and braces	15
4.3.1	Local denting	15
4.3.2	Plastic force-deformation relationships	16
4.4	Bending capacity of dented tubular members	18
4.5	Failure criteria	18
4.5.1	Local buckling	18
4.5.2	Tensile fracture	19
5	Ship Impact Analysis of Jacket Legs	20
5.1	Steel legs: Parametric study	20
5.1.1	Results and Discussion	20
5.2	Steel grouted legs: Parametric study	33
5.2.1	Results and Discussion	33
6	Ship Impact Analyses of Jacket Platforms	39
6.1	Platforms geometry	39
6.2	Impact loading scenarios	41
6.3	Impact analysis Platform A	43
6.3.1	Results and Discussion Platform A	43
6.4	Impact analysis Platform B	61
6.4.1	Results and Discussion Platform B	61
7	Effect of the Vessel Velocity in the Ship Impact Analysis: Parametric Study	84
8	Denting Effect in the Axial Capacity of Steel Tubes: Parametric Study	88
9	Conclusions and Recommendations for Further Work	92

10 Annex	95
10.1 simplified Method	95
References	103

List of Figures

3-1	Types of collisions (a) stern impact, (b) bow impact and (c) side impact. (Aldilana, 2014)	7
3-2	Deformation modes of a steel jacket from Søreide (1981)	8
3-3	Stress-strain curve for steel (Learneasy.info, 2014)	9
3-4	Plastic hinge formation in a beam under lateral load Søreide (1981)	10
3-5	Stress and strain variation in a symmetrical cross section for a beam under a transverse load from Codecogs.com (2014)	10
3-6	Composite section of steel tube filled with concrete	11
4-7	Energy dissipation for strength, ductile and shared-energy design from Veritas DNV-RP-C204 and Norsok Standard N-004	12
4-8	Deformation curve for beam, raked bow and stern impact from Veritas DNV-RP-C204 and Norsok Standard N-004	14
4-9	Deformation curve for bow with and without bulb (2-5.000 DWT) from Veritas DNV-RP-C204 and Norsok Standard N-004	14
4-10	Resistance curve for local denting from DNV-RP-C204 (2017)	15
4-11	Collapse mechanism for beams with axial flexibility from Veritas DNV-RP-C204 and Norsok Standard N-004	17
4-12	Force-deformation relationship for tubular beams with axial flexibility from Veritas DNV-RP-C204 and Norsok Standard N-004	17
4-13	Reduction moment capacity for dented tubes from DNV-RP-C204 (2017)	18
5-14	Non-dimensional Denting -vs- Non-dimensional Impact Force for D=1.3m and 1.5m	21
5-15	Non-dimensional Denting -vs- Non-dimensional Impact Force for D=1.8m and 2.0m.	22
5-16	Comparison of the energy absorbed by denting in USFOS with N-004.	23
5-17	Plastic utilization and strain distribution of impacted leg with D=1.5m and t=40mm	23
5-18	Thickness influence in the absorbed energy against global displacement for D=1.3m and 1.5m	26
5-19	Thickness influence in the absorbed energy against global displacement for D=1.8m and 2.0m	27
5-20	Diameter influence in the absorbed energy against global displacement for t=40mm, 50mm and 60mm	28
5-21	Diameter influence in the absorbed energy against global displacement for t=70mm and 80mm	29
5-22	Denting effect in the energy absorption of the steel leg	30
5-23	Comparison test results from Jones et al. (1992) D/t=11 and 60 with N-004 for local denting.	31
5-24	Comparison test results from Jones et al. (1992) D/t=21, 30 and 40 with N-004 for local denting.	31
5-25	Comparison test results (Jonnes et al.) with USFOS for Non-dimensional Impact Energy-vs-Non-dimensional global displacement	32

5-26	Grout influence in the Energy absorbed -vs- Global lateral displacement for D=1.3m and 1.5m	34
5-27	Grout influence in the Energy absorbed -vs- Global lateral displacement for D=1.8m and 2.0m	35
5-28	Utilization factor of the legs without grout and grout $f'c= 10$ MPa and 50 MPa for D=1.3m and 1.5m	36
5-29	Utilization factor of the legs without grout and grout $f'c= 10$ MPa and 50 MPa for D=1.8m and 2.0m	37
5-30	Comparison of experimental test with numerical tests in USFOS for lateral impact and global displacement of grouted legs	38
6-31	Overview Platform A	39
6-32	Overview Platform B	41
6-33	Boat impact scenarios for Platform A	42
6-34	Boat impact scenarios for Platform B	42
6-35	Comparison of impact energy against the global displacement, for the leg with grout and without it	44
6-36	Comparison of Simplified Method and USFOS of the impact force against the global displacement	44
6-37	Comparison of Simplified Method and USFOS of the non-dimensional impact force against non-dimensional dent	45
6-38	Comparison impact energy absorbed against global displacement at the upper-joint of the leg	46
6-39	Comparison impact force against global displacement at the upper-joint of the leg	46
6-40	Plastic Utilization factor and Strain distributions for leg without grout under boat impact (mid-span)	48
6-41	Plastic utilization factor and strain distributions for leg with grout under boat impact (mid-span)	49
6-42	Plastic utilization factor and strain distributions for leg without grout under boat impact (upper joint)	50
6-43	Plastic utilization factor and strain distributions for grouted leg under boat impact (upper joint)	51
6-44	Comparison of Simplified Method and USFOS of the impact force against global displacement for diagonal brace	52
6-45	Comparison of Simplified Method and USFOS of the impact force against dent for diagonal brace	53
6-46	Plastic utilization factor, and strain distribution of the diagonal brace under boat impact	54
6-47	Comparison of the impact force against the global displacement, for the horizontal brace with grout and without it -Platform A	56
6-48	Comparison of Simplified Method and USFOS of the impact force against the global displacement, for the horizontal brace without grout - Platform A	56

6-49 Comparison of Simplified Method and USFOS of the non-dimensional impact force against the non-dimensional dent, in the horizontal brace without grout - Platform A	57
6-50 Global deformation against the impact force at the joint with grout - Platform A	57
6-51 Utilization factor and strain distribution of the horizontal brace, impacted at the grouted joint - Platform A	58
6-52 Utilization factor and strain distribution of the grouted horizontal brace, impacted at mid-span - Platform A	59
6-53 Utilization factor and strain distribution of the horizontal brace without grout, impacted at mid-span - Platform A	60
6-54 Global displacement against impact energy for grouted leg and leg without grout, impacted at mid-span - Platform B	63
6-55 Global displacement against impact force for grouted leg and leg without grout, impacted at mid-span - Platform B	63
6-56 Dent against the impact force for leg without grout, impacted at mid-span - Platform B	64
6-57 Global displacement against the impact energy for grouted leg and leg without grout, impacted at the upper joint - Platform B	64
6-58 Global displacement against the impact force, for grouted leg and no leg without grout, impacted at the upper joint - Platform B	65
6-59 Dent against the impact force for leg without grout, impacted at the upper joint - Platform B	65
6-60 Utilization factor and strain distribution of the leg without grout, impacted at mid-span- Platform B	66
6-61 Utilization factor and strain distribution of the grouted leg, impacted at mid-span- Platform B	67
6-62 Utilization factor and strain distribution of leg without grout, impacted at the upper joint- Platform B	68
6-63 Utilization factor and strain distribution of grouted leg, impacted at the upper joint- Platform B	69
6-64 Global deformation against the impact energy in the diagonal brace, impacted at midspan and at the joint - Platform B	71
6-65 Global deformation against the impact force in the diagonal brace, impacted at midspan and at the joint - Platform B	71
6-66 Dent against the impact force in the diagonal brace, impacted at midspan and at the joint - Platform B	72
6-67 Dent against the dent energy in the diagonal brace, impacted at midspan and at the joint - Platform B	72
6-68 Utilization factor and strain distribution of the diagonal brace, impacted at midspan - Platform B	73
6-69 Utilization factor and strain distribution of the diagonal brace, impacted at the joint - Platform B	74

6-70	Global displacement against the impact force for horizontal brace with grout and without it, impacted at the midspan - Platform B	76
6-71	Global displacement against the impact energy for horizontal brace with grout and without it, impacted at the midspan - Platform B	76
6-72	Dent against the impact force in horizontal brace, impacted at midspan - Platform B	77
6-73	Dent against the dent energy in horizontal brace impacted at midspan - Platform B	77
6-74	Global displacement against the impact energy for horizontal brace with grout and without it, impacted at the joint - Platform B	78
6-75	Global displacement against the impact energy in horizontal brace, impacted at joint - Platform B	78
6-76	Dent against the dent energy in horizontal brace, impacted at joint - Platform B	79
6-77	Dent against the impact force for horizontal brace without grout, impacted at the joint- Platform B	79
6-78	Utilization factor and strain distribution of the horizontal brace impacted at the midspan- Platform B	80
6-79	Utilization factor and strain distribution of the grouted horizontal brace impacted at the midspan- Platform B	81
6-80	Utilization factor and strain distribution of the horizontal brace impacted at the joint- Platform B	82
6-81	Utilization factor and strain distribution of the grouted horizontal brace impacted at the joint- Platform B	83
7-82	Vessel speed effect in the base shear force for the leg impacted at mid-span	85
7-83	Vessel speed effect in the over-turning moment for the leg impacted at mid-span	86
7-84	Vessel speed effect in the base shear force for the leg impacted at the joint	86
7-85	Vessel speed effect in the over-turning moment for the leg impacted at the joint	87
8-86	Loading procedure in the dented tubes.	88
8-87	Non-dimensional axial capacity of steel tubes against non-dimensional denting.	90
8-88	Plastic Utilization of the dented steel tube under axial load.	90
8-89	Strain distribution in the dented steel tube under axial load.	91

List of Tables

4-1	Energy dissipation in bow given the R_0 brace resistance from Veritas DNV-RP-C204 and Norsok Standard N-004	15
4-2	Proposed values for ϵ_{cr} and H for different steel grades from DNV-RP-C204	19
5-3	Dimensions and characteristics of numerical tested-legs	20
5-4	Results of parametric study of single legs, impacted at mid-span for D=1.3m and 1.5m	24
5-5	Results of parametric study of single legs, impacted at mid-span for D=1.8m and 2.0m	25
5-6	Mechanical properties for concrete	33
5-7	Summary results for steel legs with grout $f'c=10$ MPa and 50 MPa . . .	33
6-8	General Mechanical properties of Platform A	40
6-9	General Mechanical properties of Platform B	40
6-10	Summary of energies absorbed by members in platform A	43
6-11	Summary results for leg in platform A	47
6-12	Summary results for diagonal brace in platform A	52
6-13	Summary results for horizontal brace	55
6-14	Summary of leg and braces sections for collision analyses - Platform B . .	61
6-15	Summary of energies absorbed by members in platform B	61
6-16	Summary results for leg in platform B	62
6-17	Summary results for diagonal brace in platform B	70
6-18	Summary results for horizontal brace in Platform B	75
7-19	Parameters used in dynamic analysis for Platform B	84
7-20	Base shear force and over-turning moment results for dynamic analysis .	85
8-21	Parameters used in numerical test for axial capacity of dented tubes . . .	89
8-22	Results of numerical test for axial capacity of dented tubes	89

List of Symbols and Abbreviations

Symbols

A	cross section area
B	width of contact area
β	buckling, beta factor
c	non-dimensional spring stiffness
c_f	axial flexibility factor
c_w	displacement factor
c_{lp}	plastic zone length factor
D	diameter
E	young's modulus of elasticity
ϵ_{cr}	critical strain
ϵ_y	yield strain
E_k	impact energy
E_p	energy dissipated by the platform
E_s	energy dissipated by the ship
f_c	concrete strength
f_y	steel yield strength
H	non-dimensional plastic stiffness
I	moment of inertia
I_x	second moment of inertia
K	equivalent axial stiffness of the member
K_1	adjacent node stiffness, end 1
K_2	adjacent node stiffness, end 2
K_{node}	equivalent axial stiffness of the node
L	member length
M_p	plastic moment capacity
M_{pc}	plastic moment capacity of the composite section
m_a	hydrodynamic added mass

m_s	mass of the ship
N_{sd}	design axial compression force
N_{Rd}	design axial compressive resistance
R_c	characteristic resistance to denting
R_o	plastic collapse load
R_{oc}	plastic collapse load of the composite section
t	wall thickness
v_s	velocity of the ship
w	critical displacement
\bar{w}	non-dimensional deformation
W	elastic section modulus
W_c	characteristic deformation for tubular members
w_d	local dent
w_g	global displacement
W_p	plastic section modulus

Abbreviations

ALS	Accidental Limit State
BS	Base Shear Force
CFTs	Circular steel concrete-filled tubes
DWT	Dead Weight Tonnes
FEA	Finite Element Analysis
FEM	Finite Element Method
FRCFT	Circular steel fiber-reinforced concrete-filled tube
HAT	Highest Astronomical Tide
LAT	Lowest Astronomical Tide
NCS	Norwegian Continental Shelf
OM	Over-turning Moment
OSV	Offshore Service Vessel
PTCFTs	Circular steel post tensioned concrete-filled tubes

1 Introduction

1.1 Background

The Oil and Gas Industry in Norway has been developed since 1960. According to the Norwegian Petroleum Directorate, the Norwegian Continental shelf (NCS) has around 74 steel jacket platforms in operation. In order to provide support to this sector, supply vessels are used for handling materials and other goods of the platforms. Consequently, the presence of supply vessels around jacket platforms constitute a high risk of collision between the facility and the visiting vessel.

The Petroleum Safety Authority (2016) provides a report about the annual trend risk level in the NCS. Two incidents that involved ship on course collision in the NCS were reported. Regarding vessels collision with facilities, one incident between a vessel and an unmanned unit during removal occurred during the same year. Between 1999 and 2000 existed and increased level of similar incidents with an average of 15 per year. Furthermore, Kvitrud (2011) presents statistics of ship collision between 2001 to 2010. The total reported incidents were 26 resulting in economic consequences, but without loss of lives or personnel injuries.

Nowadays, the number has decreased to an average of 2-3 per year (Petroleum Safety Authority, 2016). Even though the frequency of these events has decreased with the years, the severity of the consequences involving such events may have enlarged. This, due to the fact that many of the existing structures, which are from the latest 80's and 90's, were designed to withstand impact energies of 11 MJ and 14 MJ, for head-on and side collision, respectively. In addition, new supply vessels with larger weight and stronger bow are being used in the NCS, leading to new requirements from codes and standards. The codes and standards that act as guidance for ship collision loads are the Norsok Standard N-003 (2017), Norsok Standard N-004 (2013) and Veritas DNV-RP-C204 (2017). In Norsok Standard N-003 (2017), an increase of the vessel size to 10000 tons at 3m/s in ALS condition for head-on collision was made. Yet, an impact energy of 50 MJ is set as a new loading criteria for vessel supplies, unless a risk analysis of the platform suggests a different value, or operational limits are implemented. Consequently, all existing jacket platforms will need to be assessed accordingly. In case of the structure being incapable to absorb the new impact energy, mitigation measures accompanied by operational limits would be needed for avoiding unwanted consequences.

1.2 Objectives

The main objective of this study is to perform a set of structural analyses of steel jacket platforms under ship collision by means of USFOS software. Correspondingly, impact energies will be applied to new requirements expressed by the Norsok Standard N-003 (2017), Norsok Standard N-004 (2013) and Veritas DNV-RP-C204 (2017). Furthermore, to achieve the main goal, the following specific objectives will be carried out:

- A parametric study of steel tubes and composite steel tubes filled with grout are tested numerically to compare the results obtained to experimental tests and the simplified method provided by the standards mentioned above.
- Two steel jacket platforms are considered to ship impact analysis: one old existing platform, and one new platform that is under development. The effects of grout, joint check and location of impact are investigated in the capacity of the platform.
- A dynamic analysis in USFOS is performed to investigate the effect of the ship velocity in results as: shear base force and over turning moment at the foundation.
- A parametric study is carried out to assess the axial capacity of steel tubes with 50%, 55% and 60% of denting in the diameter of the cross section.

1.3 Limitations

This thesis focuses on ship collisions with jacket platforms, and it investigates the jackets ability to absorb the impact energy. For that reason, only Accidental Limit State (ALS) is considered, and ALS post-impact assessment for the remaining capacity of the platform is not carried out.

The type of platforms considered are bottom fixed steel jacket structure with four legs, in collision with typical offshore service vessels (OSV) as visiting vessels. Consequently, collisions with cruise ships and tankers are not part of the scope.

The numerical simulations are performed in USFOS against small cross sections (legs/braces), and only bow collision is taking into account for all cases. Therefore, the ship is considered as "rigid body", and the platform as "soft body".

1.4 Thesis outline

This thesis consists of ten (10) chapters:

- Chapter 1: Introduction

This chapter provides a background, and importance of performing ship impact analysis. Furthermore, it presents the objectives of the study and its outline.

- Chapter 2: Recent Research

This chapter includes a compilation of relevant material about ship impact analysis of several experimental researches, and numerical simulations that have been developed during the last 20 years in the oil and gas industry.

- Chapter 3: Theoretical Background for Ship Impact Analysis

It introduces the generalities of collision loads, in company of the basis for plastic theory.

- Chapter 4: Guidelines for Ship Impact Analysis

It summarizes the relevant guidelines and force-deformation relationships from the applicable codes, such as, Norsok Standard N-003, Veritas DNV-RP-C204 and Norsok Standard N-004.

- Chapter 5: Ship Impact Analysis of Jacket Legs

This chapter discusses the results from two parametric studies carried out in steel legs, and steel grouted legs. In addition, it presents the findings and comparison with experimental data from different sources, as well as with the simplified method provided by the guidelines.

- Chapter 6: Ship Impact Analyses of Jacket Platforms

It describes the methodology implemented to run the analysis in USFOS, simplifications, assumptions, impact load scenarios and the results from the numerical simulations performed in two jacket platforms.

- Chapter 7: Effect of the Vessel Velocity in the Ship Impact Analysis: Parametric Study

This section presents a simple dynamic approach, with the methodology and findings of the effects in the base shear force and over-turning moment, when the vessel velocity at the moment of the impact is changed.

- Chapter 8: Denting Effect in the Axial Capacity of Steel Tubes: Parametric Study

It summarizes the outcomes of a parametric study carried out in axially-free dented tubes, its aim is to register the axial capacity of the damaged steel pipes.

- Chapter 9: Conclusion and Further work

This chapter presents the conclusions from the results obtained in chapters 5, 6, 7 and 8, in addition to the recommendations for further work.

- Chapter 10: Annex

This section shows a step by step methodology and the equations used for the application of the simplified method, specifically, in the horizontal brace in the Platform A.

2 Recent Research

Investigations of ship collisions with jacket platforms have been performed with great interest. The main reason is that visiting vessels to oil and gas facilities are very common in activities as handling materials, well stimulation or lifting operations. At the same time, drifting vessels represent a high risk for the structure integrity of the platform. Impact in steel tubes have been investigated by different authors in order to describe the denting, bending and energy absorption capacity of these members. Jones et al. (1992) performed 130 impact tests for fully clamped mild steel tube. The impacts with a rigid indenter were located at the mid-span, one-quarter or near to the support. A variability of Ratios D/t : 11, 21, 30, 34.47, 40, 60 and 62.34 were considered (D = outside diameter of the tube and t =thickness of the pipe). Impact energy (E_k), global displacement (w_g), Maximum impact force (P_{max}) and denting of the pipe were reported. The results presented by the author are compared to numerical tests performed in USFOS (nonlinear computer program) in this thesis, and show a fair agreement between the experimental test and numerical simulations. Furthermore, Zeinoddini et al. (2002) conducted impact analysis on 17 steel pipes with axial pre-loading and with high yield stress (500-600 MPa). The pipe was 1m long with ratio $D/t=50$. The author carried out a dynamic analysis of the impact, reporting the dent, impact energy, impact load versus time and global displacements. The results presented show that the capacity of the pipes are influenced by the pre-loading; making the pipes more vulnerable when the compression load is larger than 50% of the resistance load.

In early years, the design of platforms were done by simple methods in combinations with linear model programs. Later on, non-linear finite element programs became more relevant. Amdahl and Eberg (1993) not only discussed the use of the USFOS program, but also, performed a comparison of its implementation in static and dynamic analyses. As a conclusion, the jacket platform can be described by static approach when the impact is applied in soft points (middle span of leg and braces). If the impact is in hard point as joints, dynamic effects are more relevant.

Ellinas and Valsgard (1985) present a state of the art in the design of steel members subjected to accidental loads in ship collisions. The report also summarizes statistics of experimental tests, theoretical methods and the consequences of this type of accidental load. The study collects important information of the mechanics of ship collisions and provides the explanation of the basic theory that allowed regulations to develop simplified methods, for assessing the capacity of legs and braces under an impact load.

Nevertheless, there is a concern about the safety of offshore platforms, due to the weight increase of vessels that transit around these facilities. As a result, this has motivated other authors such as Moan et al. (2017), to present statistics related to the growth of supply vessel size since 1975 until 2015. In 1980, the maximum energies were considered 14MJ and 11 MJ for side and head on collision respectively. With a majority of vessels between 1000 and 2000 DWT (Dead Weight Tonnes), in comparison with 2013 when the size of vessel was from 5000 to 7000 DWT. This data reveals the importance of new regulations and assessments of structural integrity of offshore structures in case of

collisions events. Additionally, vessels have new bow designs and strengthening, in order to navigate in ice conditions, what implies that in bow collisions, ships may behave as rigid structures and platforms will need to dissipate most of the energy. If strength design is desired in offshore platforms, legs and braces must be strong enough to penetrate/crush the bow, what suggests, an increase in section parameters as diameter and thickness of the structural members.

In terms of numerical simulations, programs as USFOS, ABAQUS and LS-DYNA are becoming more used in the investigation of structural behavior under impact loads of offshore structures. The reason is that experimental methods need appropriate settings like location, scaling model, assurance of the initial conditions and adequate equipment to measure. A fairly wide range of numerical simulations have been performed by different authors. Especial interest in the split of absorption energy between the interacting bodies has been shown, as this is a very challenging issue. In Storheim (2016) the author presents a parametric study of numerical simulations of a bulbous vessel colliding against braces of different sections. Conclusions of the importance of accounting for the interactions effects during collision are shown, especially for braces that are smaller in dimensions than legs. If a strength design is desired (vessel dissipates most of the energy), the recommended requirements (Norsok Standard N-004, 2013) could lead to impractical thick steel pipes. Storheim shows how smaller thicknesses than the suggested by the guidelines, can crush a bulbous bow. Recommendation of an additional compactness criteria of $R_c \geq \eta$ is made. Where, R_c is the characteristic resistance to denting and η can be taken as 1.9 for bulbs and 1.4 for side collisions. Moreover, other authors as Travanca and Hao (2014b) describe a FEM model implemented for impact analysis of merchant vessels between 2000 to 5000 DWT against offshore jacket legs. The results are compared to experimental test from Jones et al. (1992). The report includes a parametric study of different sections, end conditions, axial pre-loading and dynamic parameters, as the strain rate effects are considered. By considering a ship-platform structure interaction, the study suggests a curved-design of force-deformation relationship, and energy-deformation relationship for a bulbous bow; and compare them to a curve design presented by Veritas DNV-RP-C204 and Norsok Standard N-004.

In this respect, composite structures as concrete-filled steel tubes have been used not only with the purpose of increasing the axial capacity of columns, but also, to enhance their behavior under lateral impact loads, as it has been observed in several experimental tests. Deng et al. (2011) describes the results of twelve steel tubes, whereas nine correspond to simply supported circular steel concrete-filled tubes (CFTs), two circular steel post tensioned concrete-filled tubes (PTCFTs), and one circular steel fiber-reinforced concreted-filled tube (FRCFT). The findings include failure modes, global displacement and impact force, show that a better performance in the post-tensioned samples as the concrete got improved in its capacity under tension.

Similarly, Wang et al. (2013) illustrates the results obtained after impacting twenty-two circular concrete filled steel tubular (CFST) members of mild steel. Those specimens have a diameter of 114mm, and thickness of 1.7mm and 3.5mm. The research also takes into account distinct parameters such as axial loading, impact energy, and constrain factor.

The final report exposes both the failure modes, global displacement, and dynamic forces, as well as a FEA model to describe the impact event.

In Han et al. (2014) new experimental test on twelve CFTs with high strength concrete (75 MPa) is done under impact loads. The report includes bending capacity, global displacement, impact force-time relationships and statistics under different end conditions and impact energies. In addition, a FEA model is developed and found in good agreement with the experimental tests. Dynamic effects in the flexural capacity of the beams are also presented. Important conclusions on the influences of different concrete strengths are made, showing that for impact lateral loads this parameter showed little influence in the impact force and middle span deflection. Main reason is the section moment capacity is more ruled by yield strength of the steel tube than by the concrete strength. This goes in good agreement with the results obtained in this thesis where the impact capacity of steel tubes filled with concrete of 10 MPa and 50 MPa are very similar.

Finally, Shakir et al. (2016) summaries the dynamic response of eighty-four tests for two type of specimens: concrete with normal aggregate and recycled concrete filled steel tubes under lateral impact load. Parameters as cross sectional dimensions, indenter configuration and impact energy are evaluated. The results show that both type of tests have similar deformation shape and similar strength capacity. Besides, an additional theoretical method is presented to predict the maximum impact force, the global displacement and the energy absorption of the members.

3 Theoretical Background for Ship Impact Analysis

3.1 Energy absorption

The most unfavorable case occurs when the center of gravity of the ship is concentric to the impact point, and there is not dissipation of kinetic energy by rotation energy of the ship. The law of conservation of energy implies that the impact energy from the striking body (ship) must be transferred to elastic and plastic deformation in the platform and ship. Equation 3-1 presents the conservation of law. Here, E_k is the kinetic energy, E_s is the energy dissipated by the ship, and E_p is the energy dissipated by the platform. Furthermore, the analysis of the ship collision can be handled as quasi-static if the natural period of the structure is less than estimated impact time. This is the case for most fixed platforms. Further considerations on the split of the energy absorption is considered in section 4.1.

There are three types of impacts between a ship and platform, and they are related to which part of the ship is striking the platform. These are defined as bow collision, side collision and stern collision. Legs in a jacket platform can be subjected to all types of collision. However, diagonal and horizontal braces will be only subjected to bow and stern collisions. Figure 3-1 presents the types of collisions between a ship and jacket platform.

$$E_k = E_s + E_p \quad (3-1)$$

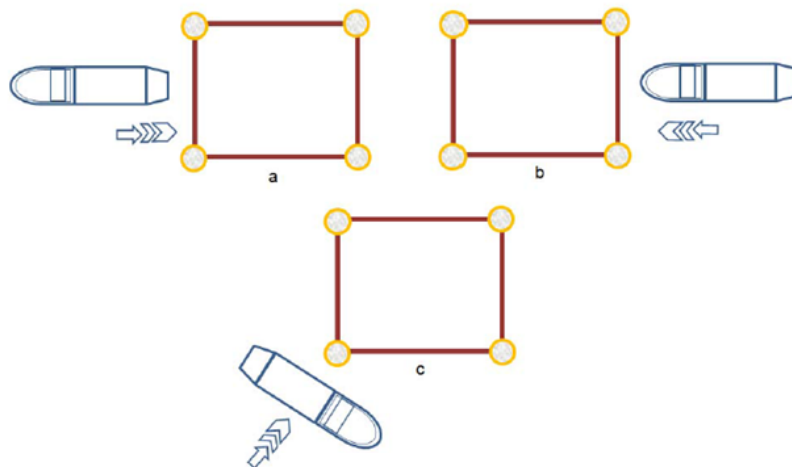


Figure 3-1: Types of collisions (a) stern impact, (b) bow impact and (c) side impact. (Aldilana, 2014)

3.2 Type of damage

The dissipation of impact energy in a platform can be divided as follows:

- Overall damage/jacket deformation.
- Global damage.
- Local damage.

Figure 3-2 shows the deformation modes of a steel jacket platform under ship collision. All three modes interact and affect each other. First, the ship will create a local damage (dent) in the member, the severity of this will depend on the type of collision, and geometry of the ship. For instance, a sharped-bow will produce more local damages than side collisions. After local damage starts, the capacity in bending of the member will be reduced due to the loss of area in the cross section. The impact force will increase making the member bend and producing plastic hinges in the beam (Fig. 3-4). At this point, energy absorption is achieved by both local and global deformation. During the process of bending membrane forces can arise if end boundary conditions allow axial restraint in the impacted member.

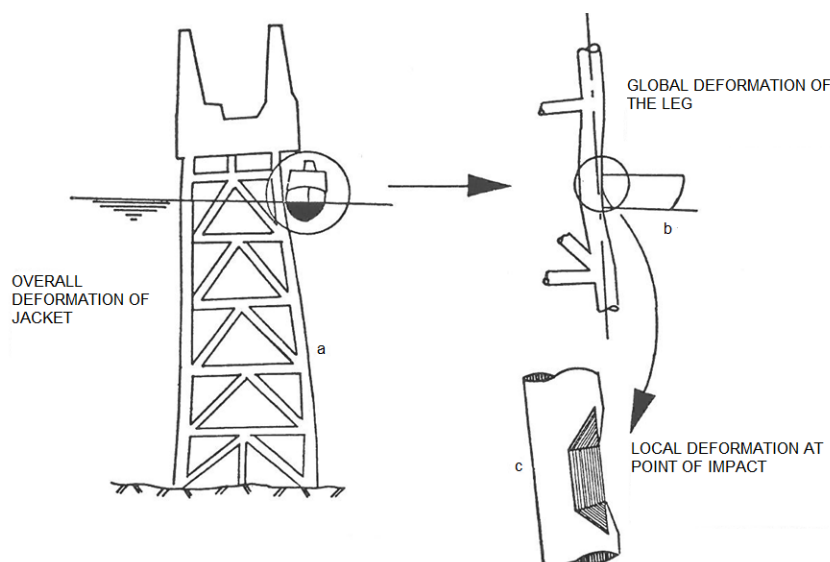


Figure 3-2: Deformation modes of a steel jacket from Søreide (1981)

3.3 Plastic theory

Collision loads involve high energies where plasticity theory is more appropriate than elastic theory, the main reason is that structural members can have large deformations beyond the elastic region.

Steel material is characterized by its ductility and ability to resist larger stresses beyond the yield strength. Consequently, the material will deform until it fractures. Figure 3-3 depicts this process of stress-strain relationship for steel under tension. At the beginning, the process is linear elastic, after reaching the yield point, plastic process starts where the member is allowed to deform without a significantly increase in the stress. When

the section is completely yielded, the material resistance to larger deformation will initiate strain hardening and reach the ultimate stress. Finally, necking will begin and the material will fracture.

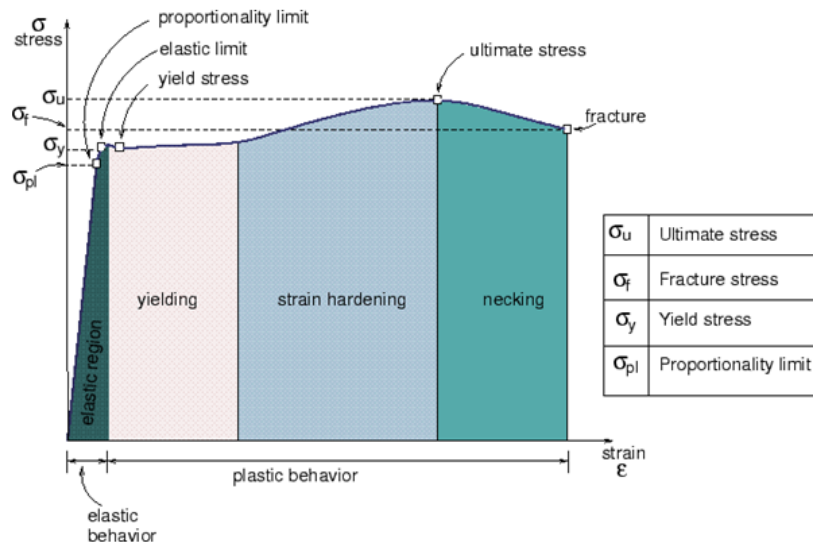


Figure 3-3: Stress-strain curve for steel (Learneasy.info, 2014)

Figure 3-4 illustrates the plastic behavior of a beam under lateral load, and the process of creating plastic hinges (plastic zones). Initially, the beam behaves elastic, but if the load is increased, yielding occurs due to the large bending moment, creating a redistribution of the moments and finding full plastification on the colored zones. The final collapse load will be expressed in terms of the plastic moment capacity (M_p) of the beam. This value corresponds to the moment where the cross section is completely yielded. Figure 3-5 shows the variation of strain and stress in a symmetrical cross section. For steel tubes the plastic moment capacity (M_p) can be calculated in terms of plastic section modulus (W_p) and its yield strength (f_y), as it is shown in equations 3-2 and 3-3, where D is the outside diameter of the pipe and t is the wall thickness.

$$M_p = W_p f_y \quad (3-2)$$

$$W_p = \frac{1}{6}[D^3 - (D - 2t)^3] \quad (3-3)$$

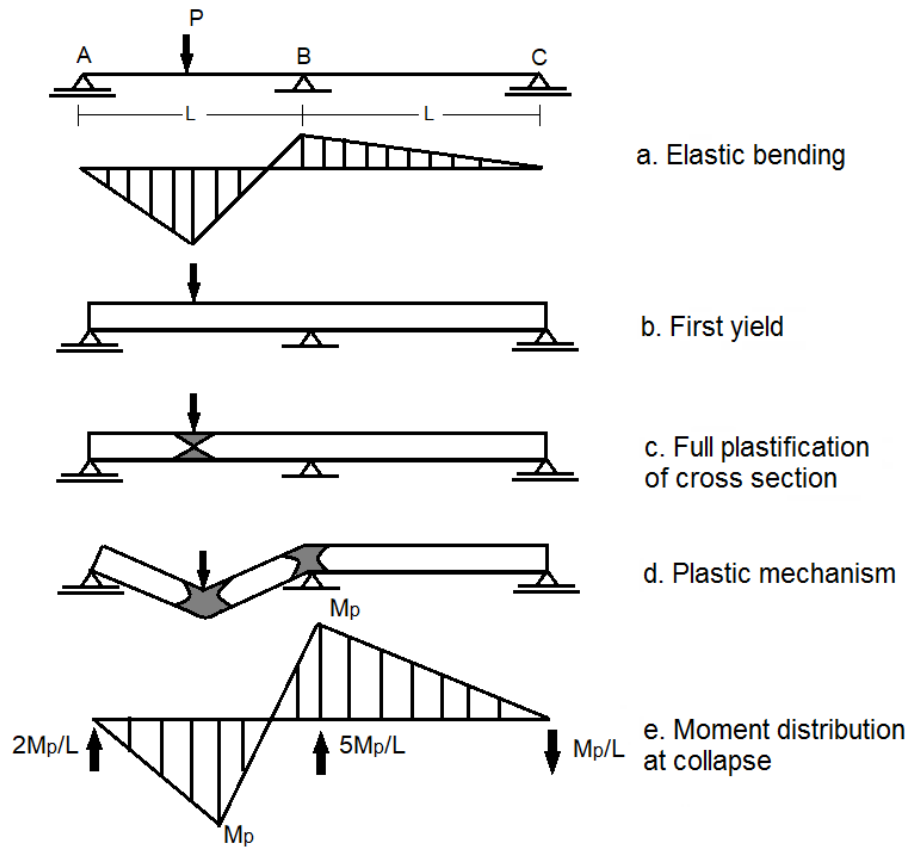


Figure 3-4: Plastic hinge formation in a beam under lateral load Sørense (1981)

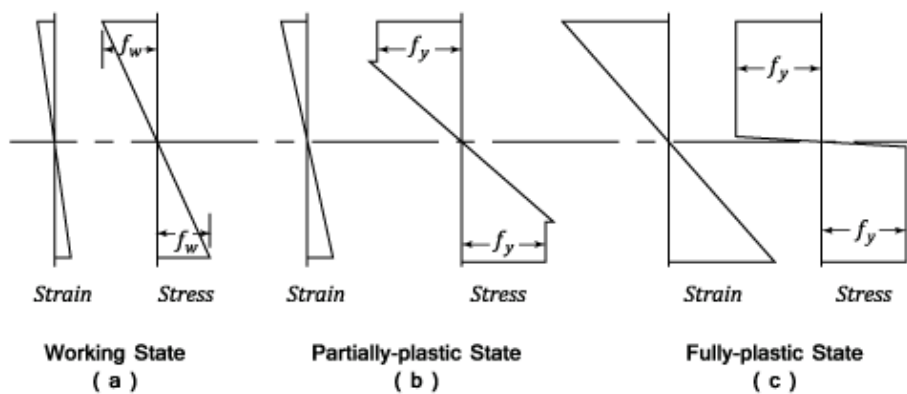


Figure 3-5: Stress and strain variation in a symmetrical cross section for a beam under a transverse load from Codecogs.com (2014)

Figure 3-6 presents a composite section of steel tube filled with concrete. The plastic

moment capacity of composite sections (M_{pc}) can be also expressed in similar terms as steel tubes. Equation 3-4 present the plastic moment capacity of the composite section as the addition between the plastic moment capacity of the steel and the plastic moment capacity of the grout column. From this equation, the critical collapse load for the composite member (R_{oc}) can be found. Equation 3-5 shows the R_{oc} for a beam with both ends fixed.

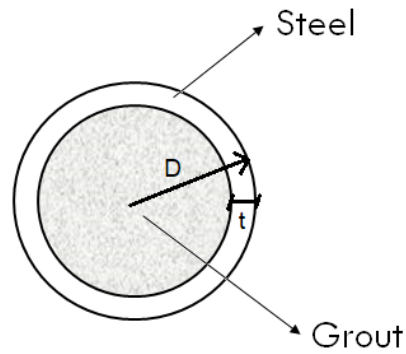


Figure 3-6: Composite section of steel tube filled with concrete

$$M_{pc} = f_y \frac{D^3 - (D - 2t)^3}{6} + f_c \frac{(D - 2t)^3}{12} \quad (3-4)$$

$$R_{oc} = \frac{8M_{pc}}{L} \quad (3-5)$$

4 Guidelines for Ship Impact Analysis

The development of this chapter is based on the guidelines given in (Norsok Standard N-003, 2017) for accidental actions as ship collisions, fires, explosions and dropped objects. Main statements for ship collisions with jacket platforms can be summarized in:

- Unless further consideration, a design value of 50MJ shall be considered for visiting vessels.
- The Impact zone in the platform is between 10 m below LAT (lowest astronomical tide), and 13 m above HAT (Highest astronomical tide).
- Impact scenarios are divided into bow, stern and side collision.
- If the natural period of the member is less than estimated impact time, the forces can be handled as quasi-static. Norsok Standard N-004 (2013) and (Veritas DNV-RP-C204, 2017) provide load-indentation and load-displacement relationship for this type of analysis.
- Unless operational restrictions are implemented for visiting vessel, for Accidental State condition (ALS), the size of 1000 DWT must be implemented, considering a corresponding velocity of 3 m/s for head-on collisions, and 2 m/s for sideways and stern collisions, respectively. Besides, an additional 10% mass for head-on and 40% mass for sides collisions are required.

4.1 Design principles

The impact load from ship collisions is governed by the kinetic energy (E_k) from the striking body (vessel). The magnitude of the kinetic energy is proportional to the mass of the ship including its hydrodynamic mass and to the squared ship velocity, at the moment of the impact. Consequently, the kinetic energy must be dissipated by the interacting bodies. Figure 4-7 depicts the type of design for ship collision based on the split of strain energy.

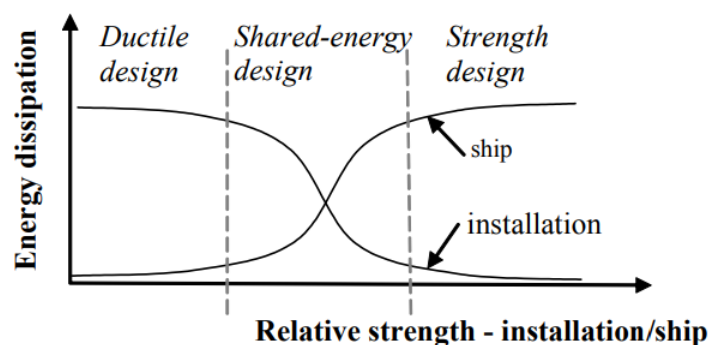


Figure 4-7: Energy dissipation for strength, ductile and shared-energy design from Veritas DNV-RP-C204 and Norsok Standard N-004

Ductile design makes reference to the fact that the striking body (vessel) is considered rigid, and all the strain energy must be dissipated by the platform. Nonetheless, the implementation of this simplification should be evaluated in detailed. Although, it is commonly used during pre-design, in some cases where there is not enough information about the type of visiting vessel or there is an indication of strong bow in the vessel. Some examples are: bulbous boat, X-bow or ice strengthened bow.

If strength design is desired, the platform installation is strengthened to be capable of crushing the vessel. This is a conservative approach that can result in an expensive solution, that could lead to very robust and thick steel cross sections.

A shared-energy approach points out that the strain energy must be dissipated by both interacting bodies, and these will deform significantly. This type of design is more realistic but more difficult to assess, as the distribution of the energy needs to be calculated at each step, and it highly depends on the way of the ship crushes, and the non-linearities of the phenomenon (bow wrapping around legs and braces, changes in the contact area among others).

The kinetic energy from the collision that must to be absorbed as strain energy can be calculated as (for fixed platforms):

$$E_k = \frac{1}{2} [m_s + m_a] v_s^2 \quad (4-6)$$

Where, m_s is the mass of the ship, m_a is the hydrodynamic added mass and v_s is the velocity of the ship at the moment of impact.

4.2 Force-deformation relationships for vessels

Figure 4-8 presents the relationship for vessels between impact force and deformation for bow, side and stern for legs with diameters 1.5m and 10m. Force-deformation relationship for bow vessels, that impact leg sections from 1.5m to 2.5m is shown in Figure 4-9. However, these relationships are limited for vessels between 2000-5000 DWT.

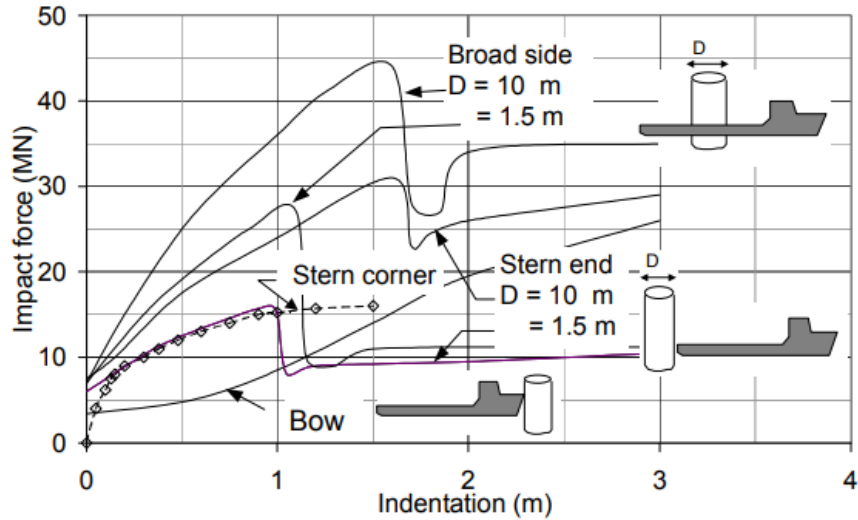


Figure 4-8: Deformation curve for beam, raked bow and stern impact from Veritas DNV-RP-C204 and Norsok Standard N-004

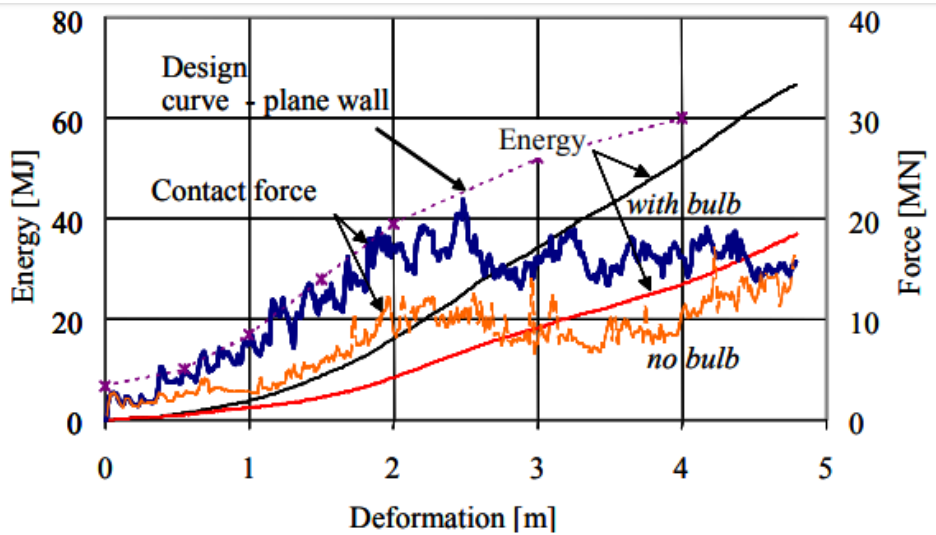


Figure 4-9: Deformation curve for bow with and without bulb (2-5.000 DWT) from Veritas DNV-RP-C204 and Norsok Standard N-004

Small tubular members as braces (diameters $\leq 1.25\text{m}$) can be able to crush the bow if the plastic collapse load in bending (R_o) is according to the values presented in Table 4-1, and the compactness parameter is fulfilled. This compactness criteria in the brace is expressed as:

$$f_y t^{1.5} D^{0.5} = \frac{2}{3} R_o \quad (4-7)$$

Contact location	Energy dissipation in bow if brace resistance R_o			
	>3 MN	>6 MN	> 8 MN	> 10 MN
Above bulb	1 MJ	4 MJ	7 MJ	11 MJ
First deck	0 MJ	2 MJ	4 MJ	17 MJ
First deck - oblique brace	0 MJ	2 MJ	4 MJ	17 MJ
Between forecastle/first deck	1 MJ	5 MJ	10 MJ	15 MJ
Arbitrary location	0 MJ	2 MJ	4 MJ	11 MJ

Table 4-1: Energy dissipation in bow given the R_o brace resistance from Veritas DNV-RP-C204 and Norsok Standard N-004

4.3 Forces-deformation relationship for legs and braces

The dissipation of impact energy in a platform-leg or brace can be divided by bending and local denting of the member. Large dissipation energy can be achieved if the joints and the surrounded structure are strong enough to allow the impact member undergo large deformations. The Veritas DNV-RP-C204 and Norsok Standard N-004 provide formulations for tensile fracture limits, local buckling and impact force-deformations relations for denting of stiffened and unstiffened tubes.

4.3.1 Local denting

For an impact against a jacket leg/brace, the contact force will increase resulting in local denting of the tube (w_d). When the contact force is greater than the plastic bending collapse resistance (R_o), the leg/brace will deform in a three-hinge mechanism. At the same time, the denting of the wall will also reduce the plastic moment capacity (M_p) of the member.

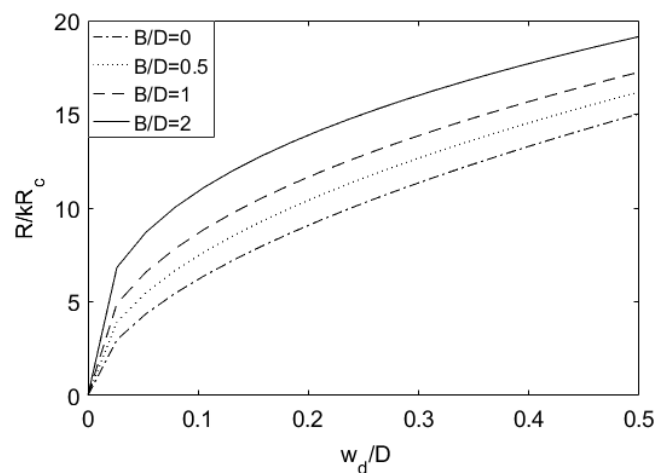


Figure 4-10: Resistance curve for local denting from DNV-RP-C204 (2017)

Figure 4-10 illustrates the resistance curve for local denting of tubes presented in Veritas DNV-RP-C204 and Norsok Standard N-004. Equation 4-8 defines the relationship dent-impact force of Figure 4-10.

$$\frac{R}{kR_c} = C_1 \left[\frac{W_d}{D} \right]^{C_2} \quad (4-8)$$

$$R_c = fy \frac{t^2}{4} \sqrt{\frac{D}{t}}$$

$$C_1 = 22 + 1.2 \frac{B}{D}$$

$$C_2 = \frac{1.925}{3.5 + \frac{B}{D}}$$

$$k = 1.0 \quad \text{for} \quad \frac{N_{sd}}{N_{Rd}} \leq 0.2$$

$$k = 1.0 - 2 \left[\frac{N_{sd}}{N_{Rd}} - 0.2 \right] \quad \text{for} \quad 0.2 < \frac{N_{sd}}{N_{Rd}} < 0.6$$

$$k = 0 \quad \text{for} \quad 0.6 \leq \frac{N_{sd}}{N_{Rd}}$$

Where, R_c is characteristic resistance to denting. B is the extension contact. The factor k accounts for the axial loading of the leg, and where N_{sd} is the design axial compression force in the member and N_{Rd} is the design axial compressive resistance.

4.3.2 Plastic force-deformation relationships

A leg/brace subjected to a collision load is mainly governed by the bending. Moreover, the load capacity may increase by the development of membrane tension. The DNV standard provides simple equations in order to account for the effect of:

- elastic flexibility of member/adjacent structure
- local deformation of cross-section
- local buckling
- strength of connections
- strength of adjacent structure
- fracture

The axial flexibility of the members influence the tension forces of the member under large deformations. Figure 4-11 shows the collapse mechanism of a supported beam with axial flexibility.

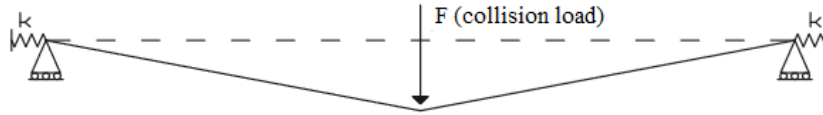


Figure 4-11: Collapse mechanism for beams with axial flexibility from Veritas DNV-RP-C204 and Norsok Standard N-004

Figure 4-12 shows the force-deformation relationship for a tubular beam, where \bar{w} is the non-dimensional deformation and it will be limited by local buckling or tensile fracture (see Sections 4.5.1 and 4.5.2). The equations for calculating the plastic collapse load (R_o), the non-dimensional deformation (\bar{w}), the equivalent axial stiffness of the member (K) and the non-dimensional spring stiffness (c) are:

$$R_o = \frac{4C_1 M_p}{L} \quad (4-9)$$

$$\bar{w} = \frac{w}{C_1 W_c} \quad (4-10)$$

$$c = \frac{4C_1 K W_c^2}{f_y A L} \quad (4-11)$$

$$\frac{1}{K} = \frac{1}{k_{node}} + \frac{L}{2EA} \quad (4-12)$$

Where, $W_c = D/2$ is the characteristic deformation for tubular beams, $C_1 = 1, 2$ for pinned and fixed end conditions, respectively, A is the cross sectional area and L is member length.

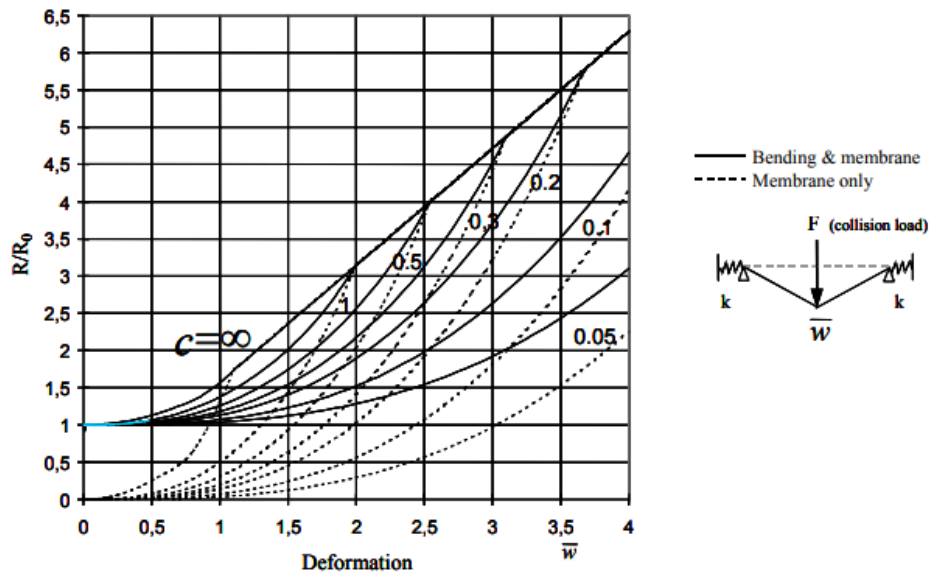


Figure 4-12: Force-deformation relationship for tubular beams with axial flexibility from Veritas DNV-RP-C204 and Norsok Standard N-004

4.4 Bending capacity of dented tubular members

Local denting in the steel member will reduce the plastic moment capacity. Figure 4-13 presents the reduction of moment capacity for dented tubes. This relationship is limited for member in compression or moderate tension and the flattened part in the denting section is considered non-effective.

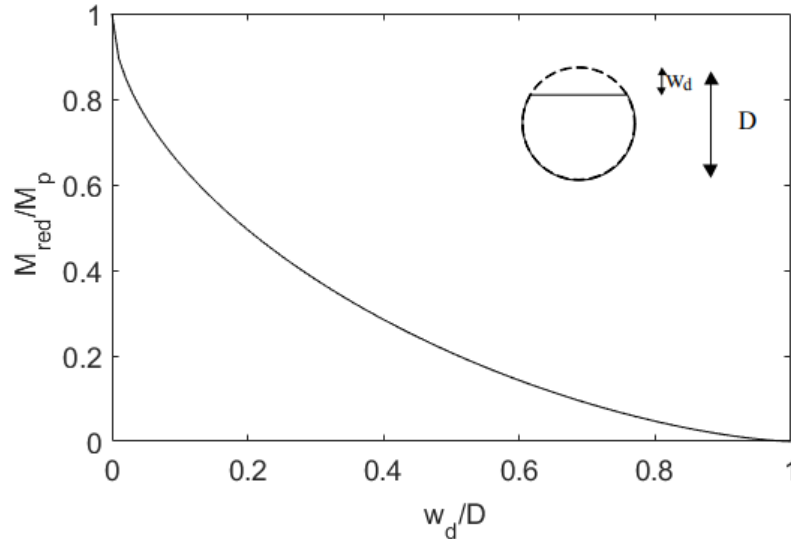


Figure 4-13: Reduction moment capacity for dented tubes from DNV-RP-C204 (2017)

4.5 Failure criteria

According to Veritas DNV-RP-C204 and Norsok Standard N-004, failure in the deformed member will take place if:

- Tensile strain exceeds the critical value (ϵ_{cr}) (see Table 4-2).
- Joint failure.
- Denting is larger than 50% of the diameter.

4.5.1 Local buckling

Local buckling will occur in the compressive side of the member. For cross sections type I and II, even after local buckling, the leg/brace will still undergo large deformations and, it will continue dissipating energy. Local buckling does not need to be taken into account if Eq.4-13 is satisfied:

$$\beta \leq \left[\frac{14C_f f_y}{C_1} \left[\frac{kL}{d_c} \right]^2 \right]^{1/3} ; \beta = \frac{D/t}{235/f_y} \quad (4-13)$$

An the axial flexibility factor (c_f) is expressed in Eq.4-14, and where c is the non-dimensional spring stiffness (see Eq. 4-11).

$$c_f = \left[\frac{\sqrt{c}}{1 + \sqrt{c}} \right]^2 \quad (4-14)$$

Where, $d_c = D$ is the characteristic dimension, $C_1 = 2$ or 1 for clamped ends or pinned end, respectively, and kL is the smallest dimension from the location of the collision to the joint. If buckling occurs, the maximum displacement may be:

$$w = \frac{d_c}{2c_f} \left[1 - \sqrt{1 - \frac{14c_f f_y}{c_1 \beta^3} \left[\frac{kL}{d_c} \right]^2} \right] \quad (4-15)$$

4.5.2 Tensile fracture

Tensile fracture will occur in the yield hinges as large rotations are developed. Rupture may be assumed to occur when lateral deflection exceeds:

$$w = \frac{c_1 d_c}{2c_f} \left[\sqrt{1 + \frac{4c_w c_f \epsilon_{cr}}{c_1}} - 1 \right] \quad (4-16)$$

Displacement factor:

$$c_w = \frac{1}{c_1} \left[c_{lp} \left[1 - \frac{c_{lp}}{3} \right] + 4 \left[1 - \frac{W}{W_p} \right] \frac{\epsilon_y}{\epsilon_{cr}} \right] \left[\frac{kl}{dc} \right]^2 \quad (4-17)$$

Plastic zone length factor

$$c_{lp} = \frac{\left[\frac{\epsilon_{cr}}{\epsilon_y} - 1 \right] \frac{W}{W_p} H}{\left[\frac{\epsilon_{cr}}{\epsilon_y} - 1 \right] \frac{W}{W_p} H + 1} \quad (4-18)$$

Where, W is the elastic section modulus, W_p is the plastic section modulus, ϵ_y is the yield strain, and H is the non-dimensional plastic stiffness that can be found from Table **4-2**.

Steel grade	ϵ_{cr}	H
S 235	20 %	0.0022
S 355	15 %	0.0034
S 460	10 %	0.0034

Table 4-2: Proposed values for ϵ_{cr} and H for different steel grades from DNV-RP-C204

5 Ship Impact Analysis of Jacket Legs

5.1 Steel legs: Parametric study

The simplified method presented by Veritas DNV-RP-C204 (2017) (see section 4.1) is similar to the introduced in Norsok Standard N-004 (2013). Given that force-deformations relationships and equations are similar, in this section, references to the N-004 are also valid for the DNV-RP-C204. The results from numerical simulations obtained from USFOS software are compared then to the Norsok Standard N-004. The parametric study includes leg-platforms with different ratios D/t (Diameter/thickness) and constant length.

The leg is impacted at mid-span as a point load. For instance, the contact extension is zero ($B=0$). Furthermore, experimental results from Jones et al. (1992) are also given in comparison with numerical results from USFOS. Dimensions and characteristics of the numerical tests are summarized in Table 5-3. The failure criteria is considered when the strain reaches its critical value of 0.15 ($\epsilon_{cr}=0.15$).

Characteristic	Value/Description
Length, L[m]	20
Diameter, D[m]	1.3, 1.5, 1.8, 2.0
Thickness, t[mm]	40,50,60,70,80
Boundary conditions	Fixed
Yield strength f_y [MPa]	355

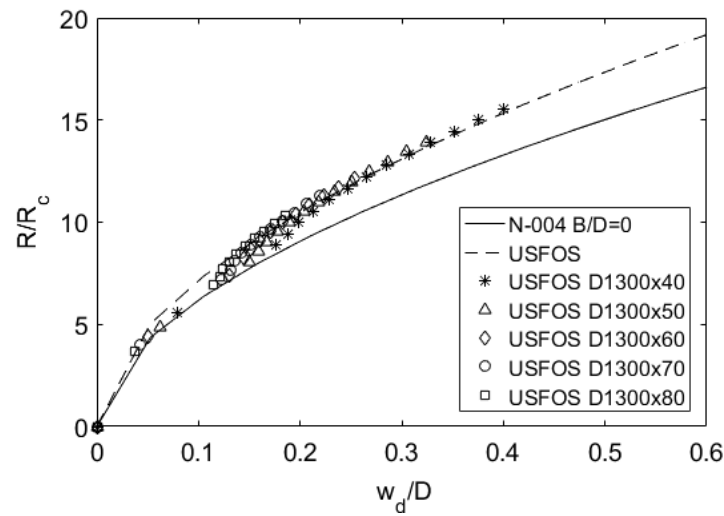
Table 5-3: Dimensions and characteristics of numerical tested-legs

Hand calculations and force-deformation relationships are performed using the simplified method referred in section 4.1, in order to predict the global displacement, denting of the wall, impact energy and total energy absorbed by the leg. An example of the process used in the simplified method is presented in the Annex in section 10.1.

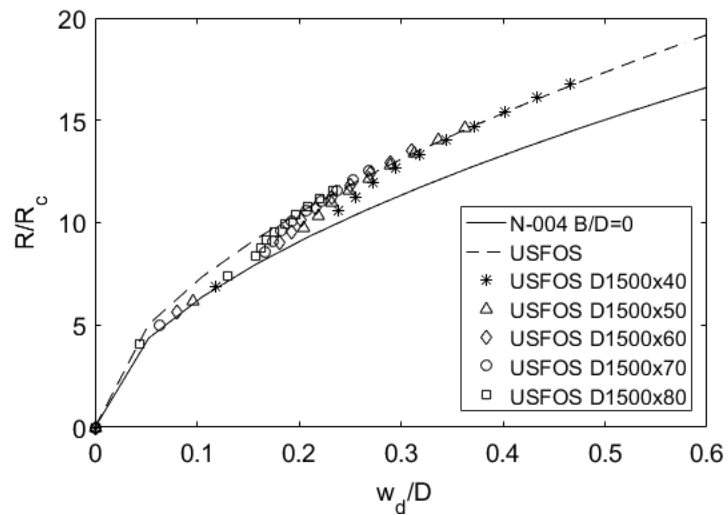
5.1.1 Results and Discussion

Tables 5-4 and 5-5 report the impact forces, global deflections in bending, denting, and impact energies from the parametric study. The comparison from the results obtained for the impact force show that the simplified method deviate between a range of 0-5%. The most dispersed values are the bending displacement (global deflection), denting and energy absorption due to the dent in the wall. The critical bending displacement of the leg is more conservative in N-004 than USFOS, as larger displacement have been observed in the numerical model, for 1.3m and 1.5m diameters, these values are between 10% and 20% larger than N-004. For large diameters as 1.8m and 2.0m, a great difference is found in the dent in the wall, and consequently, in the energy absorption by denting. The difference in these two parameters can go up to 48%, being the value reported by the

simplified method larger than the value from USFOS. Main reason to this difference is the membrane effect capture by the numerical model. Figures 5-14 and 5-15 depict a comparison of numerical test and N-004, here the non-dimensional dent against the non-dimensional impact force is shown. The figure presents a good agreement at the beginning of the curve. However, when the dent is 20-30% of the diameter the USFOS curves are shifted up as the membrane forces acting in the member offers resistance to the dent. This implies that for same impact force less denting is found in the USFOS model. Thereby, the energy absorption due to denting (area under the curve) is less than the found by using the simplified method in Norsok Standard N-004. Figure 5-16 explains in a better way the statement mentioned above.

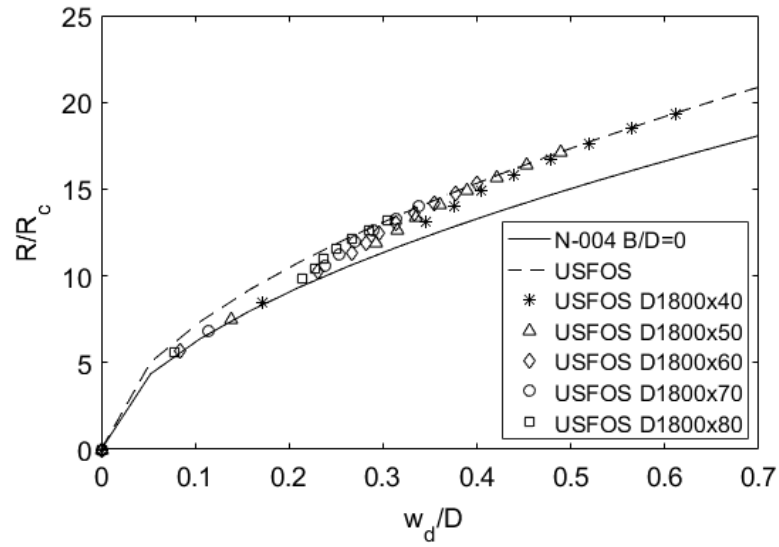


(a)

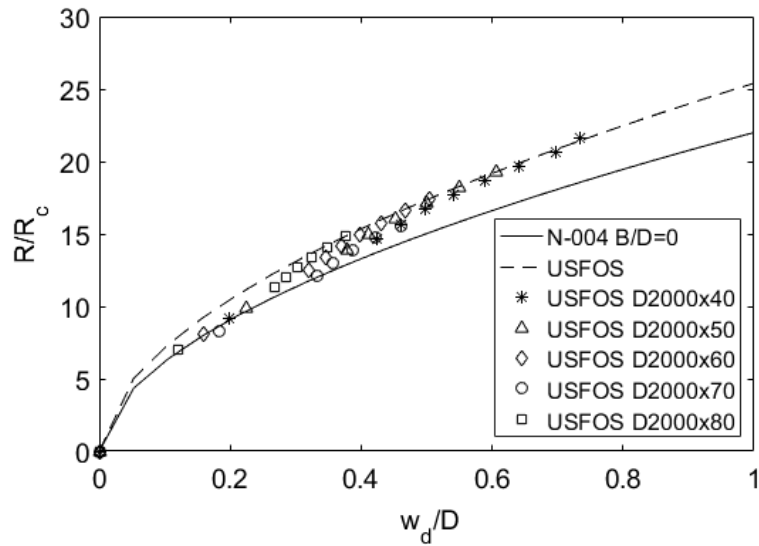


(b)

Figure 5-14: Non-dimensional Denting -vs- Non-dimensional Impact Force for $D=1.3\text{m}$ and 1.5m



(a)



(b)

Figure 5-15: Non-dimensional Denting -vs- Non-dimensional Impact Force for $D=1.8\text{m}$ and 2.0m .

The maximum impact energy absorption in the parametric study is found to be 46.85MJ for a diameter of 2m, wall thickness of 80mm and a ratio D/t of 25. On the one hand, the maximum impact in this leg is 42.05MN, and a lateral displacement of 0.77m. On the other, the minimum impact energy absorption was 13.92MJ for a 1.3m diameter, and a wall thickness of 40mm, with a maximum impact force of 12.59MN, and a lateral displacement of 1.09m.

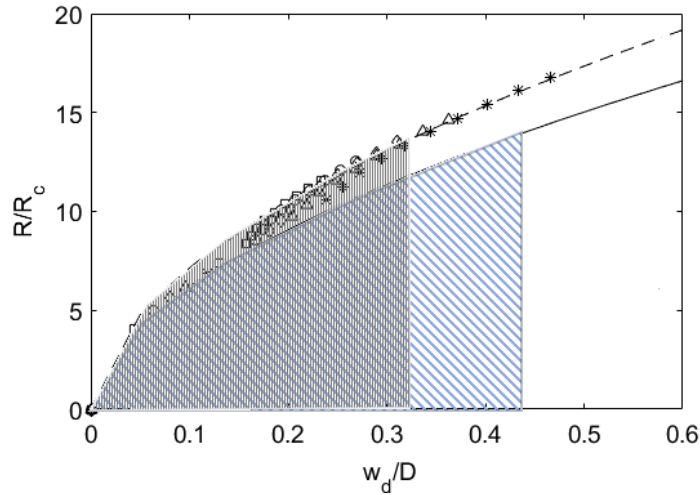


Figure 5-16: Comparison of the energy absorbed by denting in USFOS with N-004.

The interface of the program also allows to see the plastic utilization and strain distribution of the impacted member. Figure 5-17 shows an example of the plastic utilization and strain distribution for the leg with a 1.5m diameter and a 40mm wall thickness. The deformed figure displays a concentration of these parameters in the joints and in the middle of the span where plastic hinges are formed in the member.

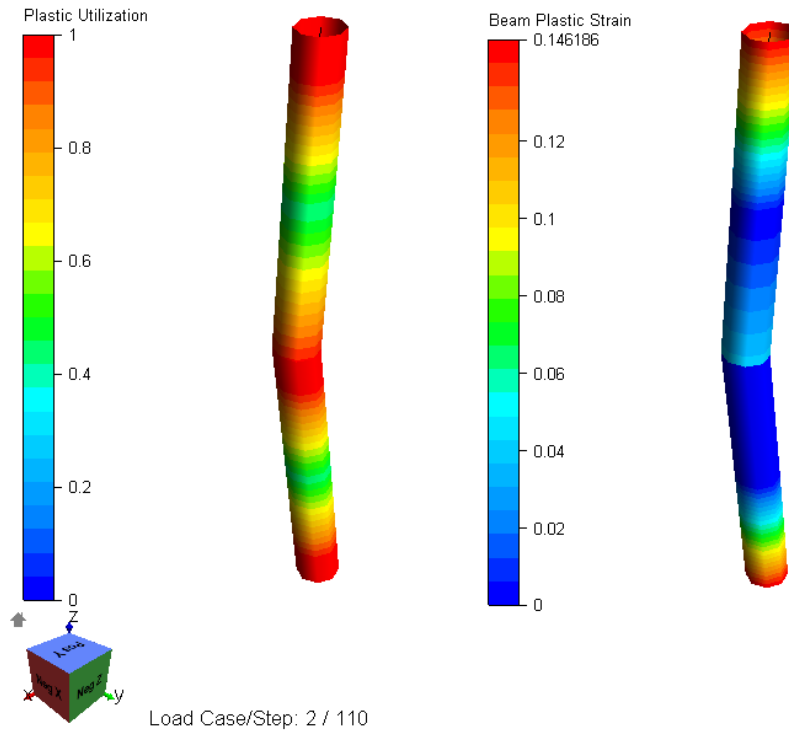


Figure 5-17: Plastic utilization and strain distribution of impacted leg with $D=1.5\text{m}$ and $t=40\text{mm}$

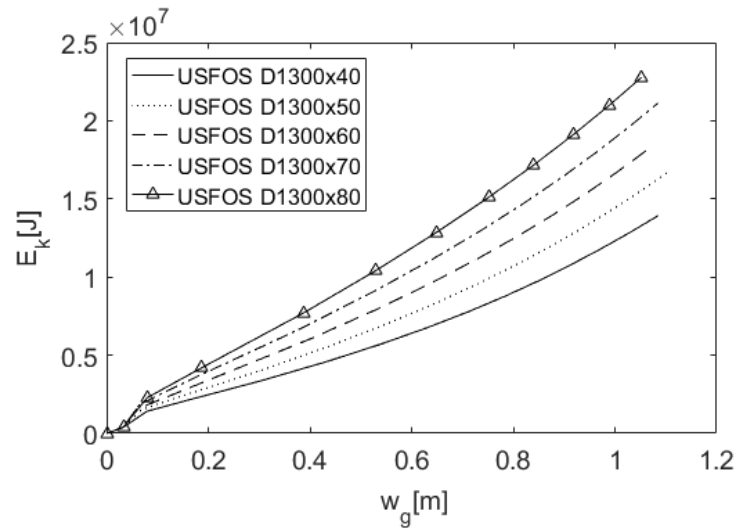
	D1300x80			D1500x80		
	Simplified Method	USFOS	%	Simplified Method	USFOS	%
Impact force [MN]	21.33	23.58	10%	25.80	28.51	10%
Energy beam [MJ]	18.77	19.38	3%	20.25	23.03	12%
Energy dent [MJ]	3.75	3.40	10%	6.49	5.96	12%
Total Energy [MJ]	22.52	22.78	1%	26.74	28.99	8%
Bending [m]	0.88	1.05	16%	0.79	0.99	21%
Dent [m]	0.27	0.24	14%	0.39	0.35	11%
	D1300x70			D1500x70		
	Simplified Method	USFOS	%	Simplified Method	USFOS	%
Impact force [MN]	19.12	21.16	10%	22.85	25.29	10%
Energy beam [MJ]	16.83	17.50	4%	18.02	20.30	11%
Energy dent [MJ]	3.96	3.63	19%	6.66	6.20	7%
Total Energy [MJ]	20.79	21.13	2%	24.68	26.47	7%
Bending [m]	0.88	1.08	19%	0.79	1.01	22%
Dent [m]	0.32	0.28	14%	0.45	0.41	9%
	D1300x60			D1500x60		
	Simplified Method	USFOS	%	Simplified Method	USFOS	%
Impact force [MN]	16.65	18.11	8%	19.89	21.58	8%
Energy beam [MJ]	14.70	14.51	1%	15.71	16.75	6%
Energy dent [MJ]	4.09	3.60	14%	6.83	6.07	13%
Total Energy [MJ]	18.79	18.11	4%	22.54	22.82	1%
Bending [m]	0.88	1.06	17%	0.79	0.98	19%
Dent [m]	0.38	0.33	16%	0.53	0.47	13%
	D1300x50			D1500x50		
	Simplified Method	USFOS	%	Simplified Method	USFOS	%
Impact force [MN]	14.10	15.73	10%	16.83	17.80	5%
Energy beam [MJ]	12.49	12.75	2%	13.33	13.25	1%
Energy dent [MJ]	4.20	4.05	4%	6.56	5.86	12%
Total Energy [MJ]	16.69	16.80	1%	19.89	19.11	4%
Bending [m]	0.89	1.10	19%	0.79	0.95	17%
Buckling [m]				0.59		
Dent [m]	0.46	0.42	10%	0.62	0.54	15%
	D1300x40			D1500x40		
	Simplified Method	USFOS	%	Simplified Method	USFOS	%
Impact force [MN]	11.27	12.59	10%	13.56	14.60	7%
Energy beam [MJ]	10.02	9.90	1%	10.78	10.87	1%
Energy dent [MJ]	4.12	4.02	2%	7.00	6.22	13%
Total Energy [MJ]	14.14	13.92	2%	17.78	17.10	4%
Bending [m]	0.90	1.09	17%	0.80	0.97	18%
Buckling [m]				0.25		
Dent [m]	0.57	0.52	10%	0.80	0.70	14%

Table 5-4: Results of parametric study of single legs, impacted at mid-span for D=1.3m and 1.5m

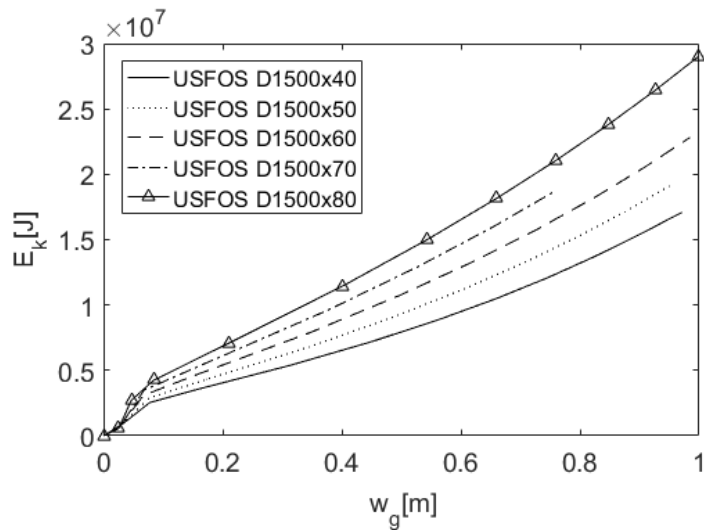
	D1800x80			D2000x80		
	Simplified Method	USFOS	%	Simplified Method	USFOS	%
Impact force [MN]	35.00	35.60	2%	41.90	42.05	0%
Energy beam [MJ]	24.50	24.66	1%	26.06	27.92	7%
Energy dent [MJ]	15.57	11.63	34%	26.15	18.92	38%
Total Energy [MJ]	40.07	36.29	10%	52.21	46.85	11%
Bending [m]	0.70	0.80	13%	0.62	0.77	19%
Buckling [m]				0.79		
Dent [m]	0.69	0.55	25%	0.96	0.75	28%
	D1800x70			D2000x70		
	Simplified Method	USFOS	%	Simplified Method	USFOS	%
Impact force [MN]	30.95	31.00	0%	37.04	36.21	2%
Energy beam [MJ]	21.06	20.98	0%	23.09	22.80	1%
Energy dent [MJ]	15.88	11.39	39%	26.59	17.98	48%
Total Energy [MJ]	36.94	32.33	14%	46.98	40.787	22%
Bending [m]	0.68	0.80	15%	0.62	0.73	15%
Buckling [m]	0.86			0.46		
Dent [m]	0.80	0.60	33%	1.11	0.82	35%
	D1800x60			D2000x60		
	Simplified Method	USFOS	%	Simplified Method	USFOS	%
Impact force [MN]	26.32	26.96	2%	32.08	31.36	2%
Energy beam [MJ]	17.95	18.27	2%	20.04	16.62	21%
Energy dent [MJ]	15.31	11.75	30%	26.99	18.34	47%
Total Energy [MJ]	33.26	30.92	8%	47.03	37.95	24%
Bending [m]	0.68	0.81	16%	0.63	0.80	22%
Buckling [m]	0.44			0.15		
Dent [m]	1.05	0.88	19%	1.57	1.21	30%
	D1800x50			D2000x50		
	Simplified Method	USFOS	%	Simplified Method	USFOS	%
Impact force [MN]	21.75	22.80	5%	27.00	26.98	0%
Energy beam [MJ]	14.87	15.70	5%	16.91	17.69	4%
Energy dent [MJ]	14.70	12.28	20%	27.32	19.85	38%
Total Energy [MJ]	29.57	27.98	6%	44.23	37.55	18%
Bending [m]	0.68	0.83	18%	0.63	0.80	22%
Buckling [m]	0.24			0.15		
Dent [m]	1.05	0.88	19%	1.57	1.21	30%
	D1800x40			D2000x40		
	Simplified Method	USFOS	%	Simplified Method	USFOS	%
Impact force [MN]	17.60	18.43	5%	21.82	21.75	0%
Energy beam [MJ]	12.06	12.36	2%	13.70	13.80	1%
Energy dent [MJ]	14.87	12.38	20%	27.54	19.20	43%
Total Energy [MJ]	26.93	24.74	9%	41.25	33.07	25%
Bending [m]	0.69	0.83	17%	0.63	0.78	19%
Buckling [m]	0.12			0.07		
Dent [m]	1.31	1.10	19%	2.00	1.47	36%

Table 5-5: Results of parametric study of single legs, impacted at mid-span for D=1.8m and 2.0m

Figures 5-18 to 5-21 present the thickness and diameter effects in the energy absorption of the leg. The figures depicts the global displacement (w_g) against the impact energy (E_k), as it can be seen, the diameter has more influence than the wall thickness in the energy absorption. Correspondingly, it can be noticed the behavior of the impact member. At the beginning where the denting takes place the curve is very steep. When the impact force is large enough, the leg starts to bend rapidly. This bending effect is presented in the second part of the curve, where it is less steeped. Figure 5-22 shows a distinction between this two stages.

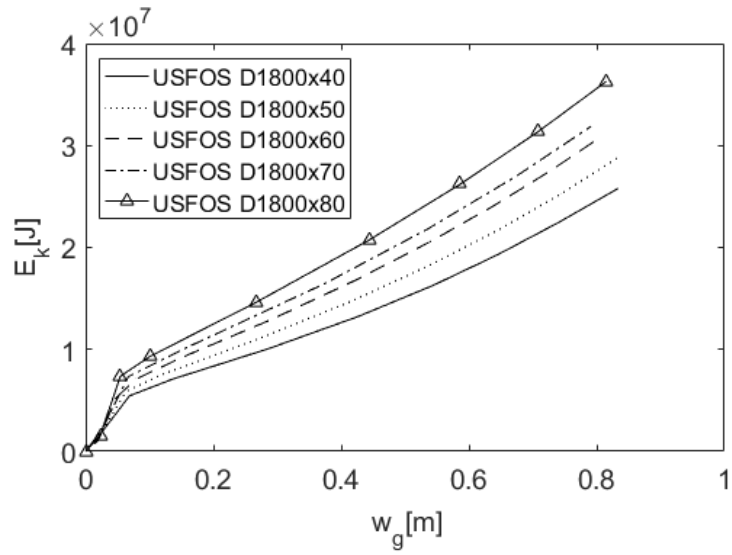


(a)

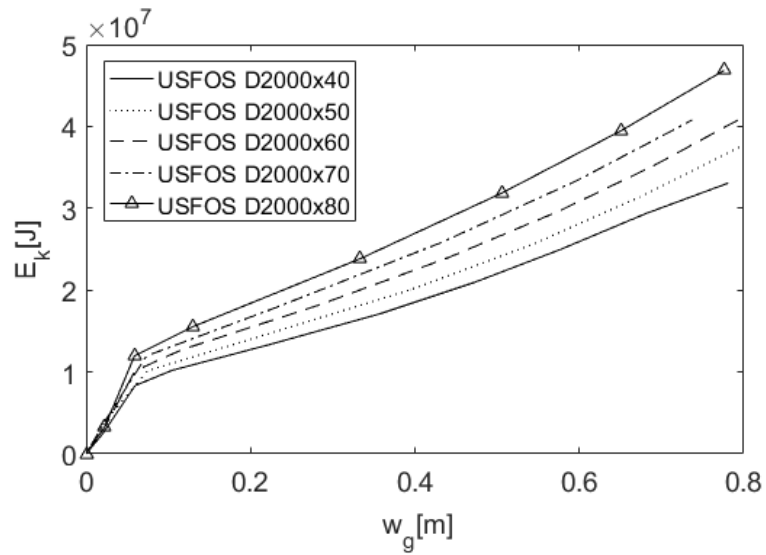


(b)

Figure 5-18: Thickness influence in the absorbed energy against global displacement for $D=1.3\text{m}$ and 1.5m

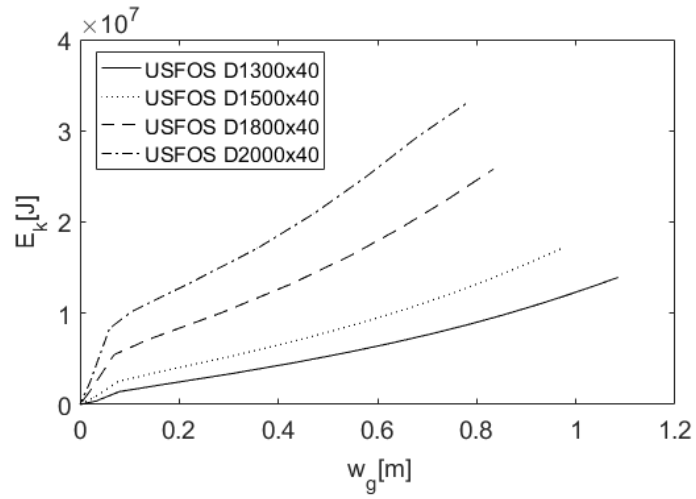


(a)

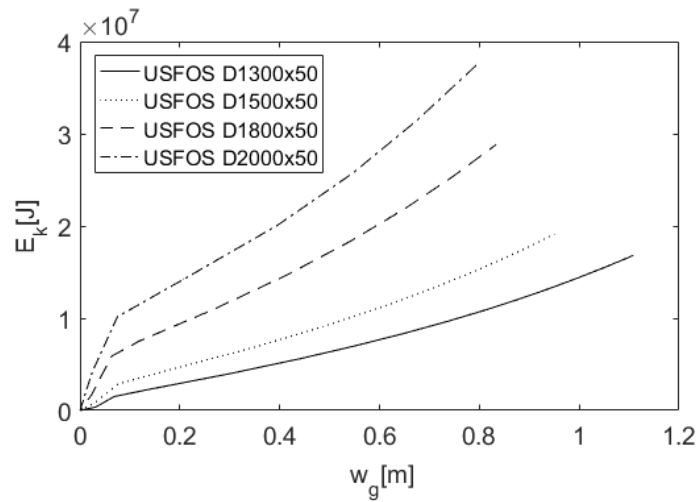


(b)

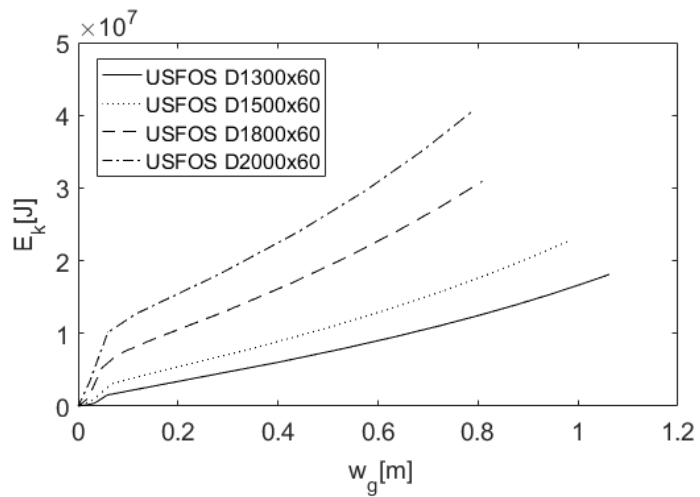
Figure 5-19: Thickness influence in the absorbed energy against global displacement for $D=1.8\text{m}$ and 2.0m



(a)

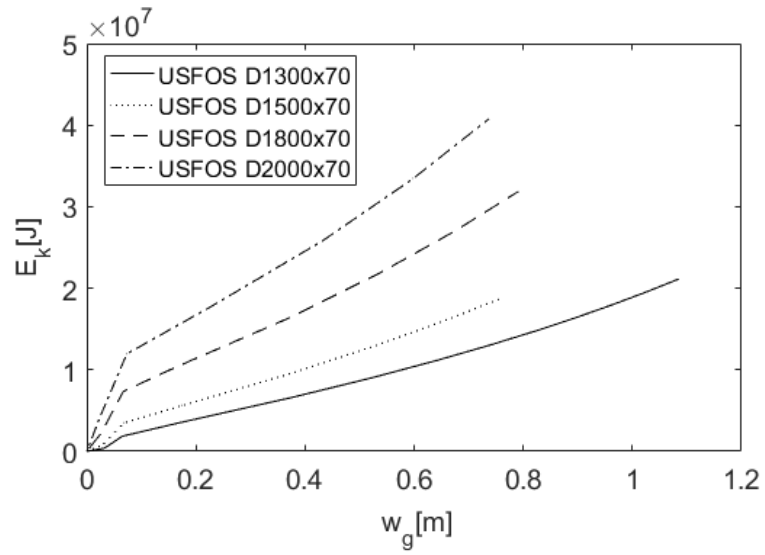


(b)

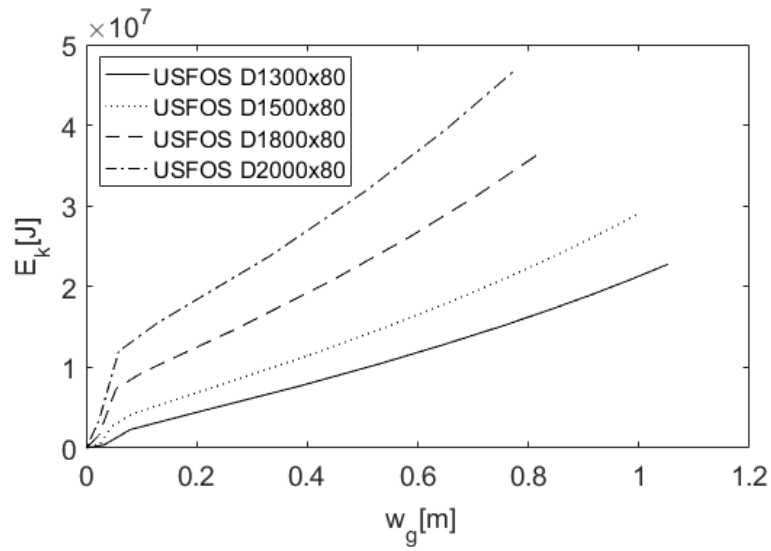


(c)

Figure 5-20: Diameter influence in the absorbed energy against global displacement for $t=40\text{mm}$, 50mm and 60mm



(a)



(b)

Figure 5-21: Diameter influence in the absorbed energy against global displacement for $t=70\text{mm}$ and 80mm

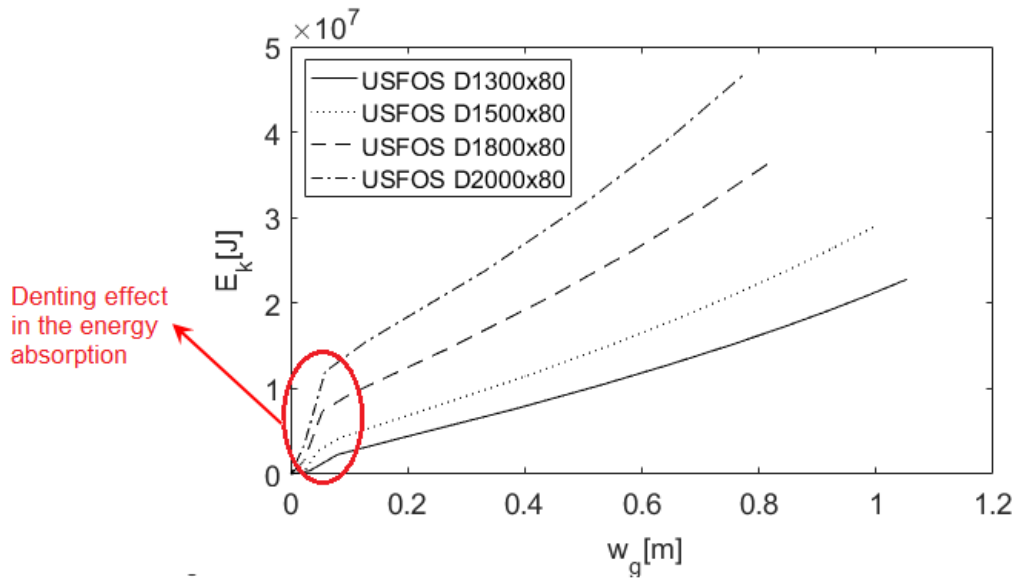


Figure 5-22: Denting effect in the energy absorption of the steel leg

Comparison with experimental tests

A comparison of the force-deformation relationship from (Norsok Standard N-004, 2013) and the numerical test from USFOS are made with the results from Jones et al. (1992). It is found that denting for experimental results are more correlated for D/t ratios between 21 to 40. Ratios of $D/t=11$ and 60 are very scattered in the graphs. For a better understanding of the results reported by Jones et al., the findings have been divide into two figures, Fig.5-24 and fig.5-23, where the former illustrates the comparison for ratios $D/t=21, 30$; and the latter the comparison between $D/t 11$ and 60. In the oil and gas industry, jacket legs typically have D/t ratios between 30 and 40. This suggests a good resemblance between the experimental tests and the force-deformation relationships provided by the guidelines, especially for ratios 21, 30 and 40, as most of the tests are located around the curves.

Figure 5-25 shows the normalized global deflection against the normalized impact energy of the experimental test ($D/t=21, 30$ and 40), and the numerical tests in USFOS with similar ratios. The results are in general in good agreement, being the ratio 30 the most similar to the numerical test.

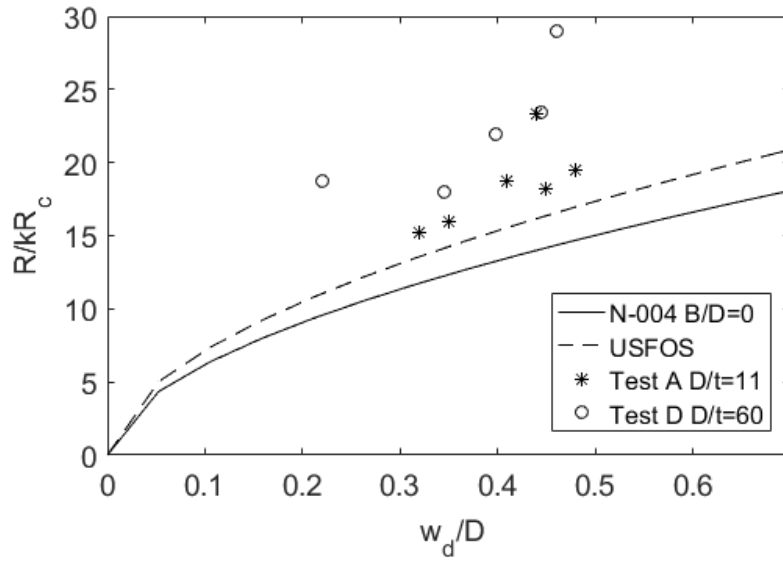


Figure 5-23: Comparison test results from Jones et al. (1992) $D/t=11$ and 60 with N-004 for local denting.

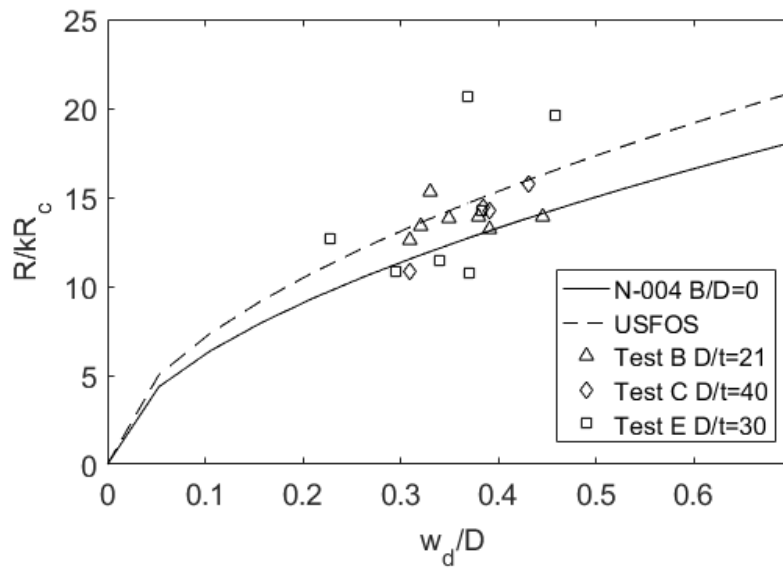
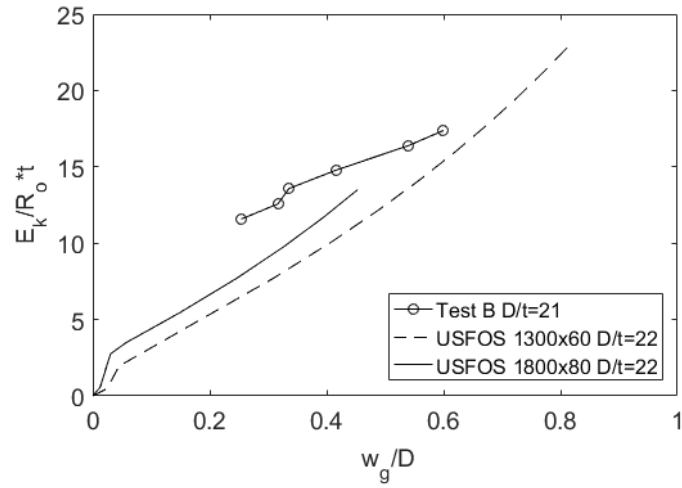
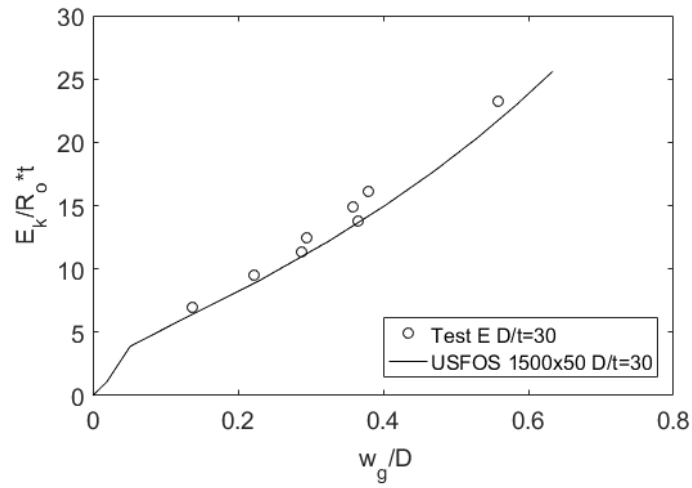


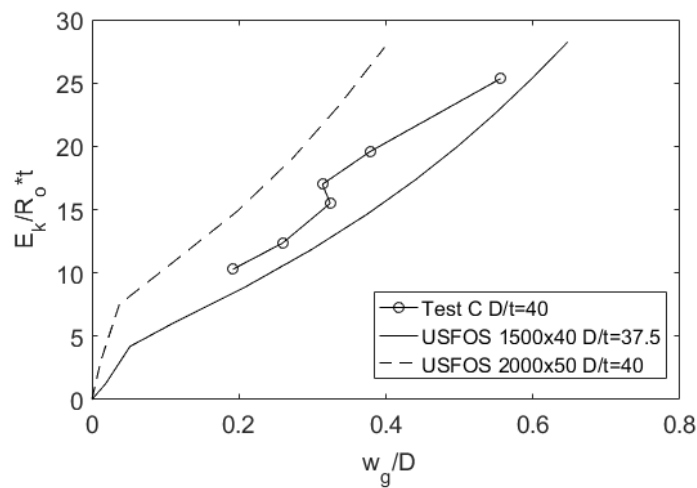
Figure 5-24: Comparison test results from Jones et al. (1992) $D/t=21$, 30 and 40 with N-004 for local denting.



(a) $D/t=21$



(b) $D/t=30$



(c) $D/t=40$

Figure 5-25: Comparison test results (Jonnes et al.) with USFOS for Non-dimensional Impact Energy-vs-Non-dimensional global displacement

5.2 Steel grouted legs: Parametric study

A similar parametric study is performed in USFOS for grouted legs with two different grout specification, $f'_c = 10$ and 50MPa . Four diameters 1.3m, 1.5m, 1.8m, and 2.0m with constant wall thickness of 40mm, and constant length of 20m are impacted at the mid-span with a point load. The grouted leg is also axially fixed at the ends allowing to the membrane forces to act in the member. The failure criteria is considered when the strain reaches the critical value of 0.15. Table 5-6 shows the grout characteristics used in the USFOS model.

Characteristic	Value/Description
Density, ρ_g [kg/m^3]	2512
Young's Modulus, E_c [GPa]	30
Strength f'_c [MPa]	10, 50

Table 5-6: Mechanical properties for concrete

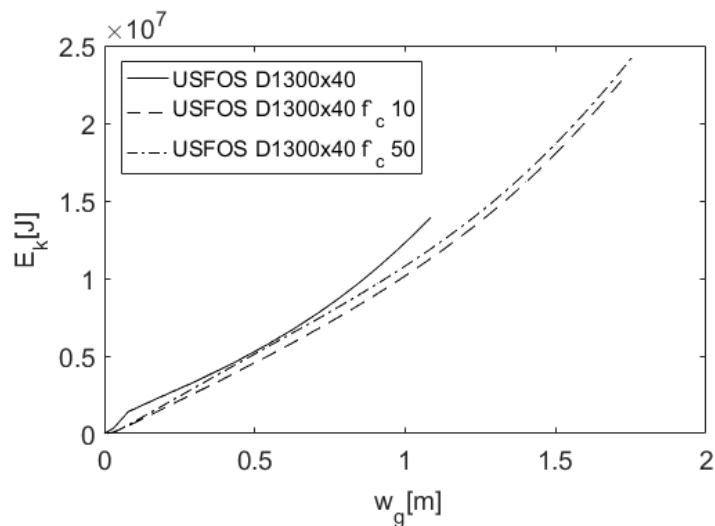
5.2.1 Results and Discussion

The capacity of the grouted members are compared to those without grout. The impact forces, global displacements, and energy absorbed for the members are summarized in Table 5-7.

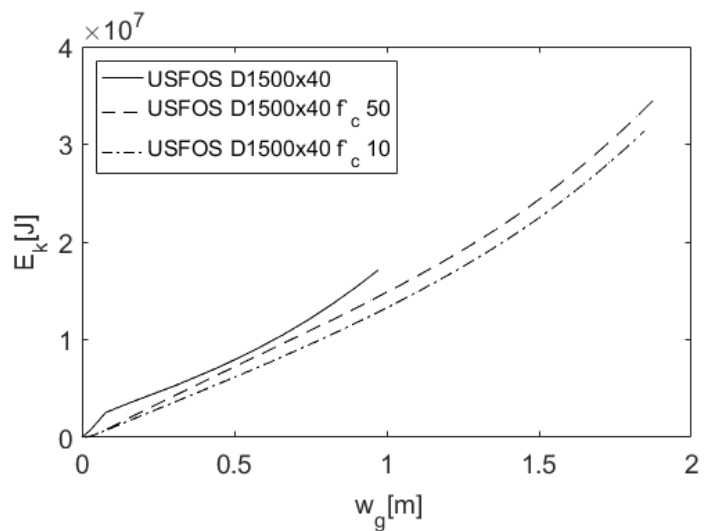
	D1300x40		
	No-grout	Grout f'_c 10 MPa	Grout f'_c 50 MPa
Impact force [MN]	12.59	23.23	24.14
Energy Absorbed [MJ]	13.92	22.74	24.45
Global displacement [m]	1.09	1.72	1.76
	D1500x40		
	No-grout	Grout f'_c 10 MPa	Grout f'_c 50 MPa
Impact force [MN]	14.60	29.18	31.56
Energy Absorbed [MJ]	17.10	31.35	34.85
Global displacement [m]	0.97	1.84	1.885
	D1800x40		
	No-grout	Grout f'_c 10 MPa	Grout f'_c 50 MPa
Impact force [MN]	18.43	39.00	40.10
Energy Absorbed [MJ]	24.74	47.53	50.00
Global displacement [m]	0.83	1.99	1.92
	D2000x40		
	No-grout	Grout f'_c 10 MPa	Grout f'_c 50 MPa
Impact force [MN]	21.75	44.82	38.30
Energy Absorbed [MJ]	33.07	50.10	50.10
Global displacement [m]	0.78	1.63	1.65

Table 5-7: Summary results for steel legs with grout $f'_c=10$ MPa and 50 MPa

From Table 5-7 it is possible to see an increment in the energy absorption of 63.3%, 83.3%, 92.1%, and 51.5% for 1.3m, 1.5m, 1.8m and 2.0m diameters respectively, in legs with grout $f'_c = 10\text{Mpa}$ and legs without it. However, there is not a large difference between the capacity for legs with grout of 10 Mpa and 50Mpa. An increment of 7%, 11.16%, 5.2% and 0% was observed for 1.3m, 1.5m, 1.8m and 2.0m diameters, respectively. This is in agreement with the findings from Han et al. (2014), where the concrete strength shows little influence in the impact forces, and midspan lateral deflections of the members. The increase of capacity of grouted members is achieved by the additional stiffness, and compressive strength during the bending of the leg.

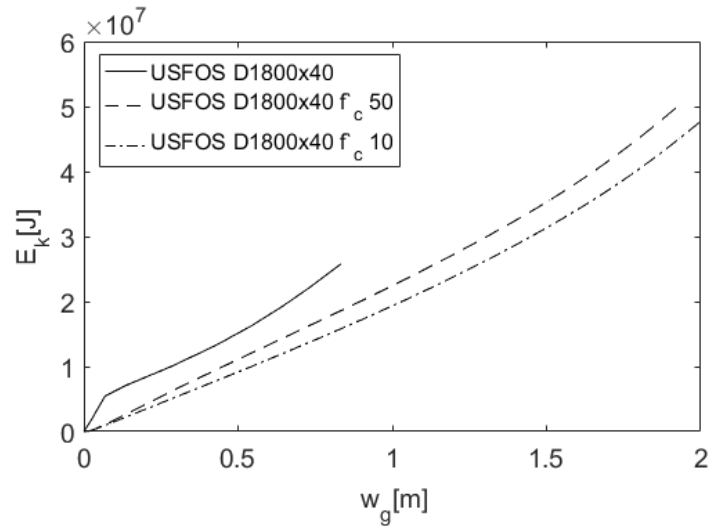


(a)

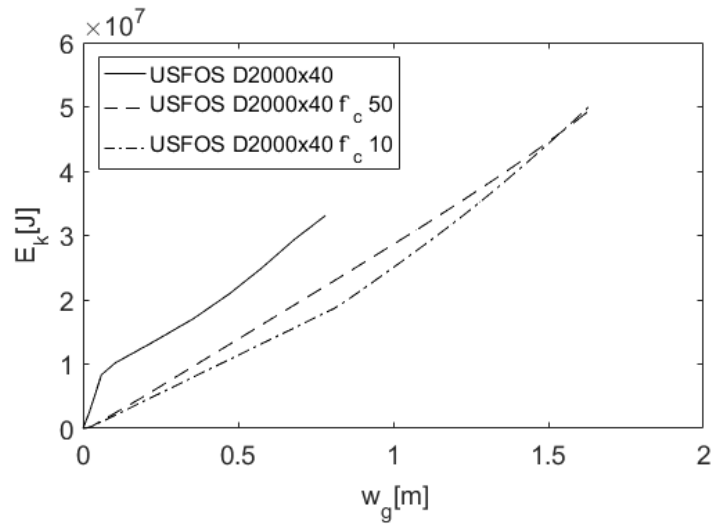


(b)

Figure 5-26: Grout influence in the Energy absorbed -vs- Global lateral displacement for $D=1.3\text{m}$ and 1.5m



(a)



(b)

Figure 5-27: Grout influence in the Energy absorbed -vs- Global lateral displacement for $D=1.8\text{m}$ and 2.0m

Figures 5-26 and 5-27 illustrate the energy absorbed against the global displacement of the legs with grout and without it. Here, the denting phenomenon (steeped part of the curve) is only visible for steel tubes without grout, as the numerical model does not allow denting in the grouted member under lateral impact load. However, leg with 1.3m diameter follows similar relationship as the grouted leg, given that, this leg cannot take much denting before it collapses in bending.

Plastic utilization factors of the grouted legs are shown in Figures 5-28 and 5-29.

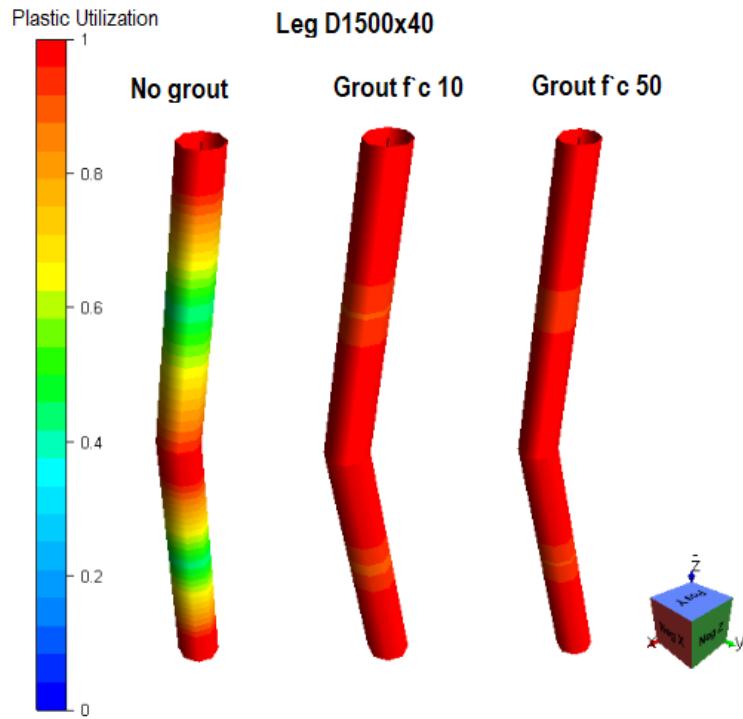
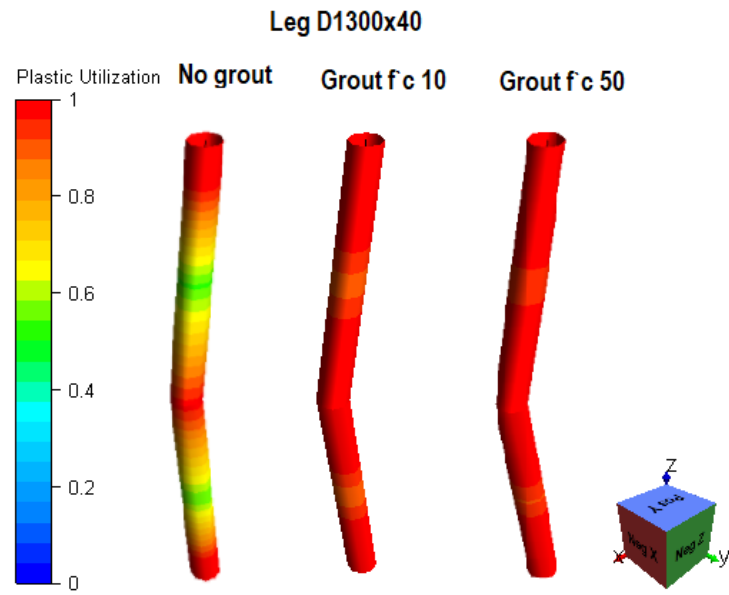
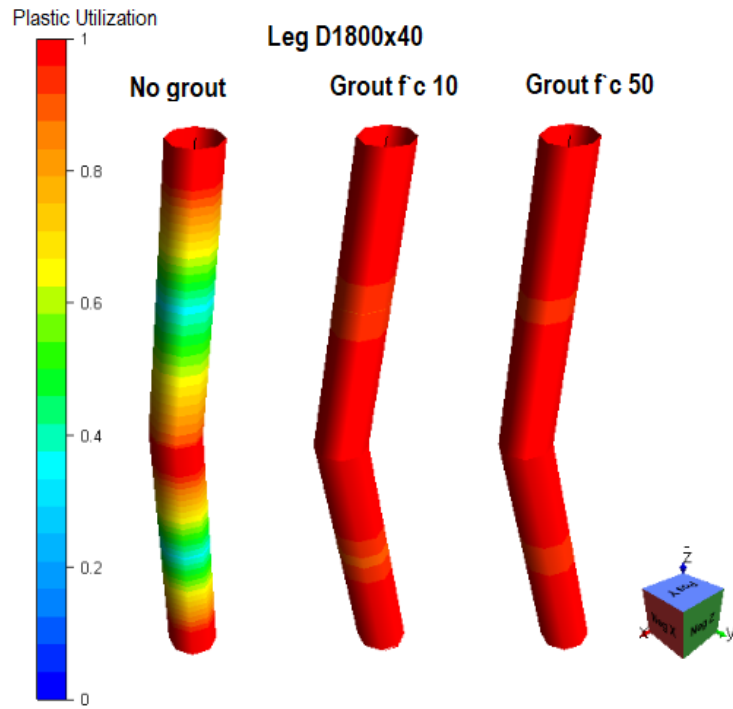
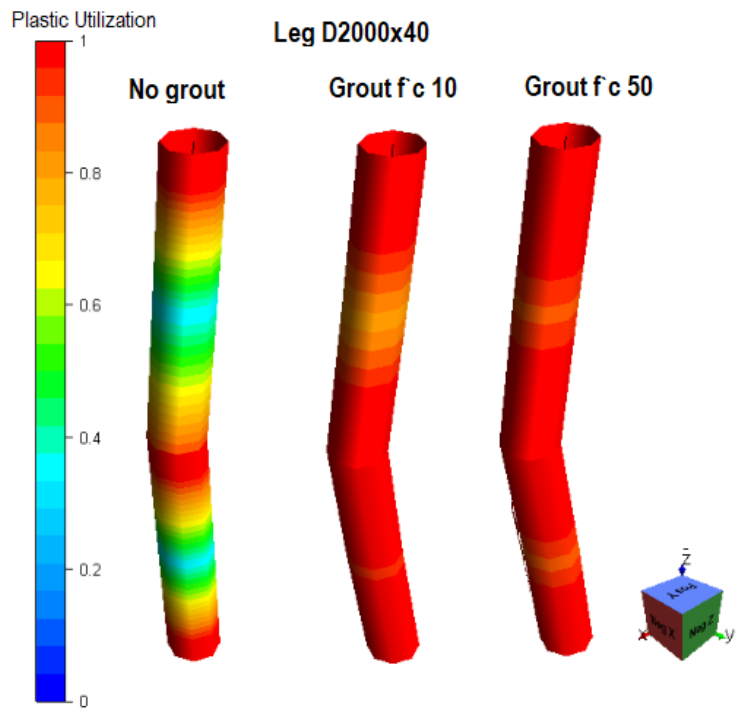


Figure 5-28: Utilization factor of the legs without grout and grout $f'_c = 10$ MPa and 50 MPa for $D = 1.3$ m and 1.5 m



(a)



(b)

Figure 5-29: Utilization factor of the legs without grout and grout $f'c= 10$ MPa and 50 MPa for $D=1.8\text{m}$ and 2.0m

Comparison with experimental tests

A wide range of experimental tests have been done for grouted legs, as these type of composite members are very useful in piers of bridges that can also be subjected to ship collisions. In the oil and gas industry, the use of composite members is limited by the marine operations, and the possibility to grout the legs in offshore/onshore. Nevertheless, some steel jacket platforms are grouted in the impact zone as an improvement of the structure. A comparison with experimental results from 4 different sources, Han et al. (2014), Deng et al. (2011), Wang et al. (2013) and Shakir et al. (2016) is done and presented in Figure 5-30. The impact energy is normalized against the plastic collapse load for the composite member (R_{oc} , see section 3.3). All experimental results are for boundary conditions where the beams were clamped, except for Deng et al. (2011) where the beam was pinned in both ends, for this particular case, the plastic collapse load was taken as $R_{oc} = 4M_{pc}/L$.

Good agreement was found between the numerical tests and the experimental results. The experimental tests are dispersed just above and over the curve lines from the USFOS model. The most dispersed results are from Wang et al. for the test with $D=114\text{mm}$ and $t=3.5\text{mm}$. This indicates, that USFOS is capable to predict the behavior of the composite member.

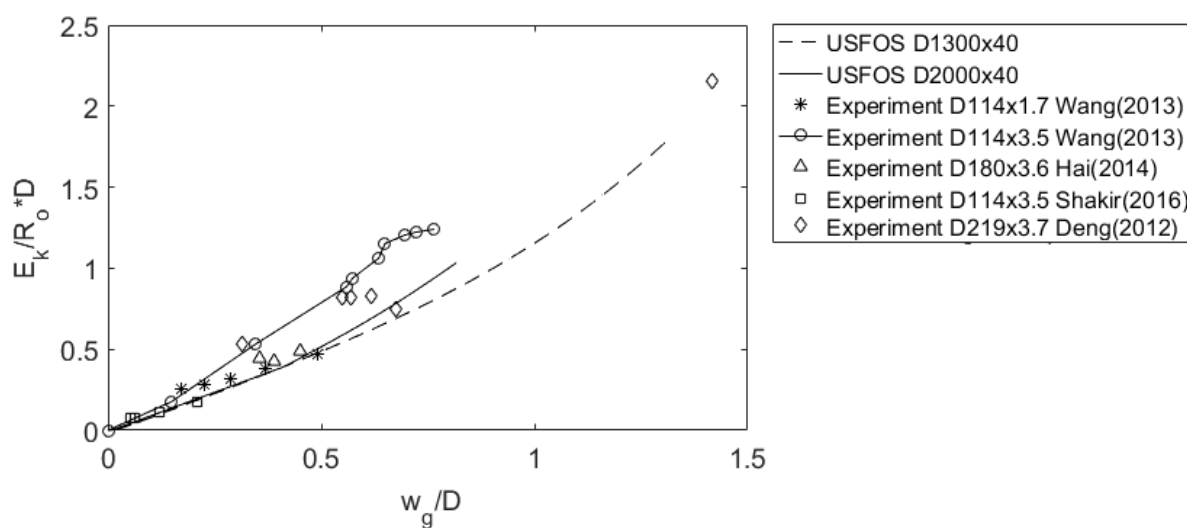


Figure 5-30: Comparison of experimental test with numerical tests in USFOS for lateral impact and global displacement of grouted legs

6 Ship Impact Analyses of Jacket Platforms

Two platforms have been subjected to boat impact analyses and carried out in USFOS. The platforms denominated as Platform A and Platform B are steel jackets with four legs, their members capacity (brace/leg) is determined by implementing a quasi-static analysis, with an impact energy of 50MJ for bow collision, this with the aim of deciding the maximum capacity of the platforms.

6.1 Platforms geometry

Platform A

Platform A is 92m high and with a water depth of 70m. This platform has a bracing perimeter filled with concrete. In Figure 6-31, the geometry of the platform is presented with the grouted bracing at elevation +10m, and the jacket legs between -12m and +16m elevations. This platform has been checked in two ways, with and without grouted members to register the increase in the capacity due to the concrete in legs and braces. The principal frames have a configuration of K-braces between plan levels and diamond braces at the plan levels. Table 6-8 summaries the mechanical properties and material data used in the analysis.

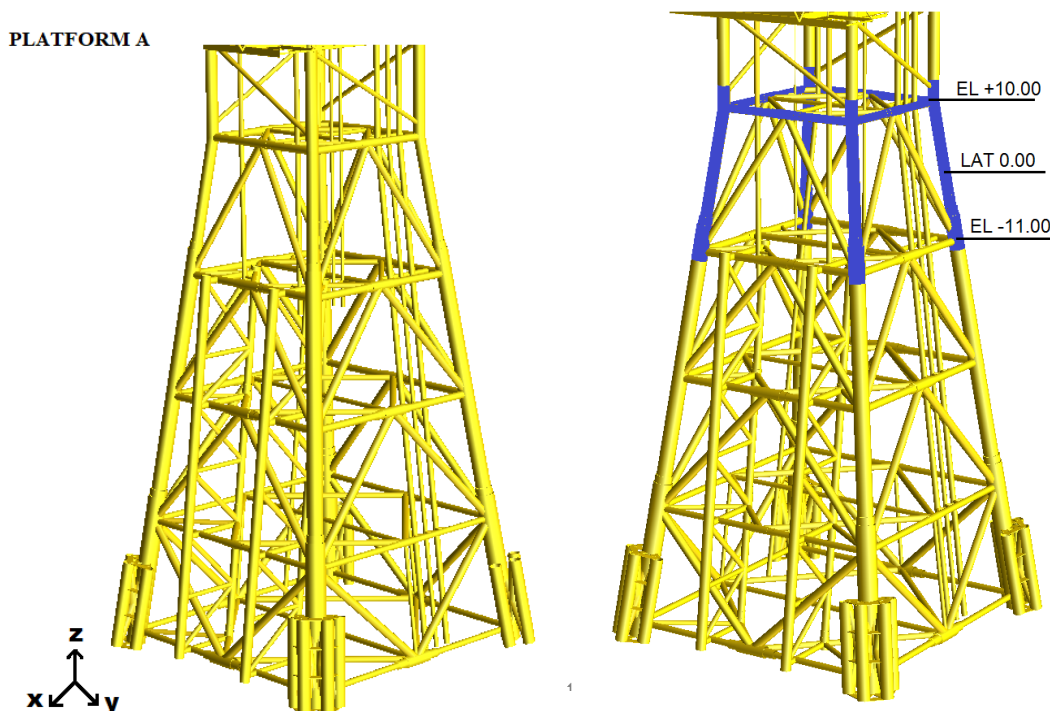


Figure 6-31: Overview Platform A

Characteristic	Value/Description
Density steel, ρ_y [kg/m^3]	7850
Young's Modulus steel, E_c [GPa]	210
Density concrete, ρ_y [kg/m^3]	2512
Young's Modulus concrete, E_c [GPa]	30
Characteristic cube strength concrete f_c [MPa]	10.3
Yield strength f_y [MPa]	340 , Topside, $t \leq 40mm$ 340 , Jacket, $t \leq 40mm$ 325 , Piles, $t \leq 63mm$

Table 6-8: General Mechanical properties of Platform A

Platform B

Platform B has a height of 94.2m and a water depth of approximate 69m. This platform is under development, and it was originally designed without grout, but for the purposes of this thesis, it has been checked based on two scenarios: with its originals sections, and with a reduction in the wall thickness in the area of impact and filled with grout. Same specification of concrete than in Platform A has been used for the second scenario.

Figure 6-32 presents the geometry of Platform B, the principal frames have a configuration of X-braces between plan levels until elevation -13.00m, K-braces from elevation +10.00m to elevation +22.00m, and X-braces at the plan levels. Table 6-9 summaries the mechanical properties and material data used in both scenarios.

Characteristic	Value/Description
Density steel, ρ_y [kg/m^3]	7850
Young's Modulus steel, E_c [GPa]	210
Density concrete, ρ_y [kg/m^3]	2512
Young's Modulus concrete, E_c [GPa]	30
Characteristic cube strength concrete f_c [MPa]	10.3
Yield strength f_y [MPa]	355

Table 6-9: General Mechanical properties of Platform B

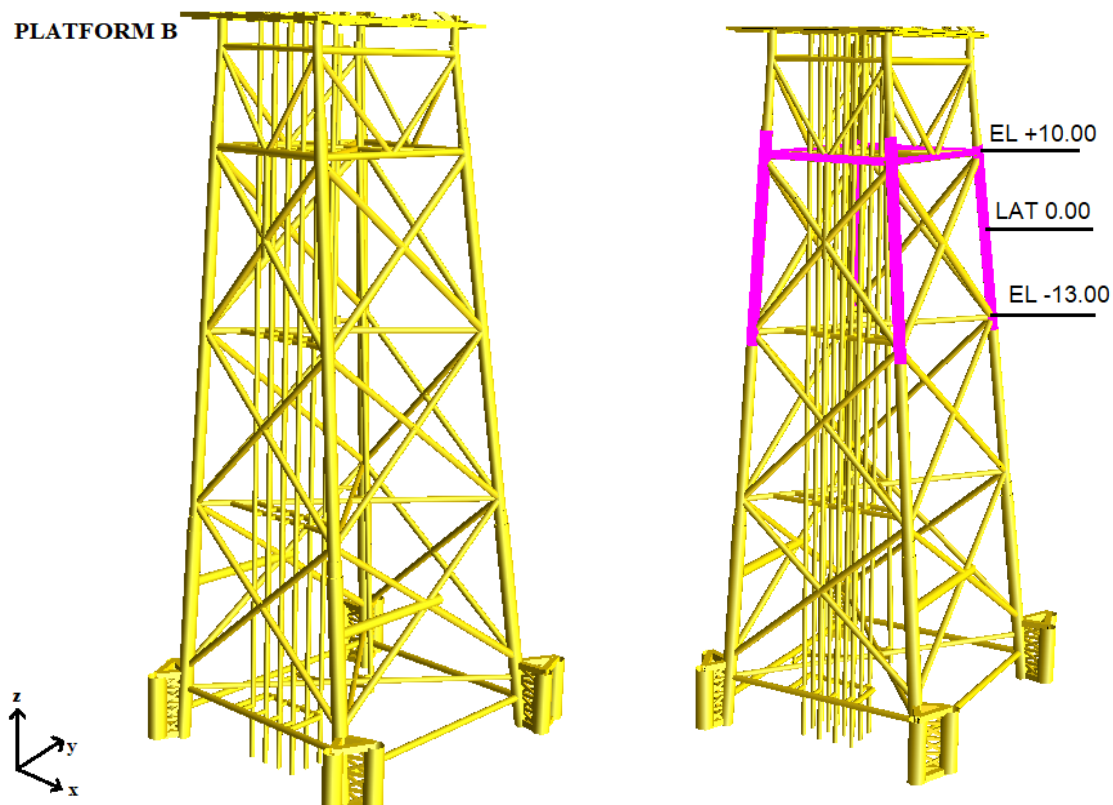


Figure 6-32: Overview Platform B

6.2 Impact loading scenarios

The impact loading scenarios for Platform A are shown in Figure 6-33, given its symmetry only one side of the platform has been considered, and five scenarios are investigated for joints and midspan legs/braces.

Figure 6-34 illustrates the impact loading scenarios for Platform B. The side where the risers are closer to the steel members is chosen, given that their proximity constitute a limitation in the boat impact analysis.

The failure criteria in the member is selected according to the design principles mentioned in the guidelines. In other words, failure occurs when the joint fails, the strain reaches a value of 0.15 or when the dent in the member is 50% of the section diameter.

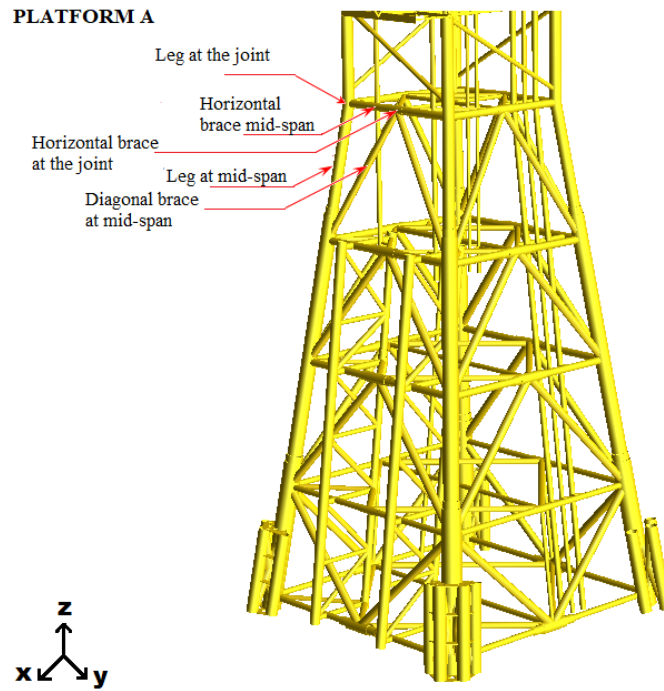


Figure 6-33: Boat impact scenarios for Platform A

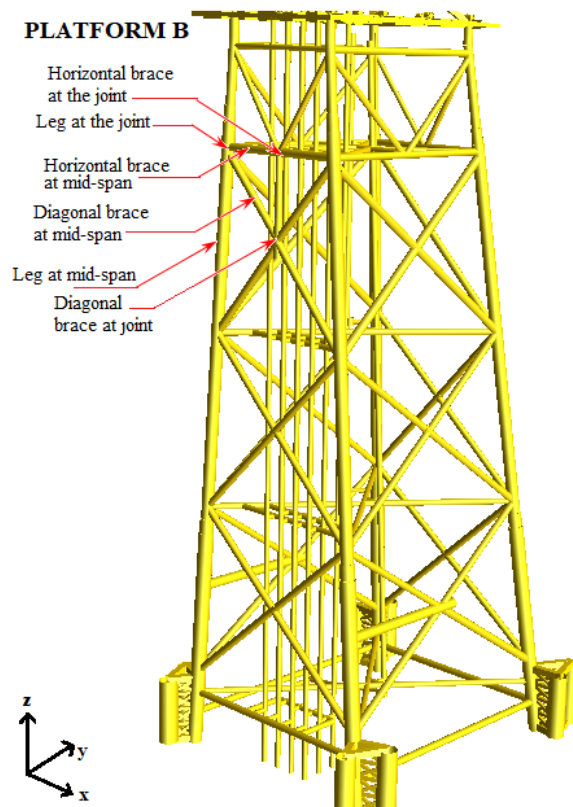


Figure 6-34: Boat impact scenarios for Platform B

6.3 Impact analysis Platform A

Platform A has been checked against impact boat with grout and without it in the zone of collision. The simplified method provided by the guidelines, is also used for comparison of the capacity of the members when they are not grouted. Annex 10.1 illustrates the procedure followed for the horizontal brace, in order to find the impact force, the global displacement, local dent, and the total energy absorbed by the member.

6.3.1 Results and Discussion Platform A

Table 6-10 presents a summary of the energies absorbed by the members, and the failure criteria selected in each impact scenario. The diagonal brace is not grouted in the platform, and it is only checked without grout, as for the joint in the horizontal brace, the only scenario considered is with grout. A detailed analysis and results are given further on this section.

Grouted Members		
Impact Location	Energy absorbed	Failure criteria
Mid-span leg	27.54 MJ	Joint failure
Joint leg	50.00 MJ	Strain
Mid-span diagonal brace	-	-
Mid-span horizontal brace	22.00 MJ	Strain
Joint horizontal brace	32.50 MJ	Strain
No-Grouted Members		
Impact Location	Energy absorbed	Failure criteria
Mid-span leg	8.06 MJ	Dent<0.5D
Joint leg	22.00 MJ	Dent<0.5D
Mid-span diagonal brace	12.13 MJ	Strain
Mid-span horizontal brace	4.92 MJ	Dent<0.5D
Joint horizontal brace	-	-

Table 6-10: Summary of energies absorbed by members in platform A

Impact with Leg

Two impact scenarios have been considered: an impact load at the upper joint of the leg and an impact load at mid-span. A maximum energy of 50MJ (bow impact) has been imposed to the leg with grout and without grout to determine the effect of the concrete in the capacity of the member. The leg has a diameter of 1.8m, with 42mm thickness and 15m free span. The free span is considered where the can sleeve ends. The leg is loaded with 30MN in compression due to the permanent and functional loads from the topside.

The leg capacity has been checked without grout, in order to compare it with the simplified method provided by Norsok Standard N-004 and Veritas DNV-RP-C204. Figure 6-35 shows the comparison of the impact energy against the global displacement for the leg with and without grout when the impact load is applied at mid-span. The red line in the curve represents the maximum energy absorption when the denting criteria of $0.5D$ is taken into account. This is expected as the leg resistance to denting R_c is very low compared to the expected plastic collapse load R_o . Figure 6-36 depicts a contrast between the simplified method and the results from USFOS regarding the impact force against the global displacement of the leg. From the figure is possible to see that the collapse load, that is noted by the last triangular marked in the figure, it is close to the plastic collapse load from the formulas presented in section 4.

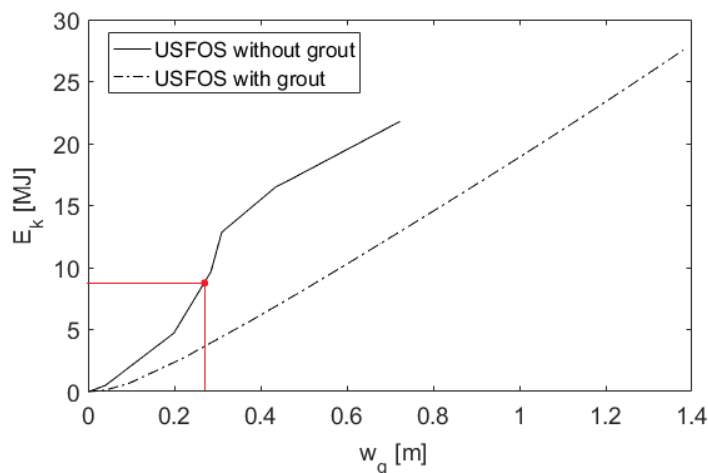


Figure 6-35: Comparison of impact energy against the global displacement, for the leg with grout and without it

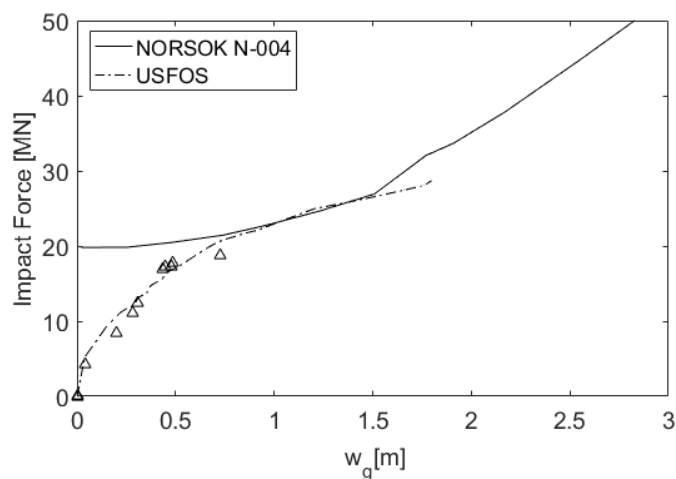


Figure 6-36: Comparison of Simplified Method and USFOS of the impact force against the global displacement

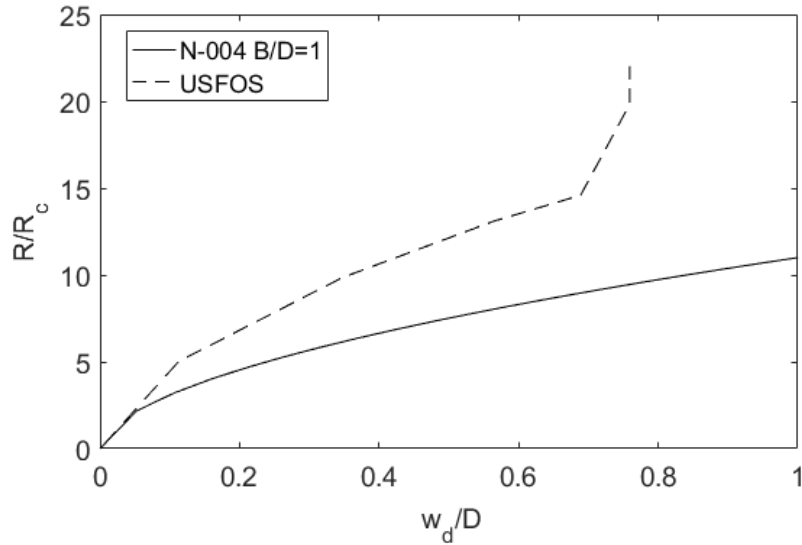


Figure 6-37: Comparison of Simplified Method and USFOS of the non-dimensional impact force against non-dimensional dent

The maximum impact force in the leg is 18.77 MN, and a total energy dissipation of 22 MJ. From this, 10 MJ are dissipated from the structure with a global displacement of 0.78 m. Due to denting, the leg is capable to absorb 12.27 MJ with 1.30 m of dent. This corresponds to more than the $0.5D = 0.86m$ allowed by the standard. The failure criteria is then ruled by the denting, when this criteria is taken into account, the maximum energy dissipated in the leg is 8.06 MJ. Where 2.07 MJ corresponds to the structure and 6.49 MJ as a result of denting absorption.

Figure 6-37 shows the non-dimensional impact force against the non-dimensional dent in the member. The difference between the simplified method and the USFOS could be explained by the membrane effect in the leg.

In the same way, for the grouted leg the maximum impact force is 23.74 MN and total energy dissipation of 27.54 MJ. In other words, this is more than three times compared to 8.06 MJ. The improvement in the capacity of the leg is notorious. However, the leg is not capable of dissipating the 50 MJ bow impact, but very close to 28 MJ broadside and stern impact.

When the impact load is applied at the grouted joint the platform has the ability to dissipate the 50 MJ energy with a maximum global displacement of 0.31 m.

The joint without grout can absorb 47.8 MJ with a displacement of 0.58 m. However, the dent in the joint is very large with 1.3 m, when the dent is considered less than $D/2$, the maximum energy absorbed is 22 MJ with a global displacement of 0.22 m. Figure 6-38 depicts the comparison of the impact energy absorbed with grouted joint and without grout, the red line is the maximum energy absorption in the joint under the $0.5D$ denting criteria.

Finally, Figure 6-39 presents the impact force against the global displacement for the grouted joint and the joint without grout.

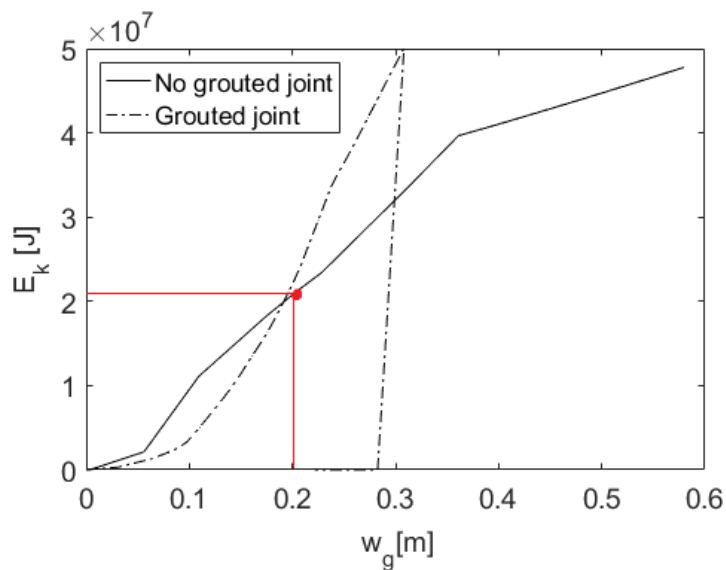


Figure 6-38: Comparison impact energy absorbed against global displacement at the upper-joint of the leg

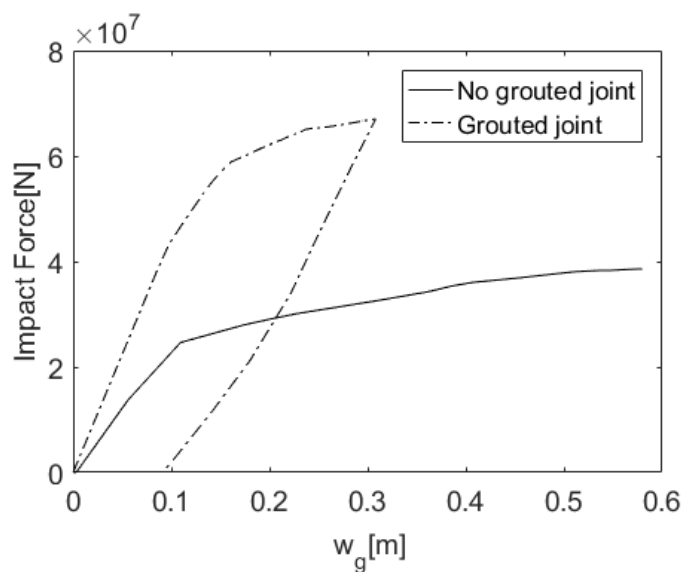


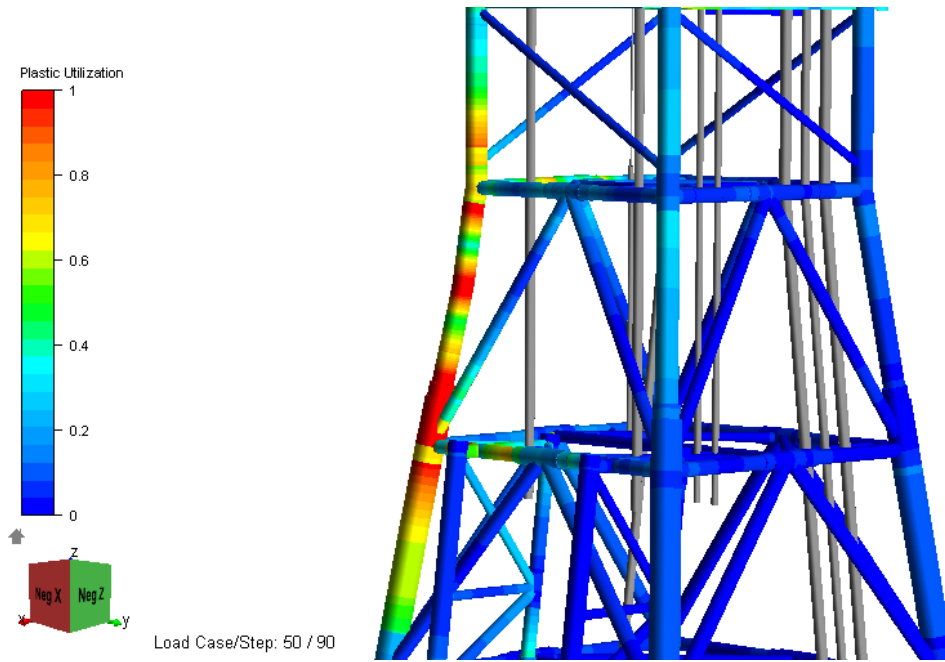
Figure 6-39: Comparison impact force against global displacement at the upper-joint of the leg

Table 6-11 shows the summary of the results for the impact boat with and without the denting criteria. Here, it is also presented the values obtained when the joint check command in USFOS is omitted. An increase in the capacity is observed, given that the number of iterations inside the program are reduced to evaluate the joint.

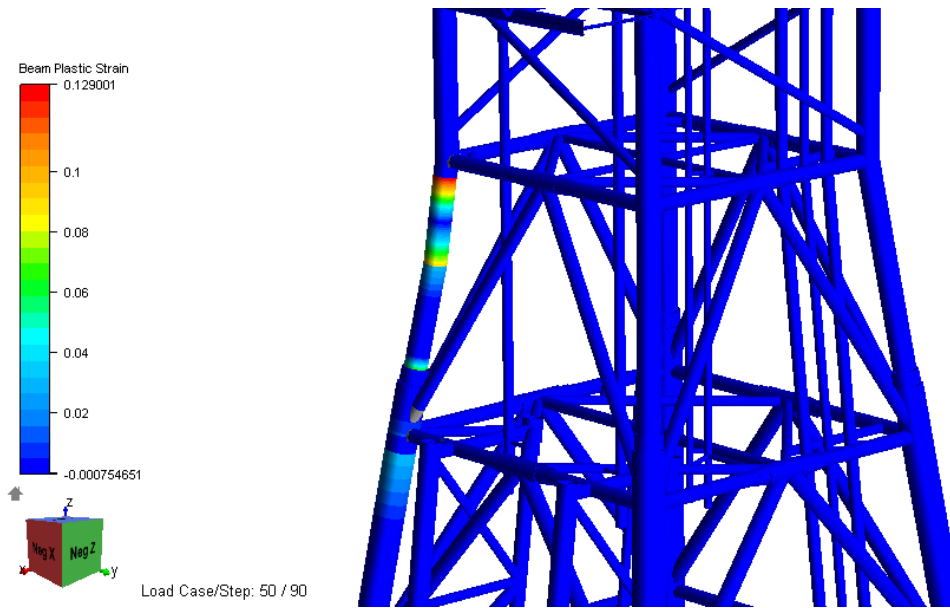
Boat Impact against Leg at mid-span					
	With grout		Without grout		Simplified Method
	Joint check	No-Joint check	Joint check	No-Joint check	
Impact force [MN]	23.74	30.85	18.77	22.45	19.57
Energy structure [MJ]	27.54	50.00	10.00	14.7	5.68
Energy dent [MJ]	-	-	12.27	13.43	3.73
Total Energy [MJ]	27.54	50.00	22.00	28.17	9.42
Global displacement [m]	1.38	2.00	0.78	0.95	0.29
Dent [m]	-	-	1.30	1.30	0.86
Energy absorption considering dent criteria Dent<D/2					
Energy structure [MJ]	-	-	2.07	2.71	5.68
Energy dent [MJ]	-	-	6.49	6.49	3.73
Total Energy [MJ]	-	-	8.06	9.20	9.42
Global displacement [m]	-	-	0.28	0.30	0.29
Dent [m]	-	-	0.87	0.87	0.86
Boat Impact against Leg at upper-joint					
	With grout		Without grout		
	Joint check	No-Joint check	Joint check	No-Joint check	
Impact force [MN]	67.00	38.61			
Energy structure [MJ]	50.00	17.80			
Energy dent [MJ]	-	30.00			
Total Energy [MJ]	50.00	47.80			
Global displacement [m]	0.31	0.58			
Dent [m]		1.30			
Energy absorption considering dent criteria Dent<D/2					
Energy structure [MJ]		8.00			
Energy dent [MJ]		14.00			
Total Energy [MJ]		22.00			
Global displacement [m]		0.218			
Dent [m]		0.87			

Table 6-11: Summary results for leg in platform A

In addition, Figures **6-40** and **6-41** present the plastic utilization and strain distribution of the members under the boat impact at the mid-span of the leg, while Figures **6-42** and **6-43** display the same, but with a boat impact at the upper joint of the leg.

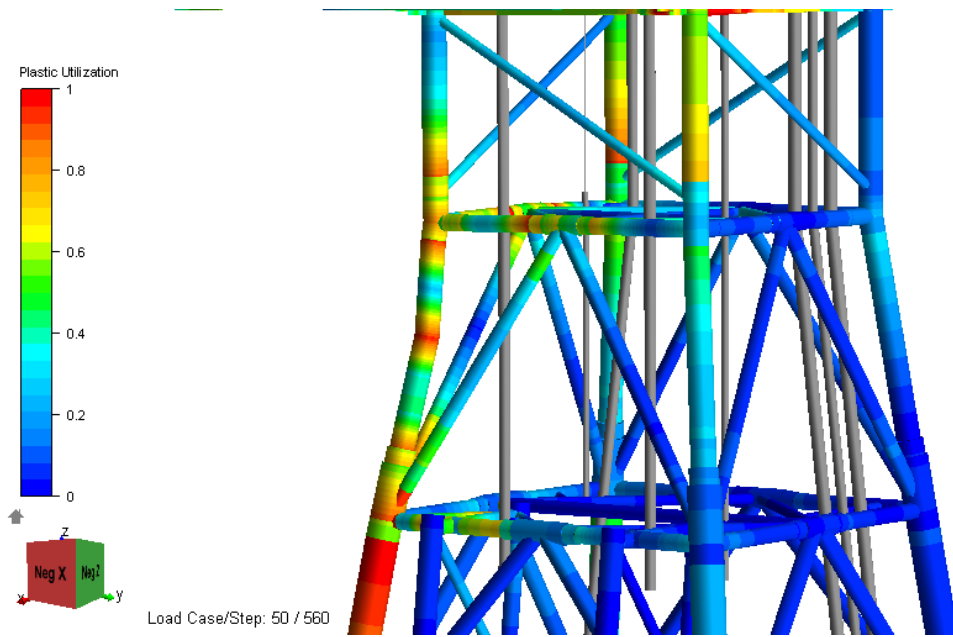


(a) Plastic Utilization

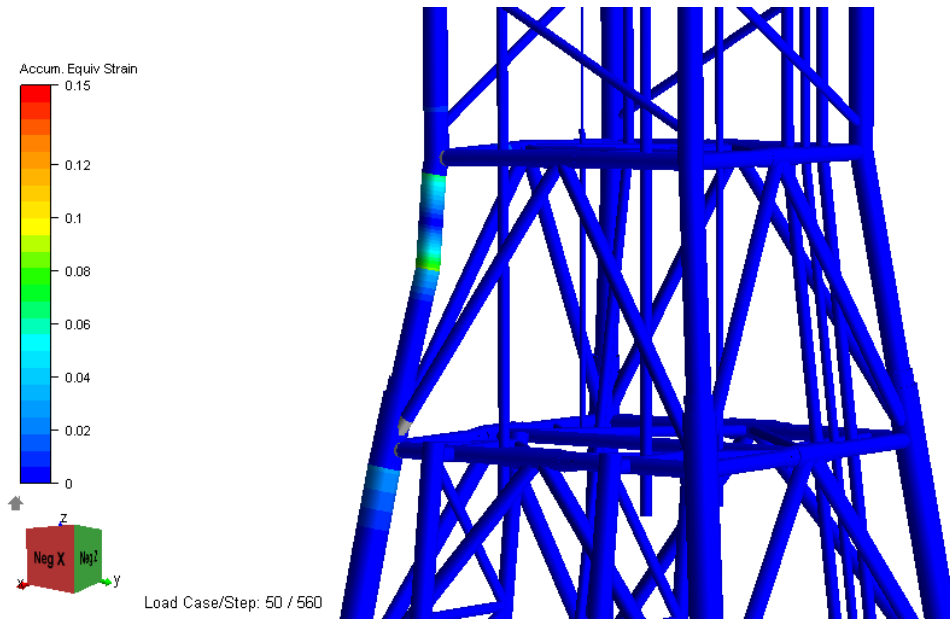


(b) Beam Strain

Figure 6-40: Plastic Utilization factor and Strain distributions for leg without grout under boat impact (mid-span)

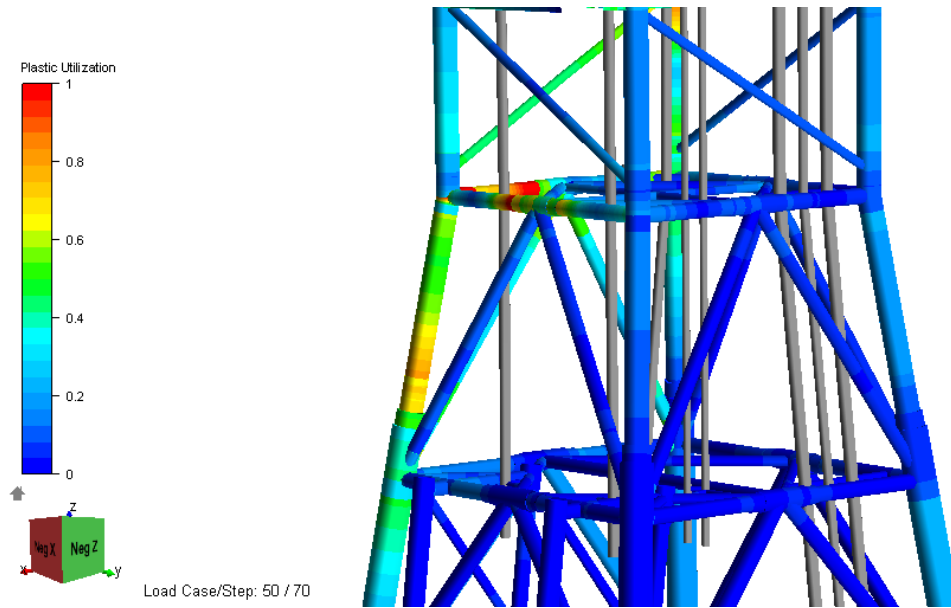


(a) Plastic Utilization

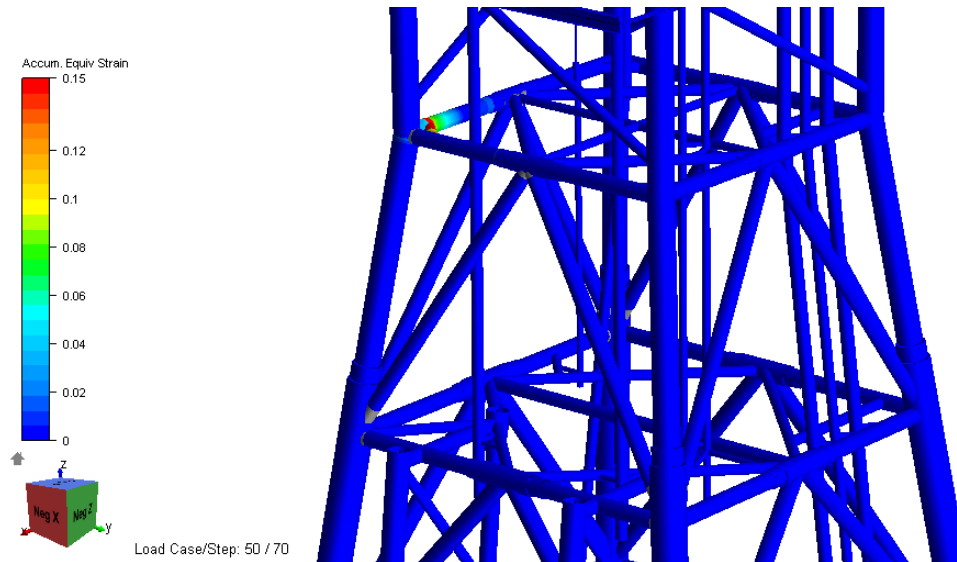


(b) Beam Strain

Figure 6-41: Plastic utilization factor and strain distributions for leg with grout under boat impact (mid-span)

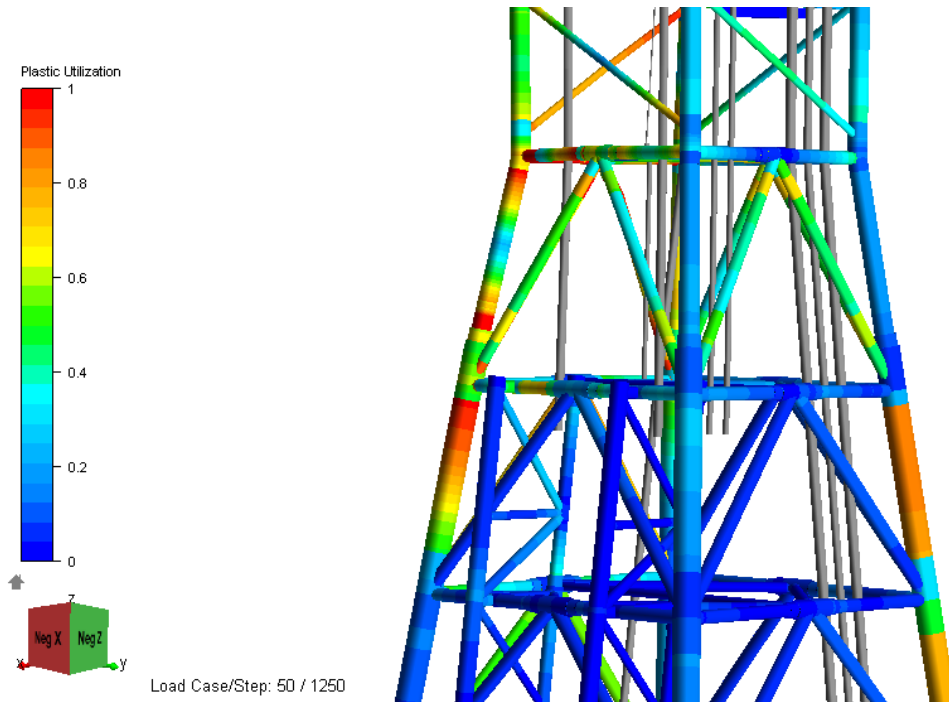


(a) Plastic Utilization

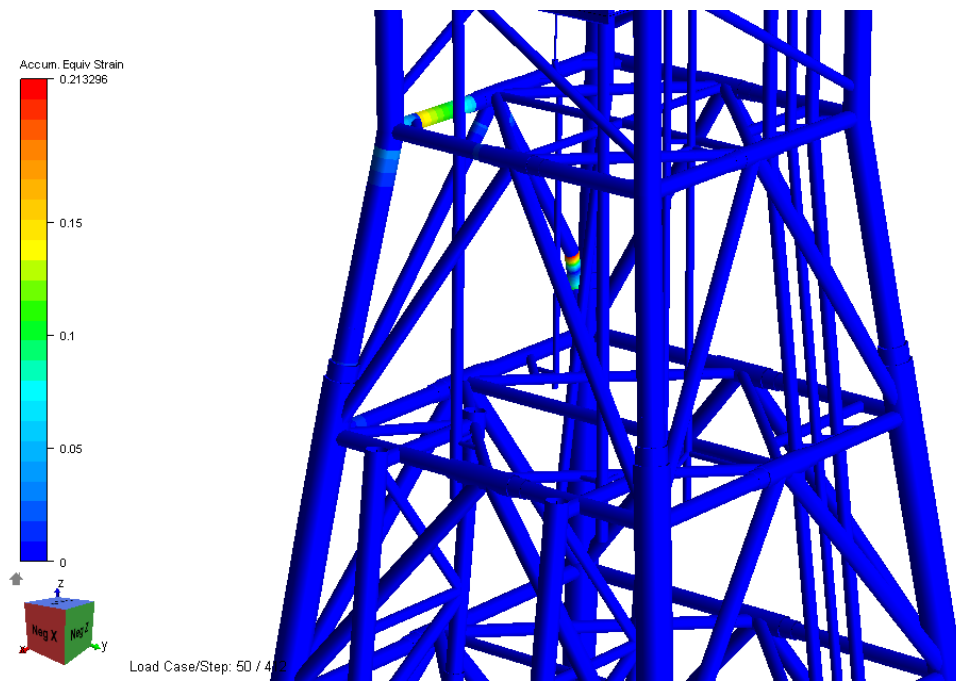


(b) Beam Strain

Figure 6-42: Plastic utilization factor and strain distributions for leg without grout under boat impact (upper joint)



(a) Plastic Utilization



(b) Beam Strain

Figure 6-43: Plastic utilization factor and strain distributions for grouted leg under boat impact (upper joint)

Impact with Diagonal Brace

The diagonal brace is 18 m long, and it has a diameter of 1.10 m with 40mm thickness. Table 6-12 summaries the results of the impact boat at the middle of the span. The maximum impact force in the brace corresponds to 10.27 MN, the global displacement is 1.69m and a total dissipation energy of 12.13 MJ. The brace has little capacity of dissipate energy by denting as only 11% of the total energy is equivalent to dent. Moreover, when the joint check is not performed, a small increase in the capacity is registered, from 12.13 MJ to 18.00 MJ in the energy absorbed.

	Boat Impact against diagonal brace at mid-span		
	Joint check	No-joint check	Simplified Method
Impact force [MN]	10.27	13.10	10.98
Energy structure [MJ]	10.75	15.9	9.48
Energy dent [MJ]	1.38	2.10	2.00
Total Energy [MJ]	12.13	18.00	11.46
Global displacement [m]	1.69	1.80	0.86
Dent [m]	0.18	0.25	0.26

Table 6-12: Summary results for diagonal brace in platform A

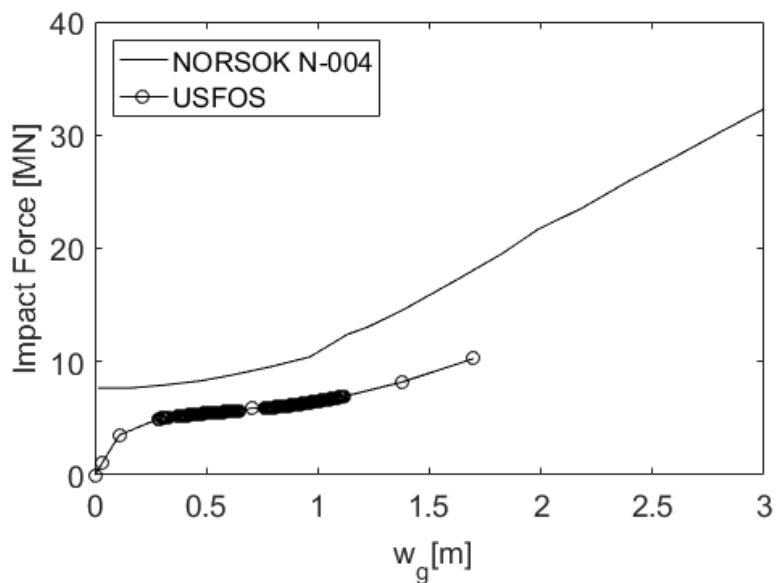


Figure 6-44: Comparison of Simplified Method and USFOS of the impact force against global displacement for diagonal brace

Figure 6-44 depicts a comparison between the simplified method and the USFOS results for the impact force against the global displacement. The figure shows a lower collapse

load than the plastic collapse load, the reason is that the denting reduces the plastic moment capacity of the member, and starts bending at a lower impact force. However, the maximum impact force estimated by simplified method is only 6.9% greater than the impact force predicted by the USFOS analysis.

Figure 6-45 illustrates the denting of the brace compared to the Norsok Standard N-004. The brace is in tension before the collision, meaning that the brace will be more resistant to denting as expected by the force-deformation relationship from the guidelines. Furthermore, the membrane effect in the member plays an important role in the resistance to dent.

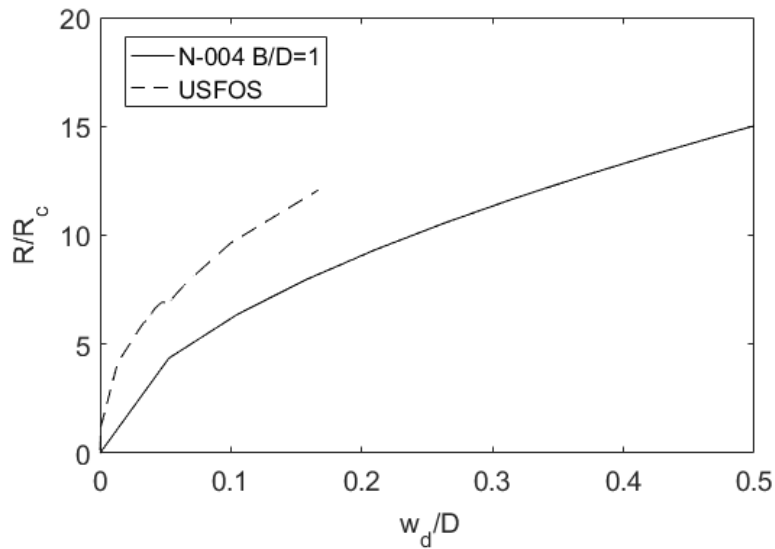
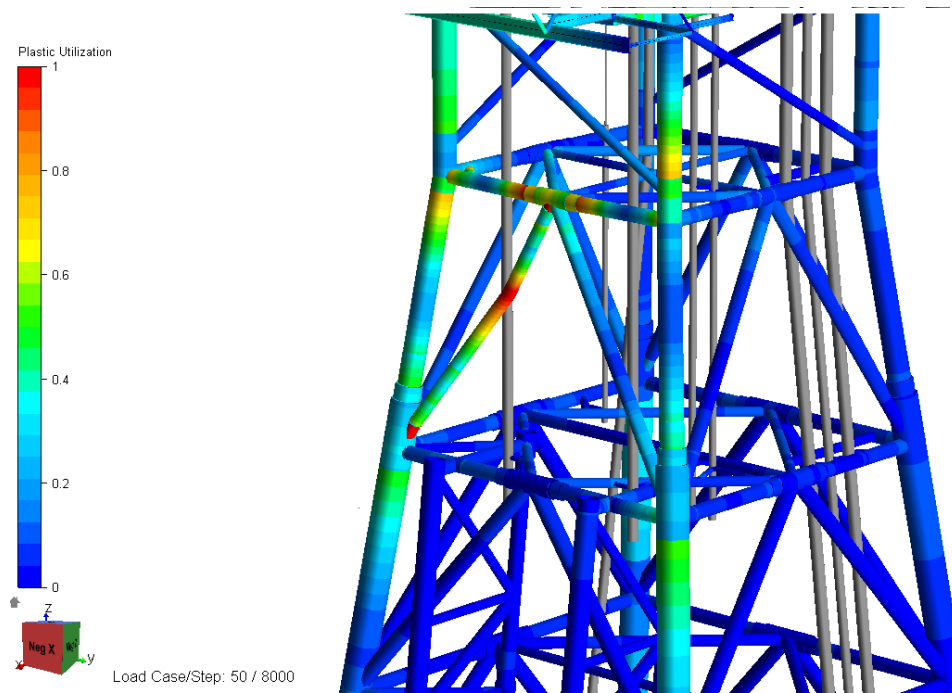
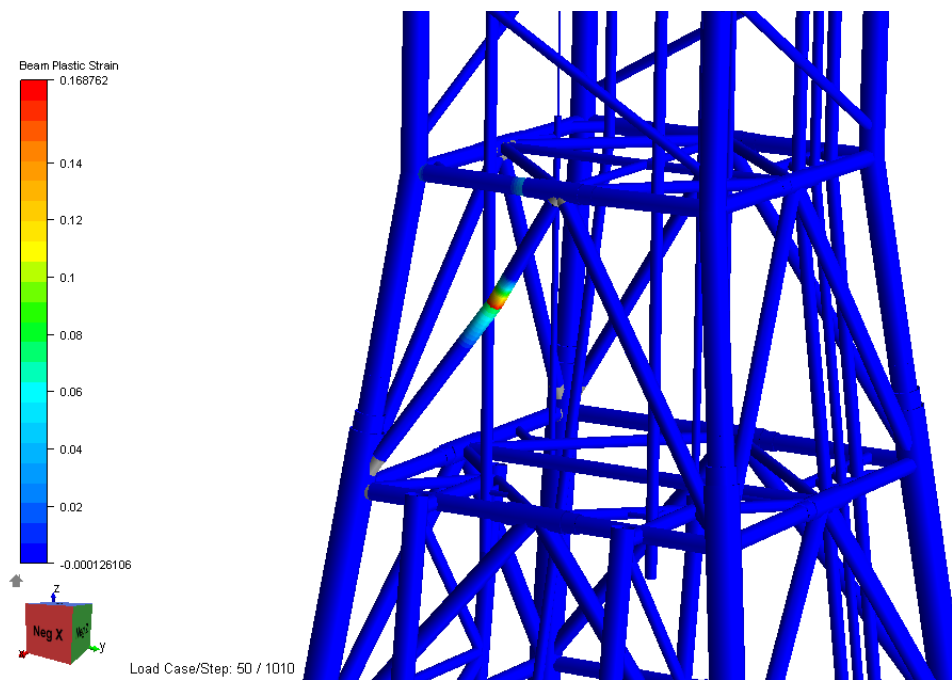


Figure 6-45: Comparison of Simplified Method and USFOS of the impact force against dent for diagonal brace

Figure 6-46 presents the plastic utilization and strain distribution in the brace. It can be noticed that the failure in the member occurs when the strain reaches the critical value of 0.15 in the middle of the span.



(a) Plastic Utilization



(b) Beam strain

Figure 6-46: Plastic utilization factor, and strain distribution of the diagonal brace under boat impact

Impact with Horizontal Brace

For the horizontal brace two scenarios have been considered, one impact load at the middle of the span, and another one at the joint. The horizontal brace has a diameter of 1.2m with 35mm wall thickness and 6m free-span. Annex 10.1 details the application of the guidelines from Veritas DNV-RP-C204 and Norsok Standard N-004, that are referred as the simplified method in this section.

Further, the results are summarized in Table 6-13 indicates that the maximum impact force in the brace without grout is 22.29 MN and with a total energy absorption of 15.5 MJ, while the joint check is not taken into account, the energy absorption is 33.12 MJ, this implies an increase of more than 50%. However, the denting is larger than the allowed by the standard with a dent of 0.87m. Consequently, the maximum total energy absorption that complies with the denting allowance is 4.92 MJ. When the brace is grouted, the total energy absorption is 22 MJ with an impact force 25MN and a global displacement of 0.67m.

Boat Impact against horizontal brace at mid-span					
	With grout		Without grout		Simplified Method
	Joint check	No-Joint check	Joint check	No-Joint check	
Impact force [MN]	25.00	26.95	22.29	27.96	21.54
Energy structure [MJ]	22.00	27.08	8.11	25.71	2.24
Energy dent [MJ]	-	-	7.39	7.41	4.48
Total Energy [MJ]	22.00	27.08	15.5	33.12	6.71
Global displacement [m]	0.67	1.30	0.51	1.20	0.10
Dent [m]	-	-	0.87	0.87	0.60
Energy absorption considering dent criteria Dent<D/2					
Energy structure [MJ]	-	-	0.65	0.65	2.24
Energy dent [MJ]	-	-	4.28	4.28	4.48
Total Energy [MJ]	-	-	4.92	4.92	6.71
Global displacement [m]	-	-	0.10	0.10	0.10
Dent [m]	-	-	0.60	0.60	0.60
Boat Impact against horizontal brace at the joint					
	Joint check	No-Joint check			
Impact force [MN]	40.51	47.1			
Energy structure [MJ]	32.50	50			
Energy dent [MJ]	-	-			
Global displacement [m]	0.75	1.3			
Dent [m]	-	-			

Table 6-13: Summary results for horizontal brace

Figure 6-47 compares the global displacement against the impact energy between the horizontal brace with and without grout. The red line indicates the maximum energy absorption when the denting criteria is taken into account. Figure 6-49 shows the denting of the member without grout compared to the simplified method from Norsok Standard

N-004. The results from USFOS are very close to the force-deformation relationship from the guidelines. Similar results are also seen in Figure 6-48, that depicts the impact force against the global displacement from USFOS, in comparison with the simplified method.

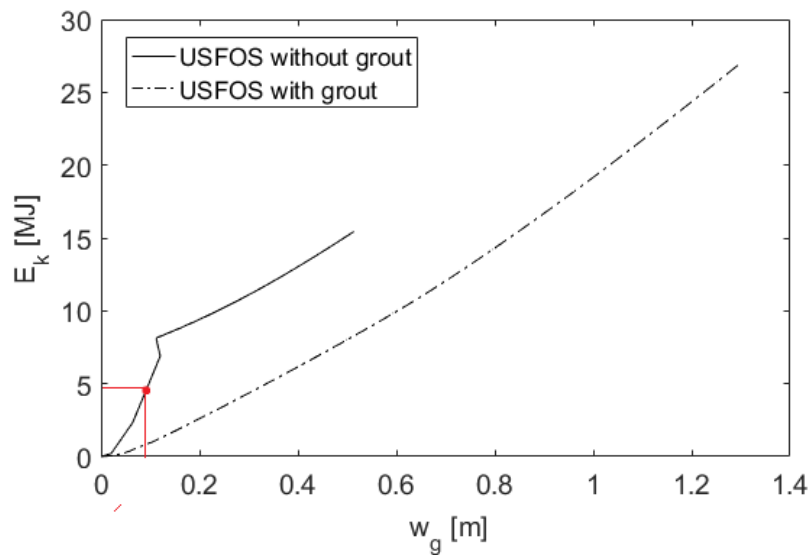


Figure 6-47: Comparison of the impact force against the global displacement, for the horizontal brace with grout and without it -Platform A

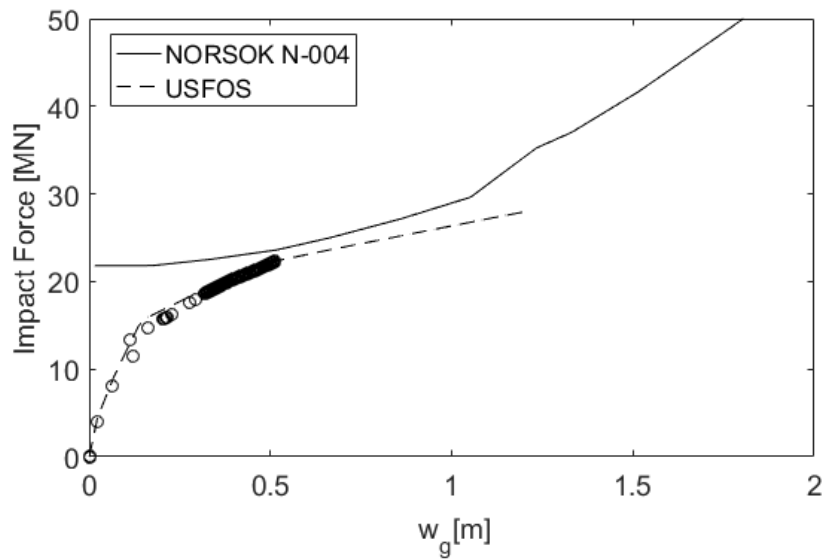


Figure 6-48: Comparison of Simplified Method and USFOS of the impact force against the global displacement, for the horizontal brace without grout - Platform A

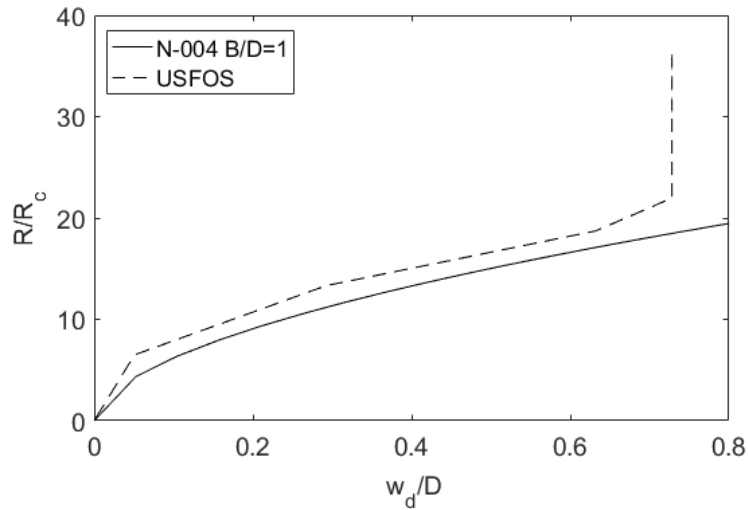


Figure 6-49: Comparison of Simplified Method and USFOS of the non-dimensional impact force against the non-dimensional dent, in the horizontal brace without grout - Platform A

For the scenario of boat impact at the joint of the horizontal brace, only grouted joint has been considered. The maximum impact force is 40.51MN, a lateral displacement of 0.75m, and with a total energy absorption of 32.5MJ. Figure 6-50 presents the global displacement against the impact force in the joint. Figures 6-51 to 6-53 present the plastic utilization, and strain distribution in the horizontal brace impacted at the mid-span and at the joint. When the joint is impacted the failure in the member occurs when it reaches the critical strain of 0.15.

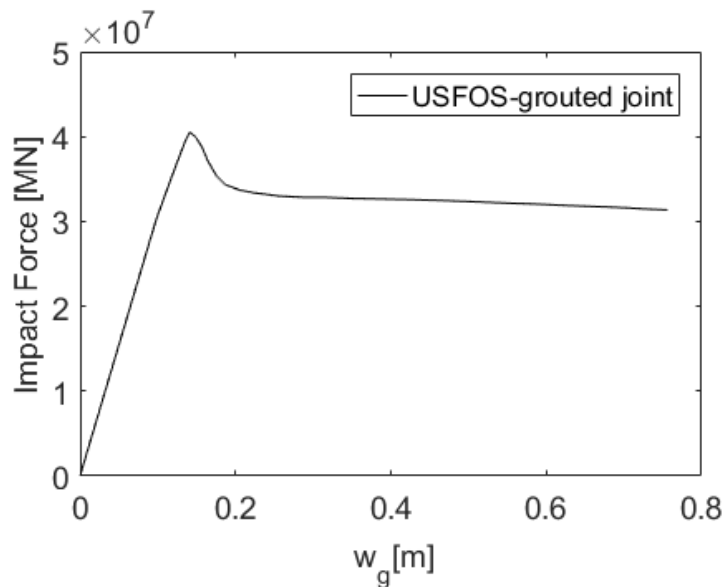
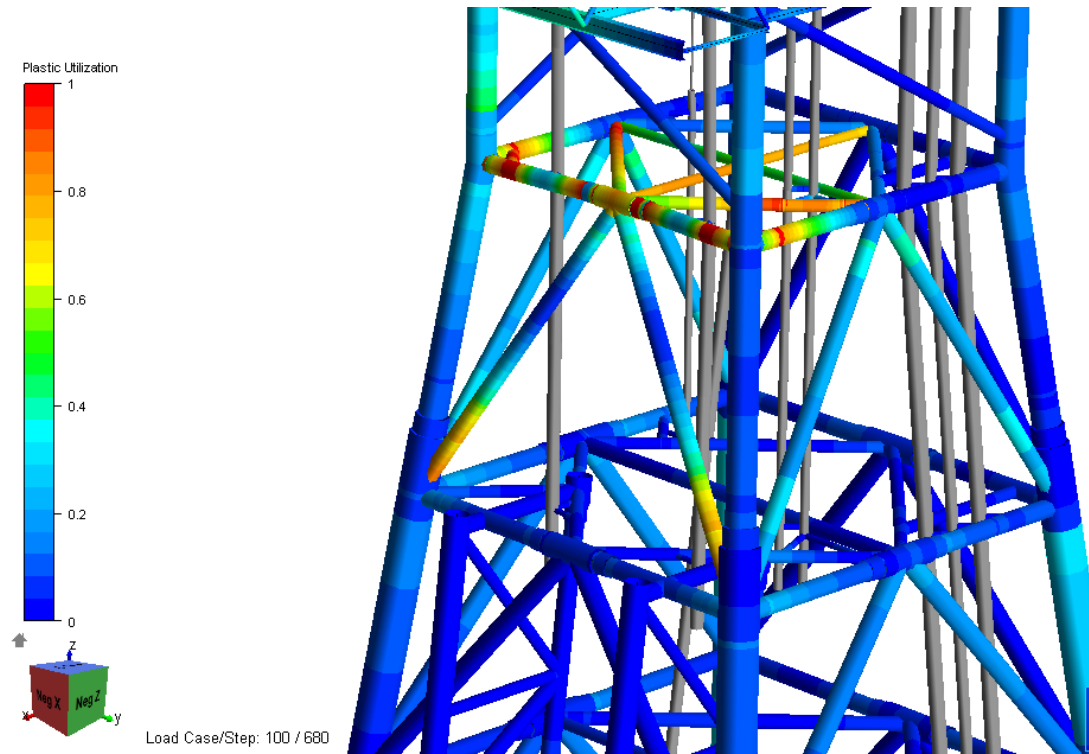
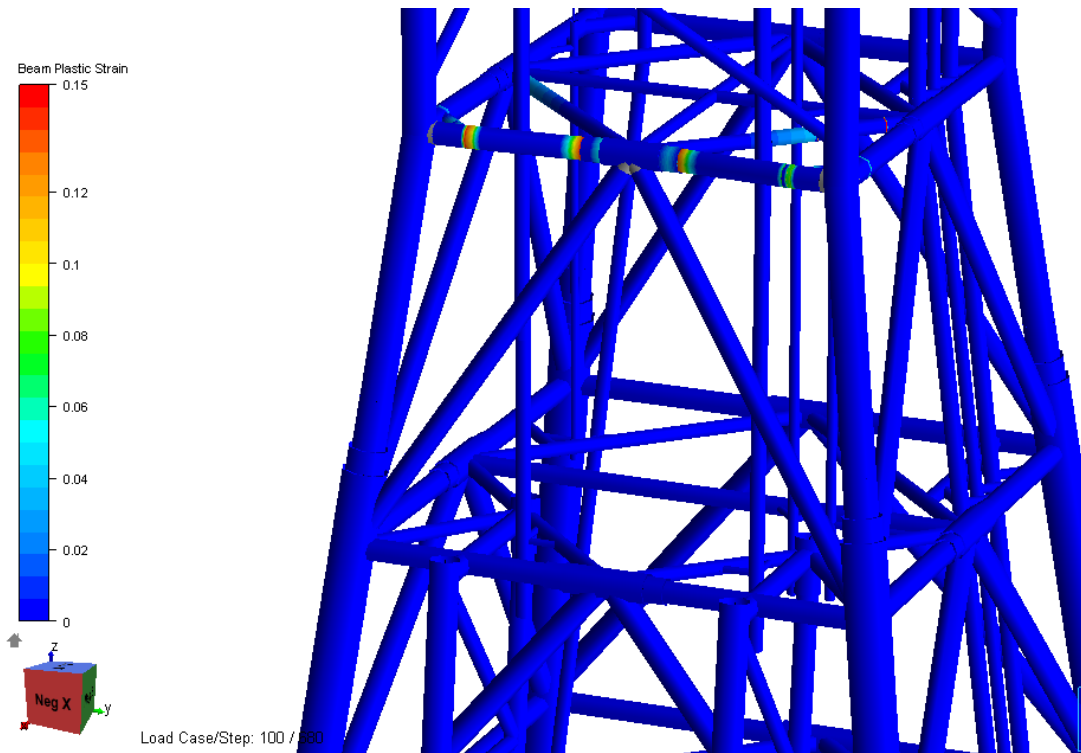


Figure 6-50: Global deformation against the impact force at the joint with grout - Platform A

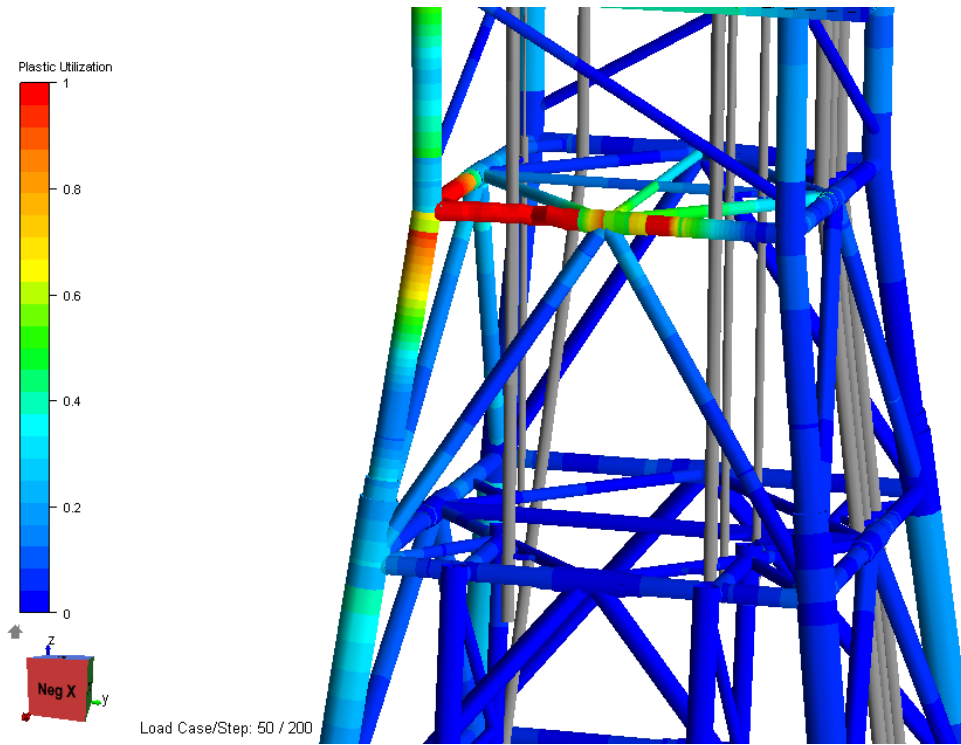


(a) Plastic Utilization

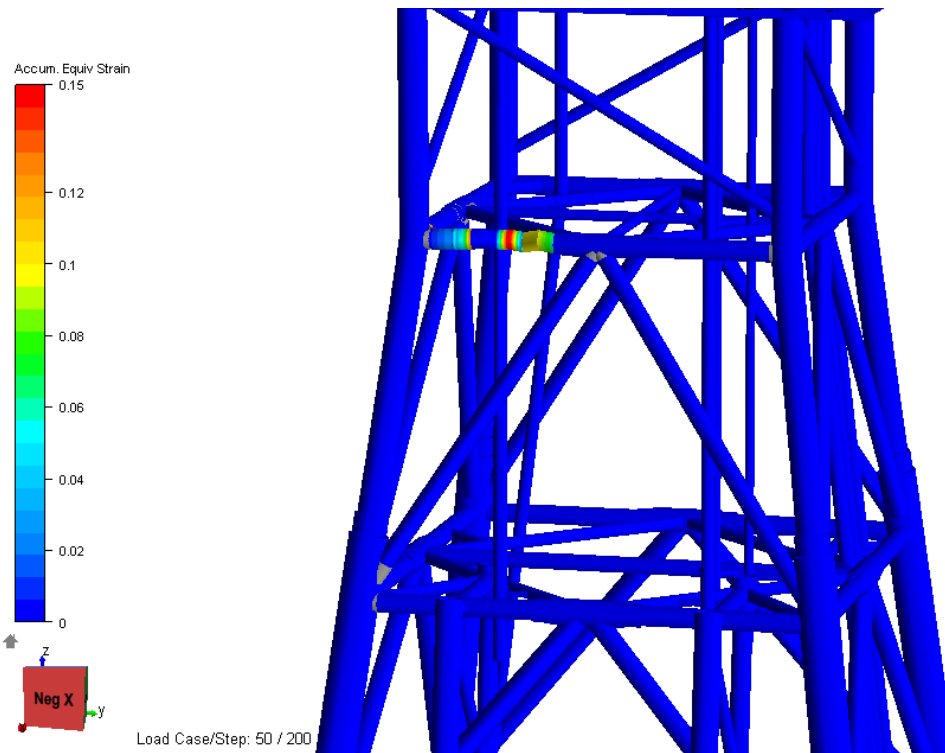


(b) Beam Strain

Figure 6-51: Utilization factor and strain distribution of the horizontal brace, impacted at the grouted joint - Platform A

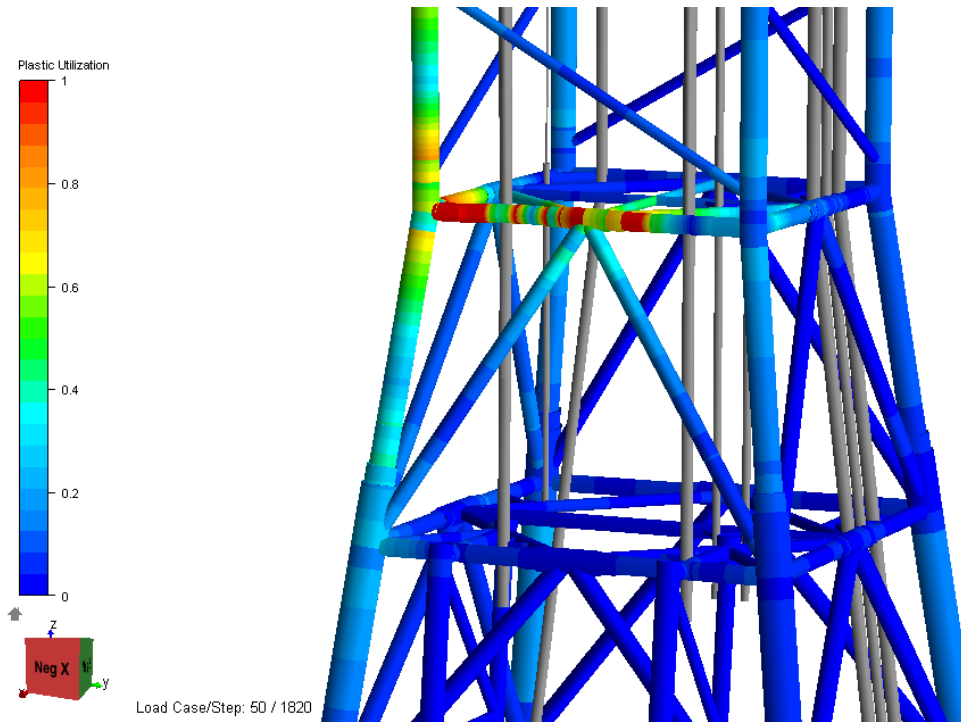


(a) Plastic Utilization

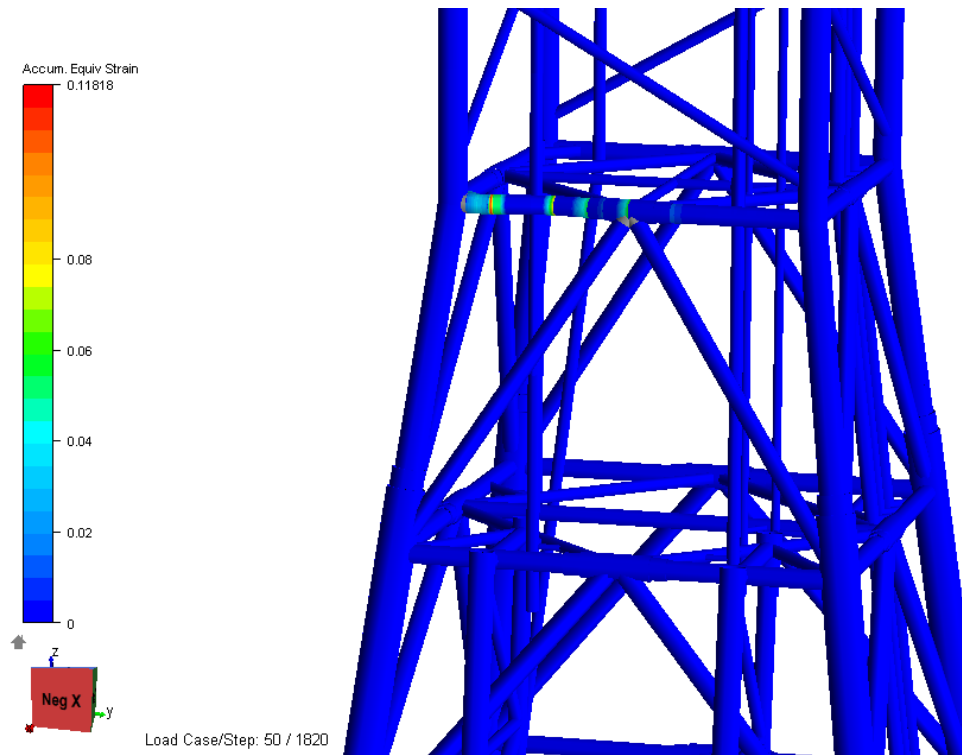


(b) Beam Strain

Figure 6-52: Utilization factor and strain distribution of the grouted horizontal brace, impacted at mid-span - Platform A



(a) Plastic Utilization



(b) Beam strain

Figure 6-53: Utilization factor and strain distribution of the horizontal brace without grout, impacted at mid-span - Platform A

6.4 Impact analysis Platform B

Platform B is a recently designed platform to withstand a large energy collision, and as consequence the wall thickness for legs and braces are very robust, and the members are not grouted. In this section, two impact analyses have been performed: one with its original sections, and another one with grouted members and with a reduction of the wall thickness, to determine the capacity of the members under collision. Both scenarios are compared in terms of global displacement, impact force and impact energy absorption. For this chapter, comparison with the simplified method from Norsok Standard N-004 is omitted. Table 6-14 presents a summary of the sections for leg and braces under the two scenarios. Originally, the ratios D/t are between 17 to 22, whereas, for the grouted members, the ratios D/t have been changed to be between 25 to 35.

Sections	Grouted-reduced members	No Grouted members
Leg [mm]	D1600x45	D1600x72
Leg joint [mm]	D1600x50	D1600x85
Diagonal brace [mm]	-	D995x47
Diagonal brace joint [mm]	-	D1100x65
Horizontal brace [mm]	D1000x35	D1000x45
Horizontal brace joint [mm]	D1000x40	D1000x55

Table 6-14: Summary of leg and braces sections for collision analyses - Platform B

6.4.1 Results and Discussion Platform B

Table 6-15 summaries the results of the boat impact analyses for Platform B, it includes the energies absorbed by the members and the chosen failure criteria. The details of each impact scenario are presented further in this chapter.

Impact Location	Grouted-reduced members	
	Energy absorbed	Failure criteria
Mid-span leg	50.00 MJ	Strain
Joint leg	50.00 MJ	Joint
Mid-span diagonal brace	-	-
X-joint, diagonal brace	-	-
Mid-span horizontal brace	11.00 MJ	Max. lateral displacement 1.4m
Joint horizontal brace	15.00 MJ	Max. lateral displacement 1.4m
Impact Location	No-Grouted Members	
	Energy absorbed	Failure criteria
Mid-span leg	50.00 MJ	Joint
Joint leg	36.00 MJ	Dent<0.5D
Mid-span diagonal brace	21.00 MJ	Strain
X-joint, diagonal brace	23.15 MJ	Joint
Mid-span horizontal brace	17.30 MJ	Max. lateral displacement 1.4m
Joint horizontal brace	21.69 MJ	Max. lateral displacement 1.4m

Table 6-15: Summary of energies absorbed by members in platform B

Impact with Leg

The original section of the leg has a diameter of 1.6m and a wall thickness of 72mm; moreover, when the leg is grouted the wall thickness is changed to 45mm. Two impact scenarios have been considered: an impact load at the upper joint of the leg and an impact load at mid-span. Table **6-16** summaries the results of the impact analyses; yet, only the cases when the joint check command has been employed are reported. The maximum impact force at mid-span for the leg without grout is 28.55MN, the lateral displacement is 1.84m and impact energy absorption is 50MJ. Similarly, the dent deformation is 0.43m and the denting energy corresponds to 9.00MJ.

Boat Impact against Leg at mid-span		
	With grout	Without grout
Impact force [MN]	18.84	28.55
Energy structure [MJ]	50.00	41.00
Energy dent [MJ]	-	9.00
Total Energy [MJ]	50.00	50.00
Global displacement [m]	2.50	1.84
Dent [m]	-	0.43
Boat Impact against Leg at upper-joint		
	With grout	Without grout
Impact force [MN]	35.00	38.61
Energy structure [MJ]	50.00	10.61
Energy dent [MJ]	-	39.39
Total Energy [MJ]	50.00	50.00
Global displacement [m]	1.11	0.4
Dent [m]	-	1.05
Energy absorption considering dent criteria Dent<D/2		
Energy structure [MJ]	-	8.00
Energy dent [MJ]	-	24.00
Total Energy [MJ]	-	36.00
Global displacement [m]	-	0.35
Dent [m]	-	0.8

Table 6-16: Summary results for leg in platform B

When the leg is grouted, the maximum impact force 18.84MN with a lateral displacement 2.50m, and an impact energy absorption of 50MJ. Figures **6-54** and **6-55** depict the comparison behavior for the leg with and without grout impacted at mid-span.

Thus, the upper joint deflects 0.4m, and is capable of absorbing 36MJ, and the failure occurs when the denting is larger than 50% of the diameter section. The grouted joint is deformed 1.1m and absorbs 50MJ. Furthermore, Figures **6-57** and **6-58** show the

global displacement against the impact energy and the impact force in the upper joint. Nonetheless, for the upper joint without grout, there is a sudden change in stiffness when the brace behind fails due to the compression on the joint. Having said that, it can be explained why when deflection reaches 0.2m, there is a drop in the impact force. Correspondingly, same phenomenon is found during the denting of the cross section (see Figure 6-59).

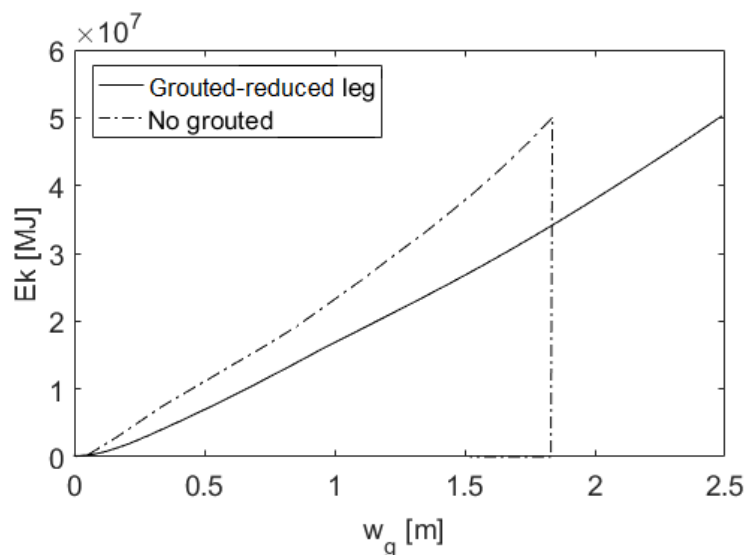


Figure 6-54: Global displacement against impact energy for grouted leg and leg without grout, impacted at mid-span - Platform B

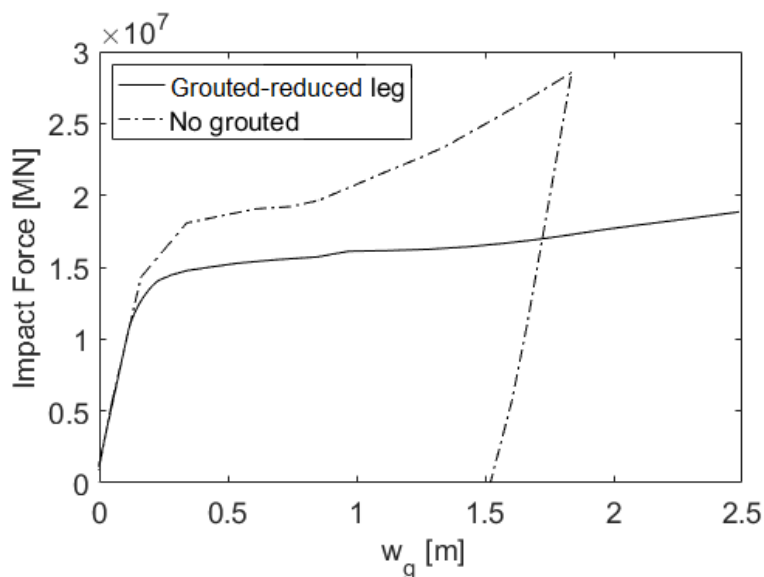


Figure 6-55: Global displacement against impact force for grouted leg and leg without grout, impacted at mid-span - Platform B

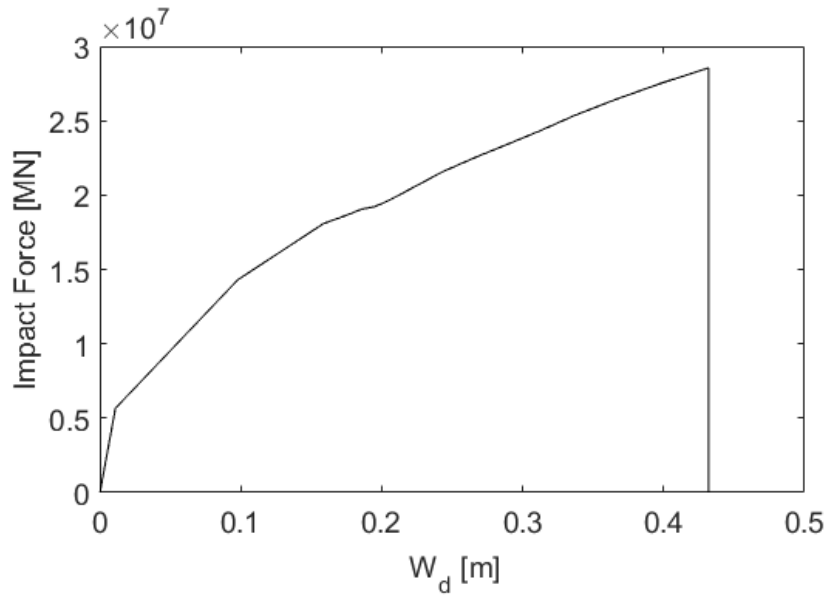


Figure 6-56: Dent against the impact force for leg without grout, impacted at mid-span - Platform B

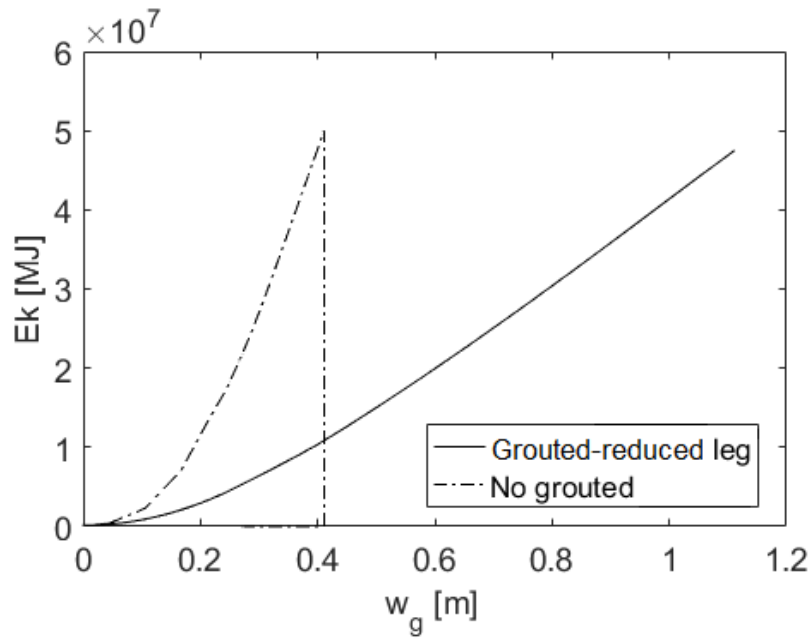


Figure 6-57: Global displacement against the impact energy for grouted leg and leg without grout, impacted at the upper joint - Platform B

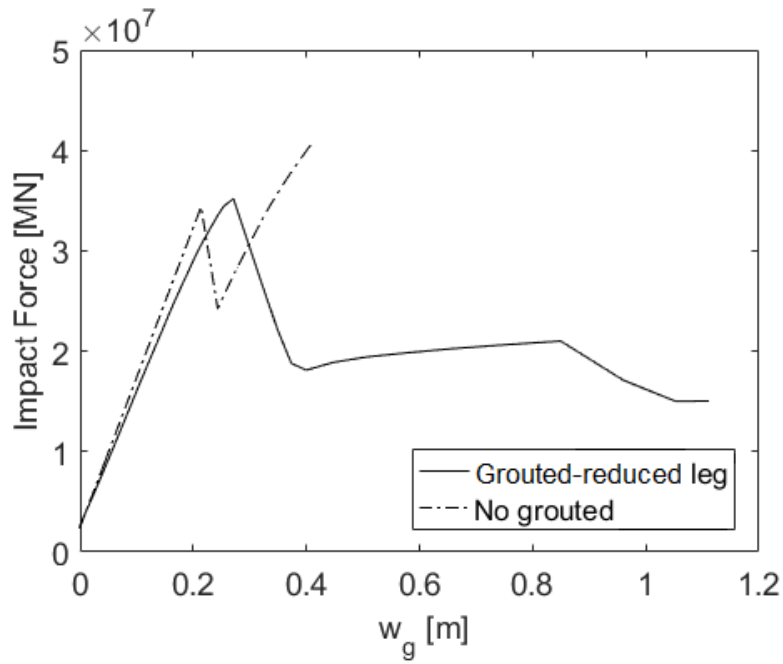


Figure 6-58: Global displacement against the impact force, for grouted leg and no leg without grout, impacted at the upper joint - Platform B

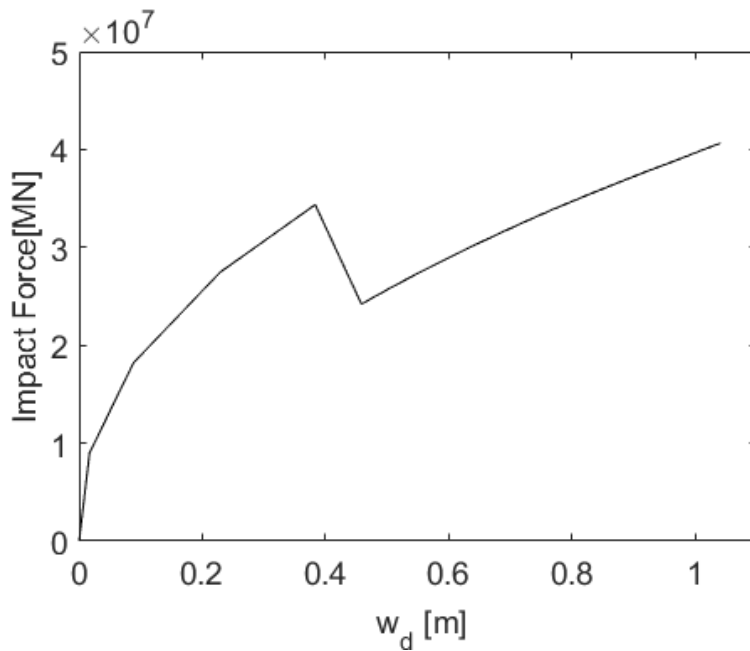
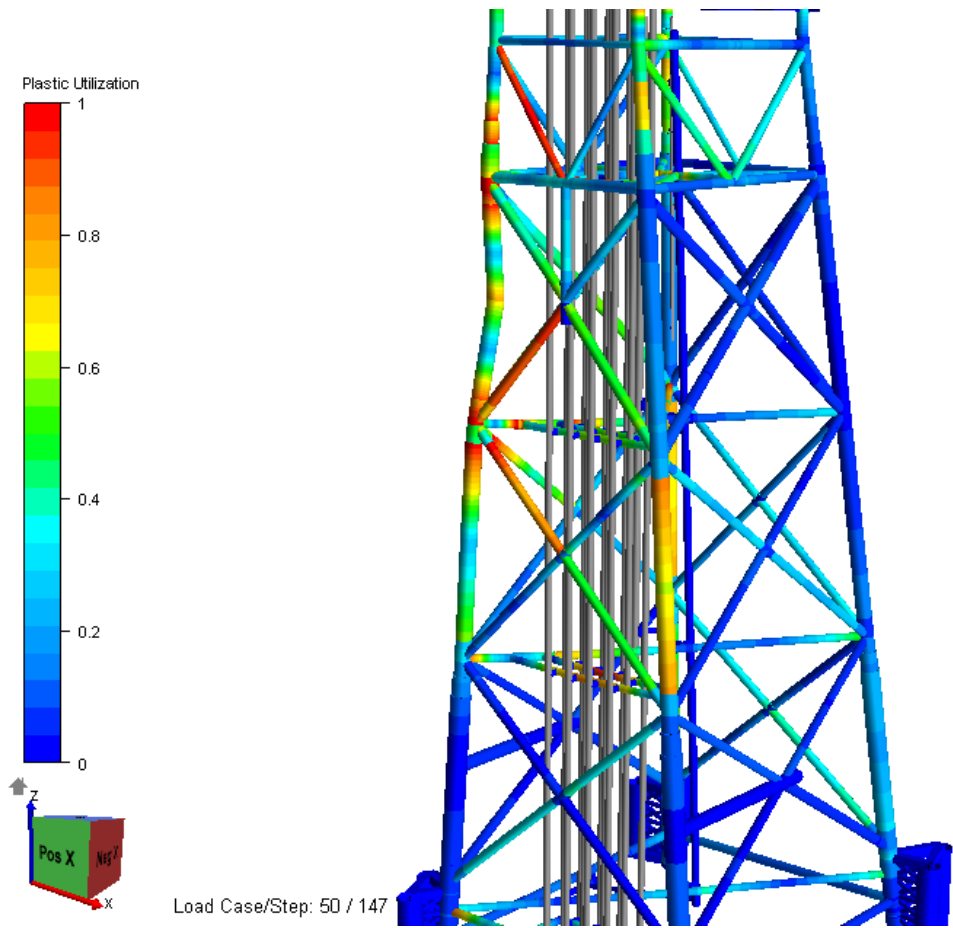
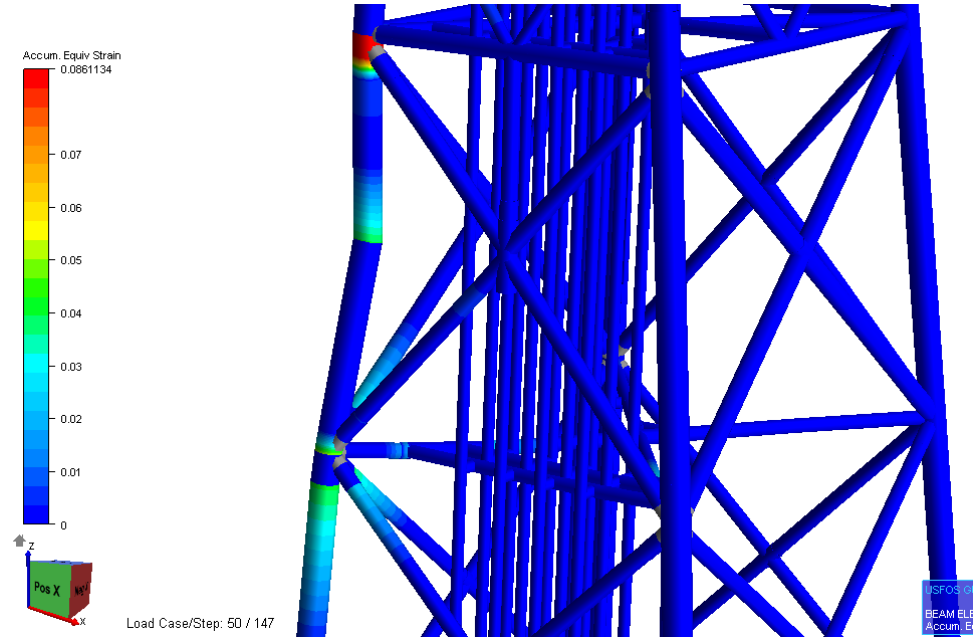


Figure 6-59: Dent against the impact force for leg without grout, impacted at the upper joint - Platform B

From Figure 6-60 to 6-63 the plastic utilization and strain distribution can be seen in the leg under boat impact.

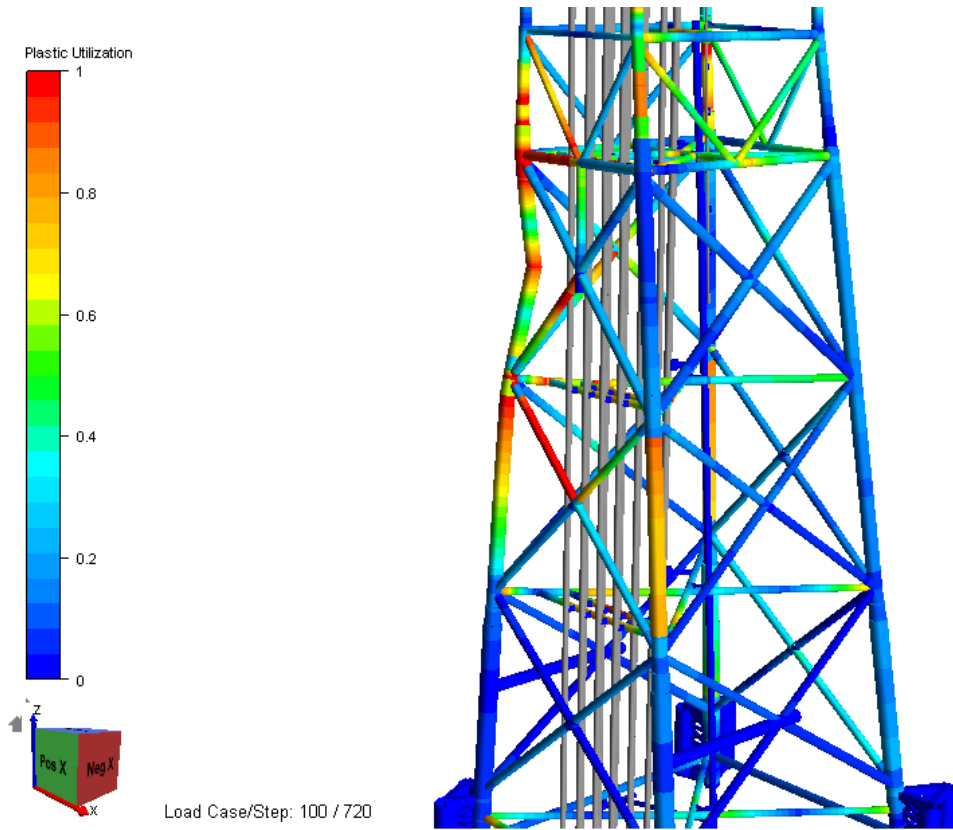


(a) Plastic Utilization

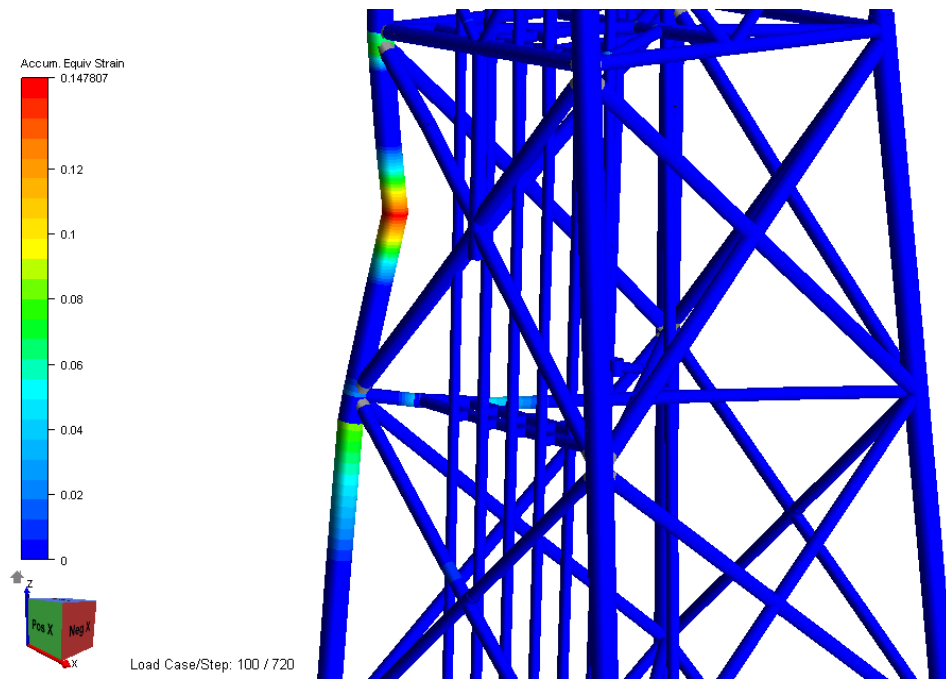


(b) Beam Strain

Figure 6-60: Utilization factor and strain distribution of the leg without grout, impacted at mid-span- Platform B

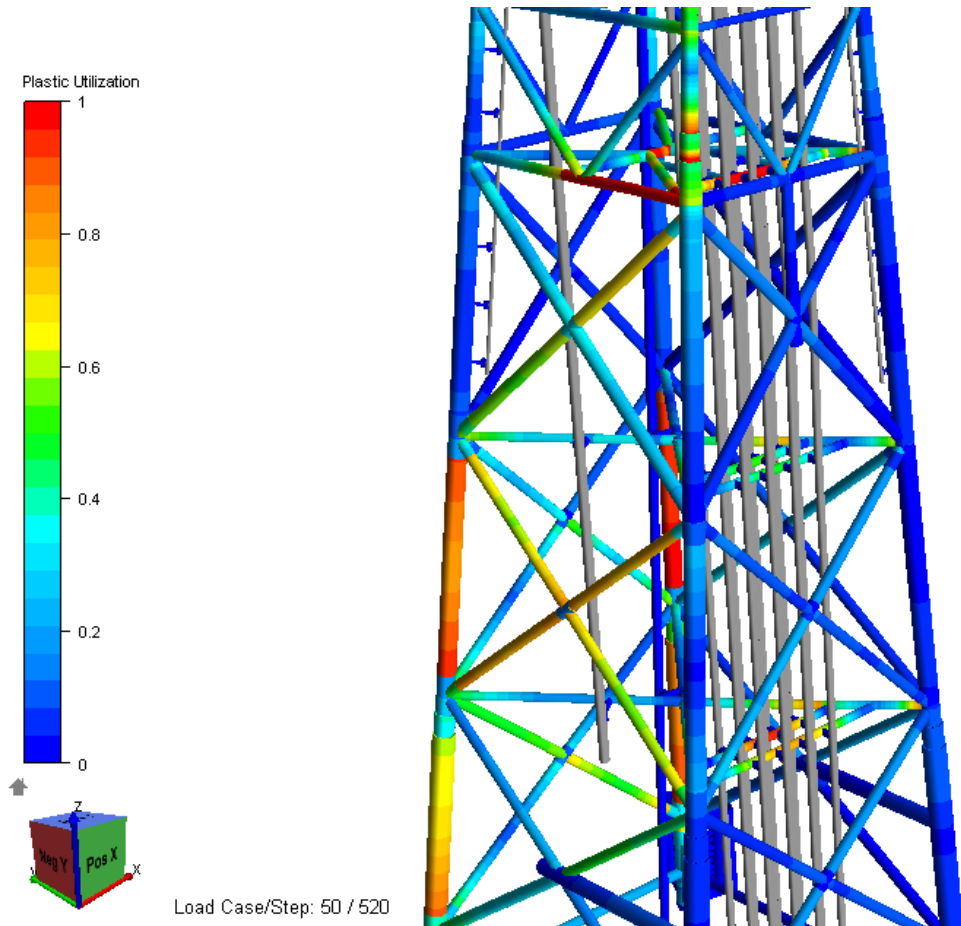


(a) Plastic Utilization

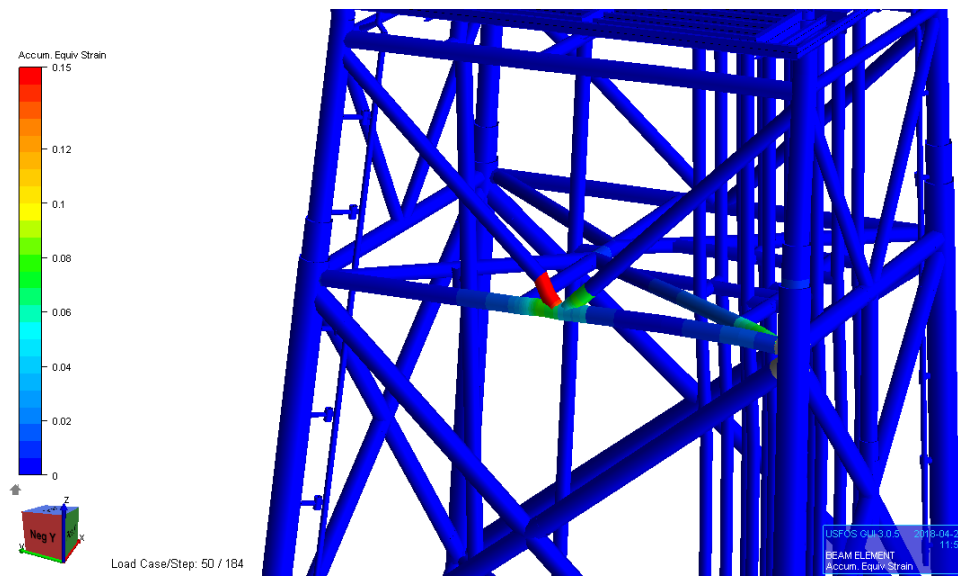


(b) Beam Strain

Figure 6-61: Utilization factor and strain distribution of the grouted leg, impacted at mid-span- Platform B

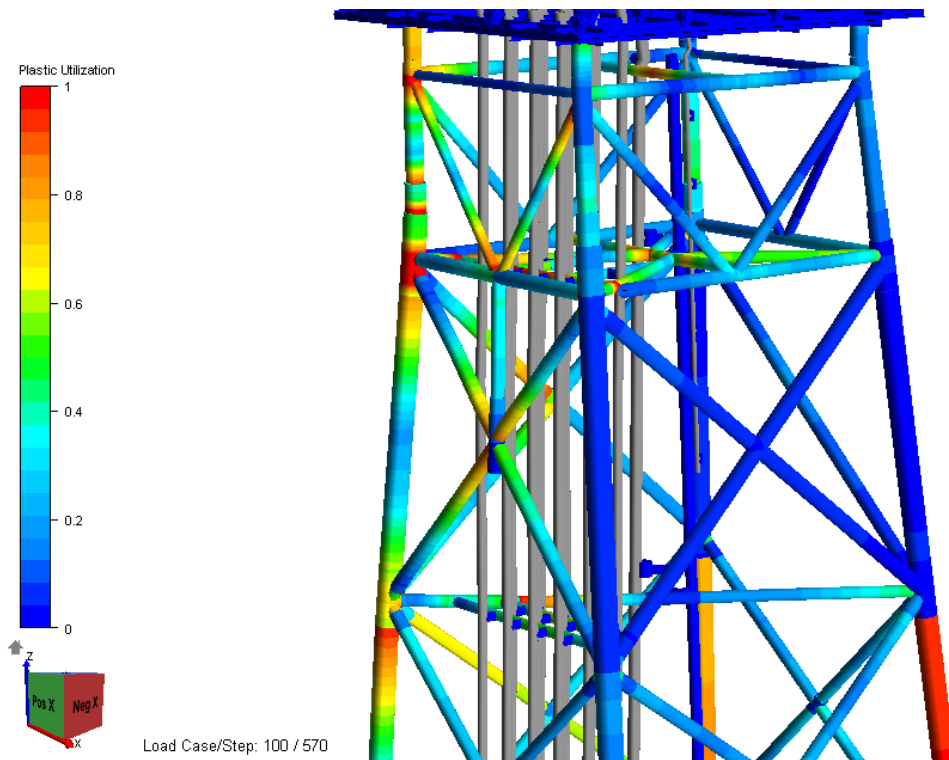


(a) Plastic Utilization

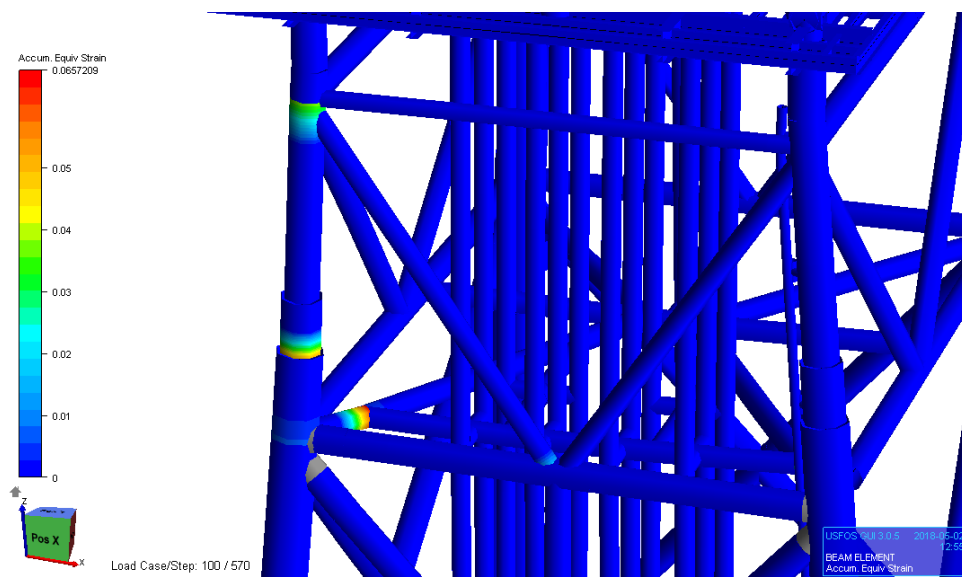


(b) Beam Strain

Figure 6-62: Utilization factor and strain distribution of leg without grout, impacted at the upper joint- Platform B



(a) Plastic Utilization



(b) Beam Strain

Figure 6-63: Utilization factor and strain distribution of grouted leg, impacted at the upper joint- Platform B

Impact with diagonal brace

The diagonal brace is impacted in two locations: at mid of the span and at the joint of the X-brace. Table **6-17** summaries the results for the diagonal brace. The maximum impact force in the mid-span is 17.28 MN with a global displacement of 1.36m, and energy absorption of 21 MJ. The diagonal brace fails when it reaches the critical strain in the upper-joint.

The maximum impact force at the joint is 21.17MN and a lateral displacement of 1.50m. The joint dissipates a total 23.15MJ, and it fails when the X-joint breaks.

Figure **6-64** presents the global deformation against the impact energy at the mid-span and at the joint. Furthermore, Figure **6-65** illustrates the comparison of the global deformation against the impact force for the impacts at mid-span and at the joint.

The brace dissipates more dent energy at the mid-span than at the joint. This is possible, as the wall thickness of the joint is larger than at the middle of the span. Figures **6-67** and **6-66** depict the comparison of the dent against the impact force and dent energy, for the impacts at the mid-span and at the joint of the diagonal brace.

Boat Impact against diagonal brace at mid-span	
Impact force [MN]	17.28
Energy structure [MJ]	15.5
Energy dent [MJ]	5.50
Total Energy [MJ]	21.00
Global displacement [m]	1.36
Dent [m]	0.45
Boat Impact against diagonal brace at X-joint	
Impact force [MN]	21.17
Energy structure [MJ]	18.6
Energy dent [MJ]	4.55
Total Energy [MJ]	23.15
Global displacement [m]	1.50
Dent [m]	0.33

Table 6-17: Summary results for diagonal brace in platform B

Finally, Figure **6-68** and Figure **6-69** show the plastic utilization and strain of the diagonal brace impacted at mid-span and at the joint. For the impact at the midspan, the failure is produced in the upper joint, when the strain reaches the critical value of 0.15. Conversely, for impacted joint, the maximum stain is found in the vertical brace, connected to the upper horizontal brace. However, the fail is produced on the joint itself.

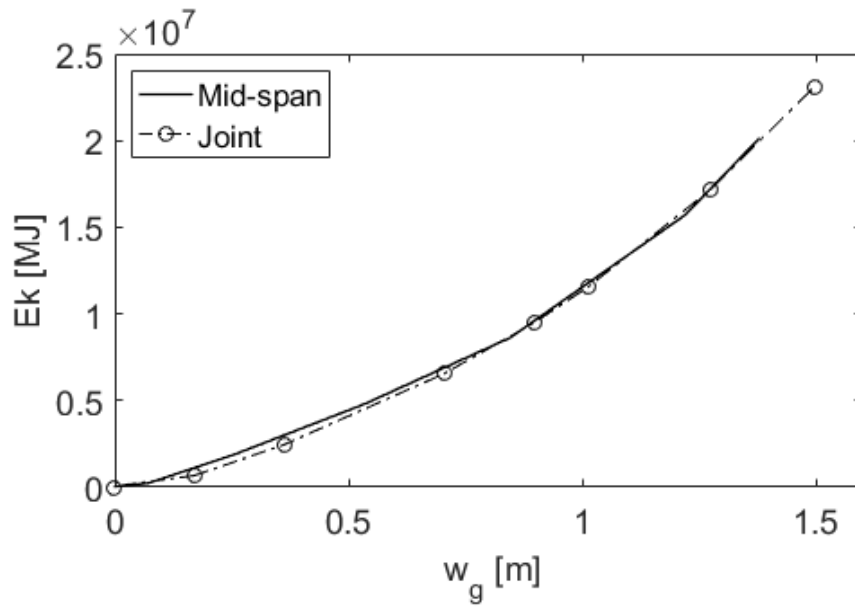


Figure 6-64: Global deformation against the impact energy in the diagonal brace, impacted at midspan and at the joint - Platform B

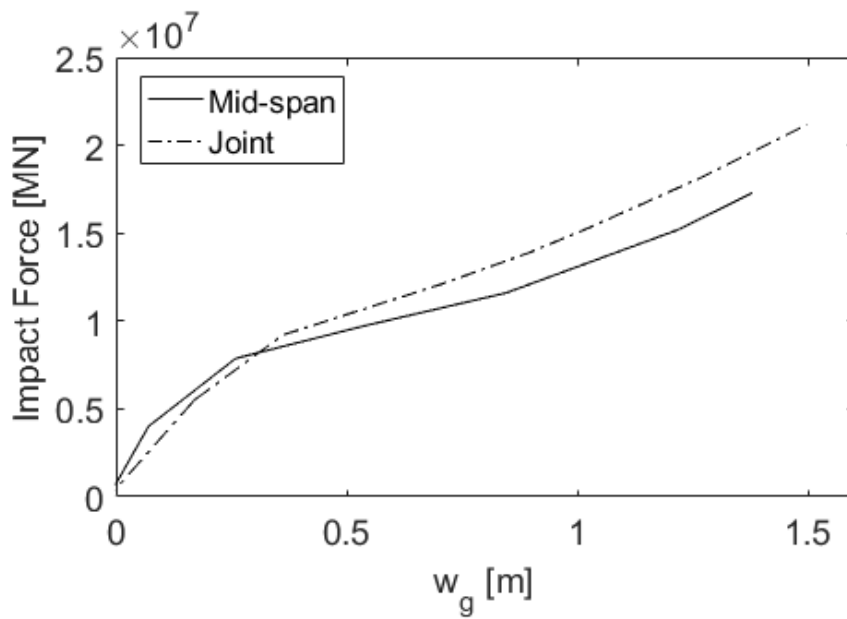


Figure 6-65: Global deformation against the impact force in the diagonal brace, impacted at midspan and at the joint - Platform B

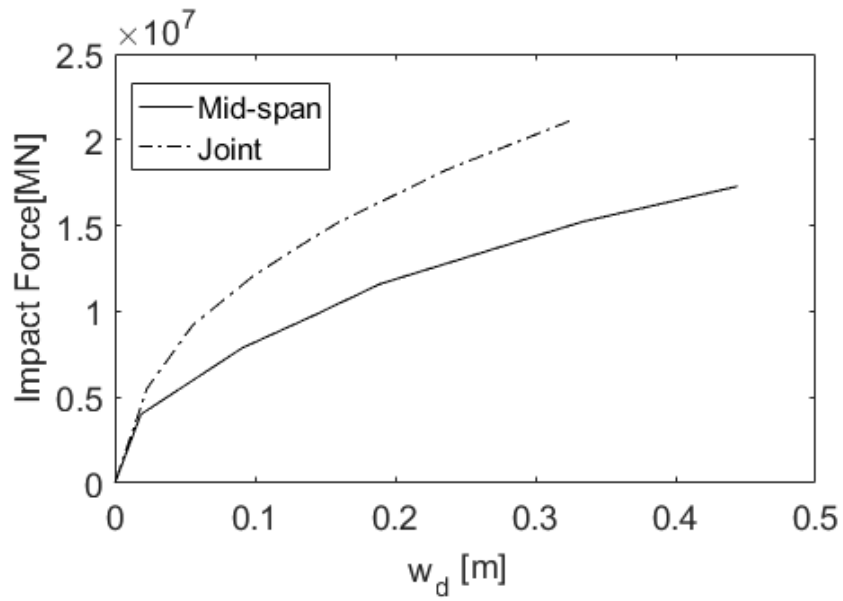


Figure 6-66: Dent against the impact force in the diagonal brace, impacted at midspan and at the joint - Platform B

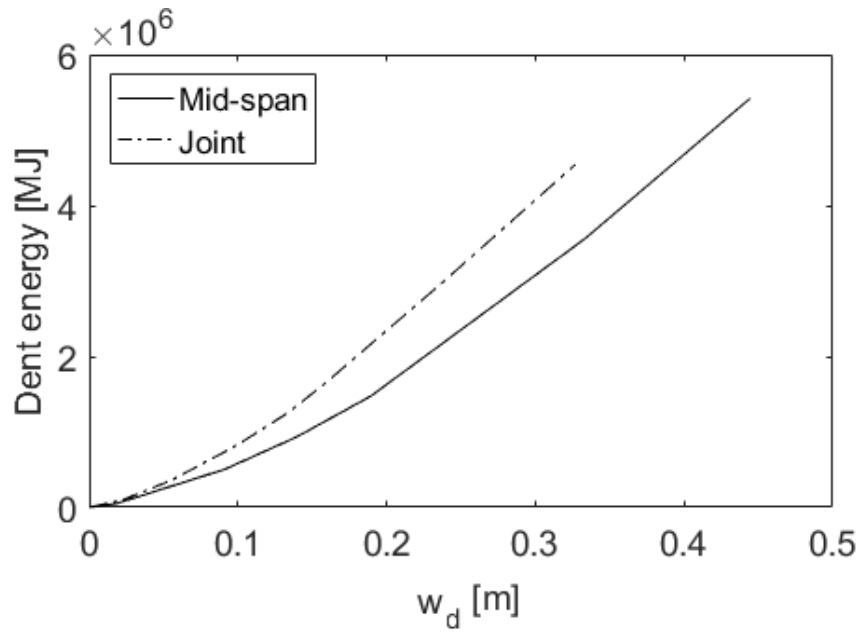
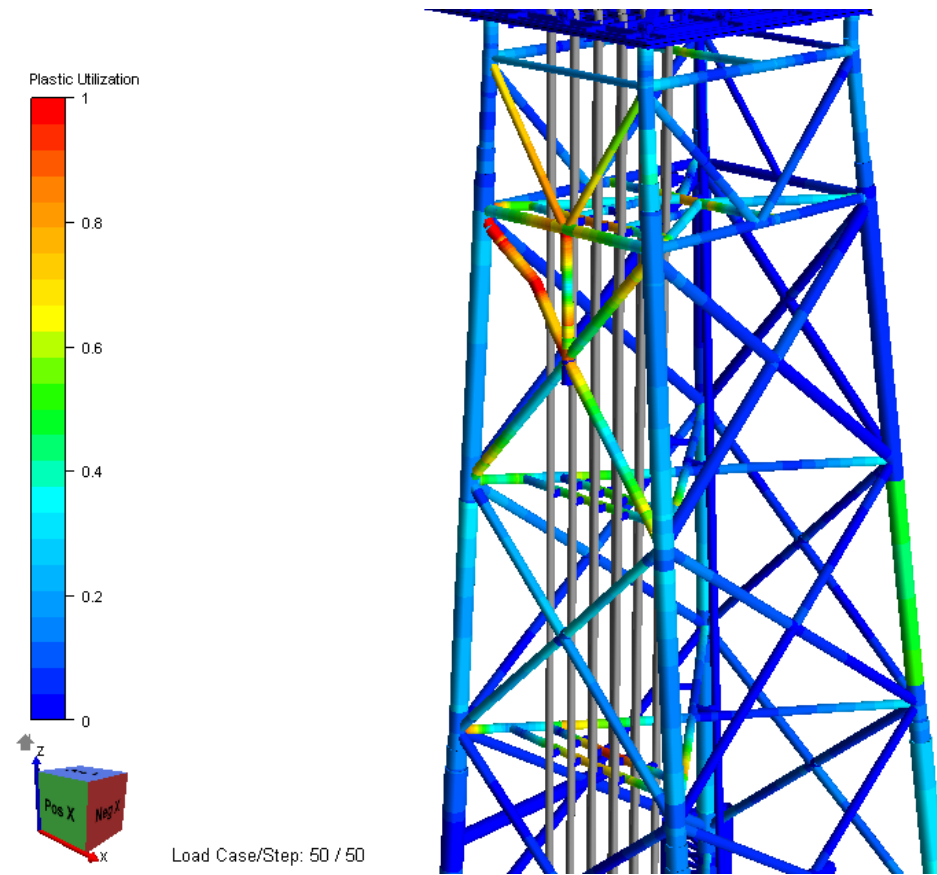
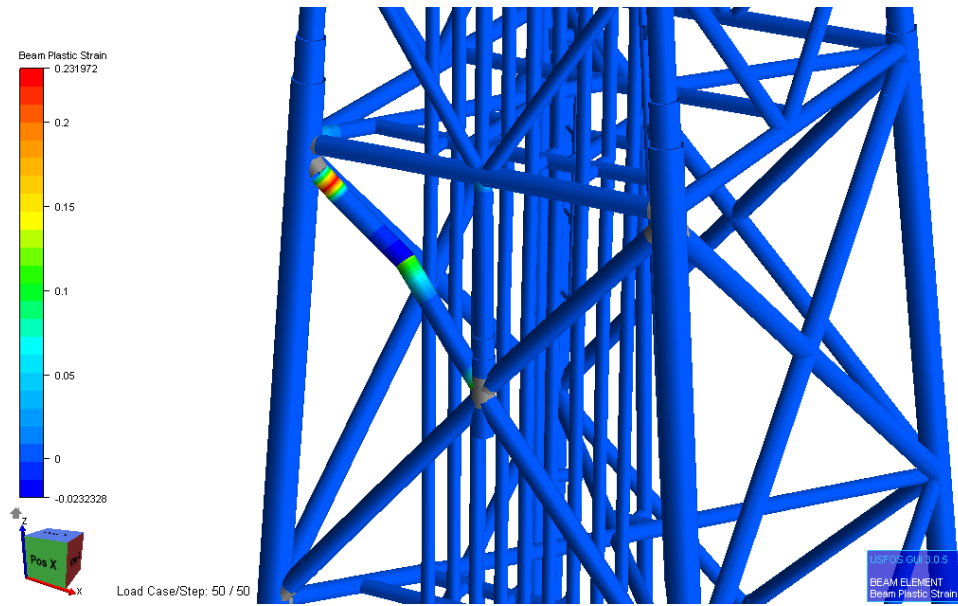


Figure 6-67: Dent against the dent energy in the diagonal brace, impacted at midspan and at the joint - Platform B

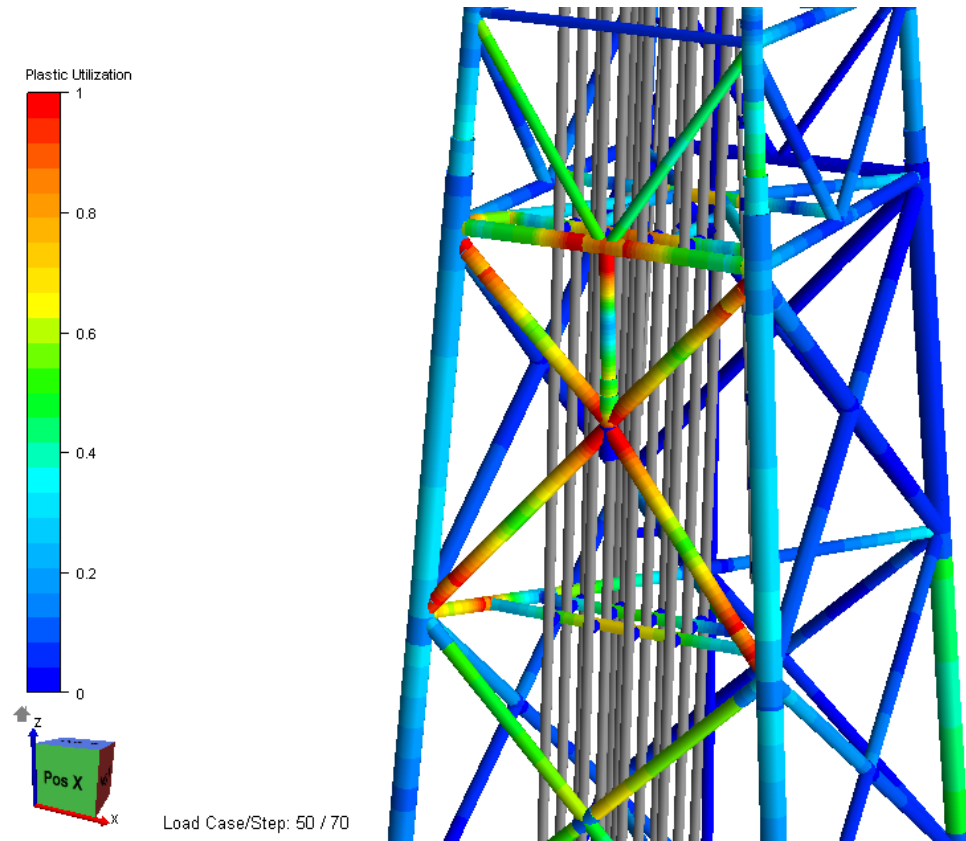


(a) Plastic Utilization

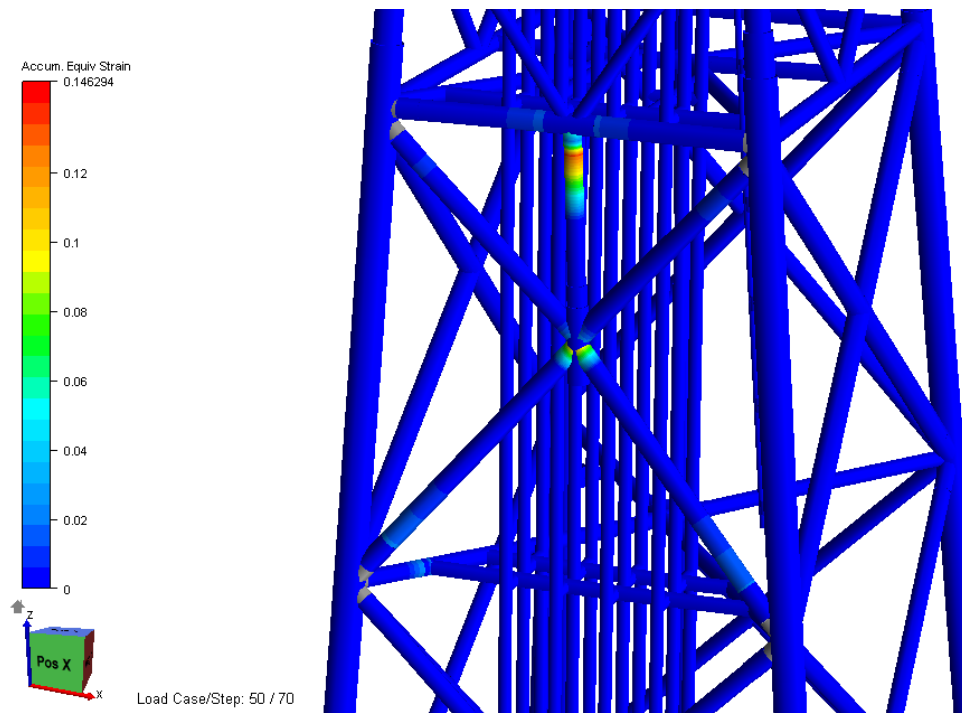


(b) Beam Strain

Figure 6-68: Utilization factor and strain distribution of the diagonal brace, impacted at midspan - Platform B



(a) Plastic Utilization



(b) Beam Strain

Figure 6-69: Utilization factor and strain distribution of the diagonal brace, impacted at the joint - Platform B

Impact with horizontal brace

The horizontal brace has been grouted and impacted in two locations: at mid of the span and the joint. Table 6-18 summaries those results. In the first place, a difference in energy absorption under both scenarios has been found. In this respect, the grouted horizontal brace can dissipate at 11 MJ, whereas a brace without grout dissipates at 17.30 MJ. Thus, it can be suggested that this main distinction takes place because of the capacity of the ungrouted brace to dissipate energy by denting. The grouted brace has a global displacement of 1.28m in comparison to 1.06m from the brace without grout. Figure 6-70 and Figure 6-71 present the correlation of the horizontal brace impacted at a mid-span with and without grout.

Failure in the brace without grout is produced at the joint, as illustrated in Figure 6-78, the figure depicts the plastic utilization and strain on the brace without grout. On the contrary, for the grouted horizontal brace, the failure is produced when the strain reaches 0.15 at mid span (see Figure 6-79).

The maximum impact force at the joint is 19.20 MN with a lateral displacement of 1.45m, the same deformation is chosen for the grouted joint. The reason is that failure of the joint is taken before the joint collapse with the risers behind. The energy absorption is larger in the joint without grout due to its capability to dissipates energy by denting. Figure 6-74 and Figure 6-75 present the global deformation against the impact energy and impact force at the joint. Furthermore, Figure 6-80 and 6-81 show the plastic utilization and strain for the impacted joint.

Boat Impact against horizontal brace at mid-span		
	With grout	Without grout
Impact force [MN]	13.00	17.08
Energy structure [MJ]	11.00	11.63
Energy dent [MJ]	-	5.67
Total Energy [MJ]	11.00	17.30
Global displacement [m]	1.28	1.06
Dent [m]	-	0.5
Boat Impact against horizontal brace at the joint		
	With grout	Without grout
Impact force [MN]	15.80	19.30
Energy structure [MJ]	15.00	17.09
Energy dent [MJ]	-	4.60
Total Energy [MJ]	15.00	21.69
Global displacement [m]	1.45	1.45
Dent [m]	-	0.35

Table 6-18: Summary results for horizontal brace in Platform B

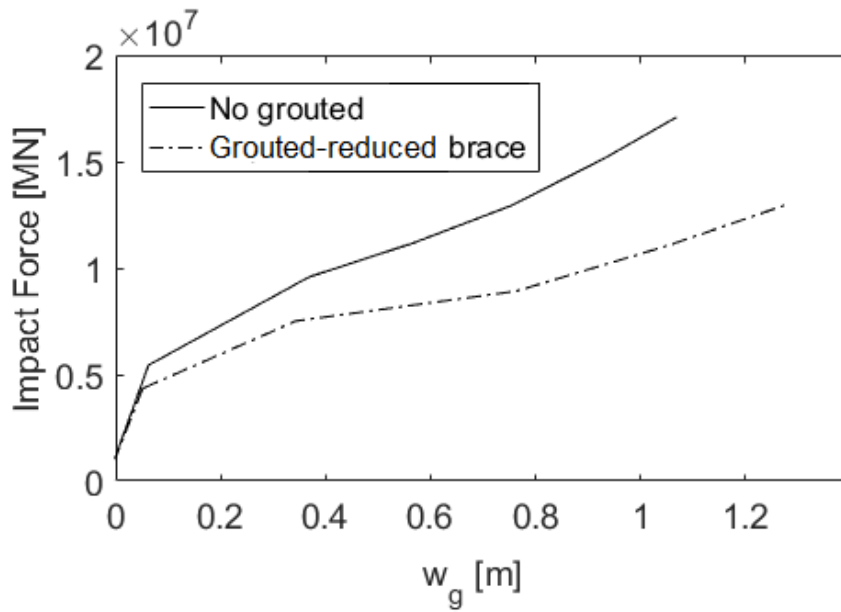


Figure 6-70: Global displacement against the impact force for horizontal brace with grout and without it, impacted at the midspan - Platform B

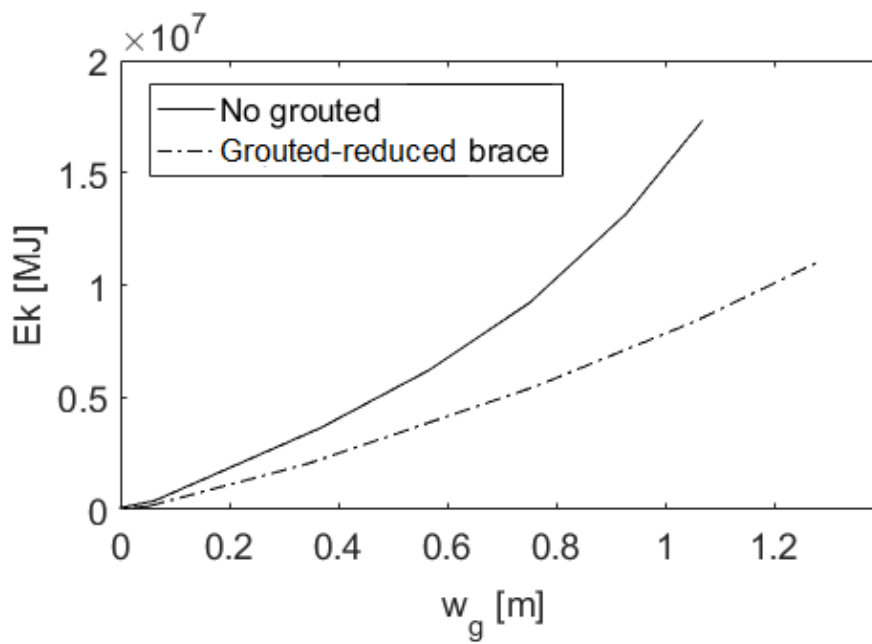


Figure 6-71: Global displacement against the impact energy for horizontal brace with grout and without it, impacted at the midspan - Platform B

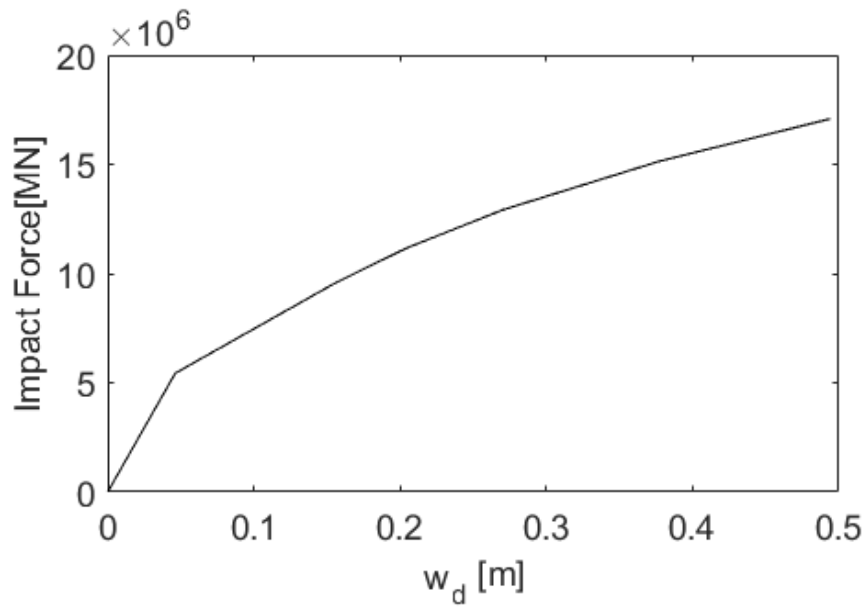


Figure 6-72: Dent against the impact force in horizontal brace, impacted at midspan - Platform B

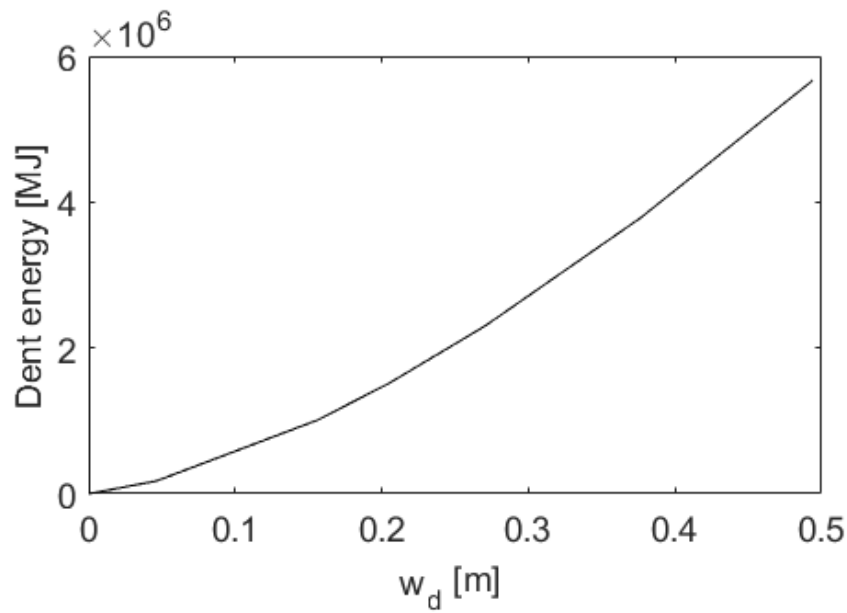


Figure 6-73: Dent against the dent energy in horizontal brace impacted at midspan - Platform B

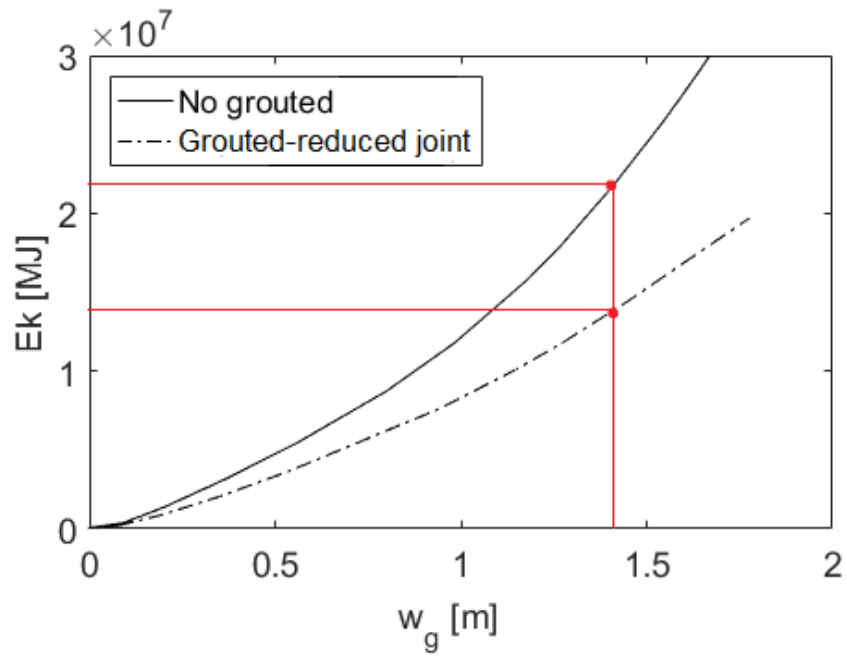


Figure 6-74: Global displacement against the impact energy for horizontal brace with grout and without it, impacted at the joint - Platform B

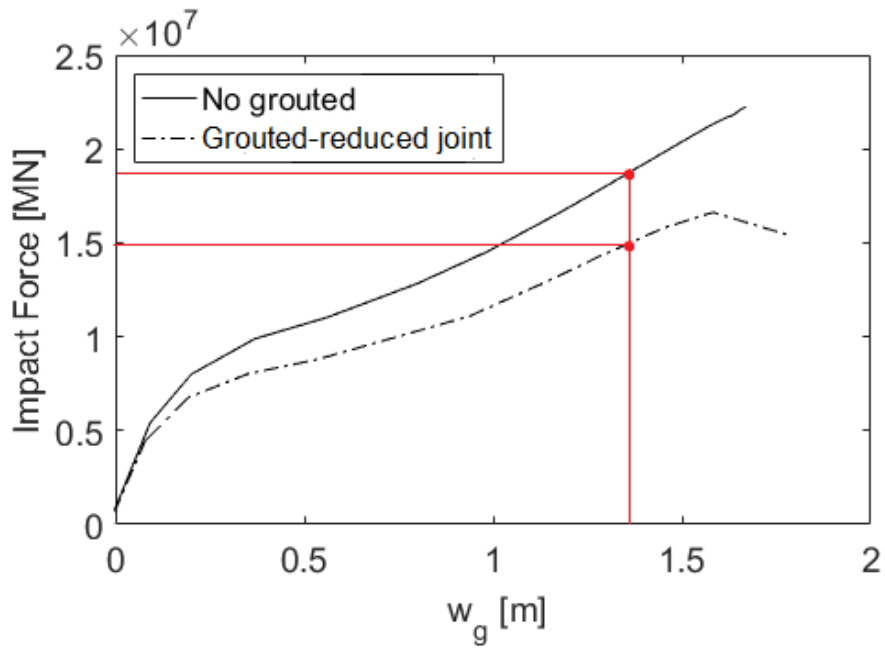


Figure 6-75: Global displacement against the impact energy in horizontal brace, impacted at joint - Platform B

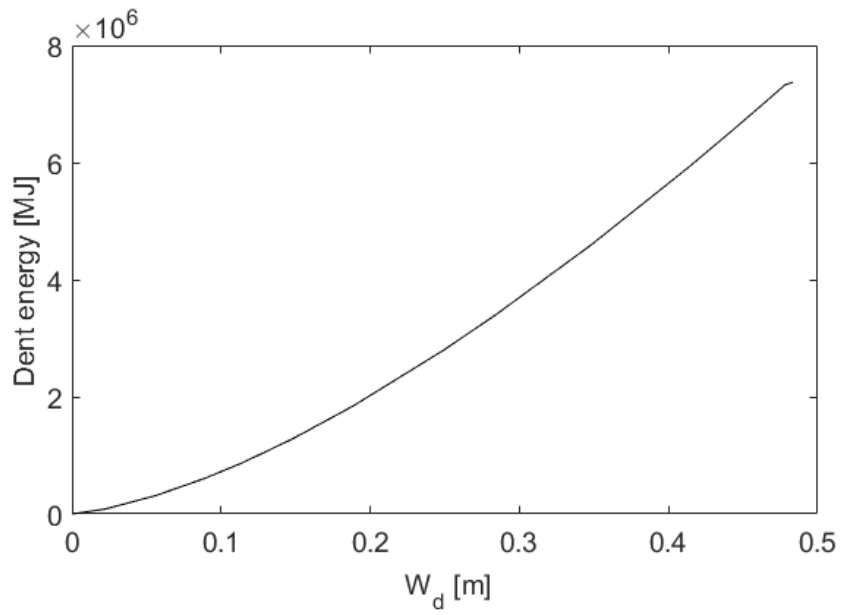


Figure 6-76: Dent against the dent energy in horizontal brace, impacted at joint - Platform B

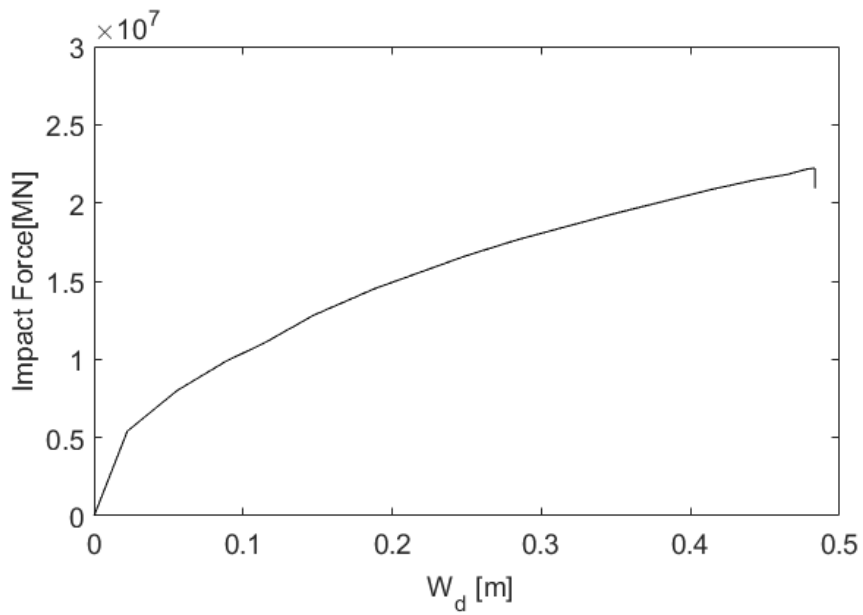
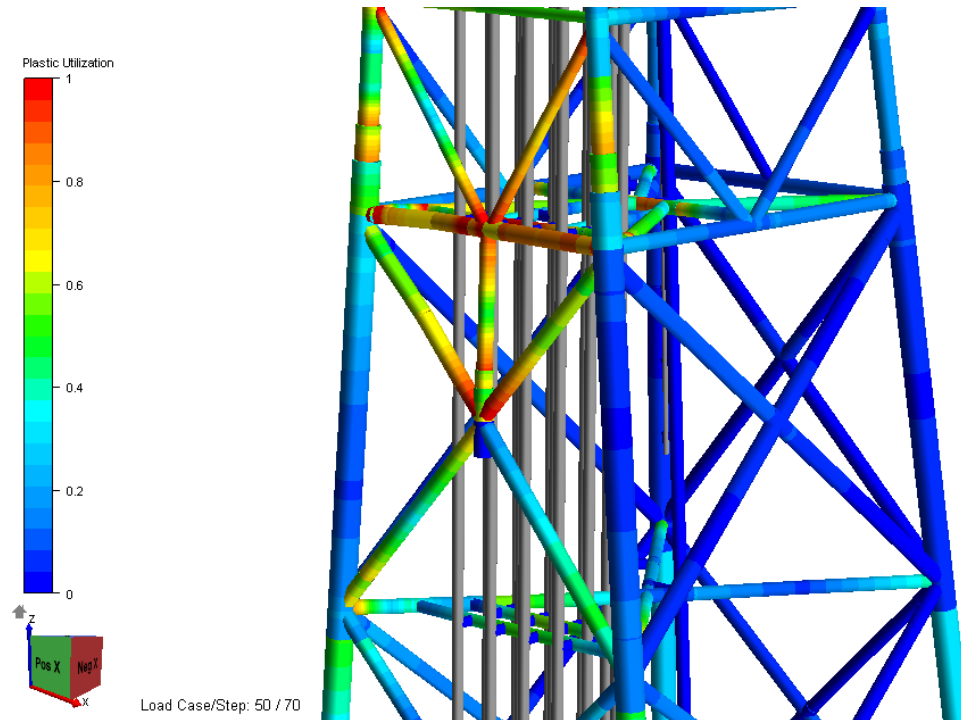
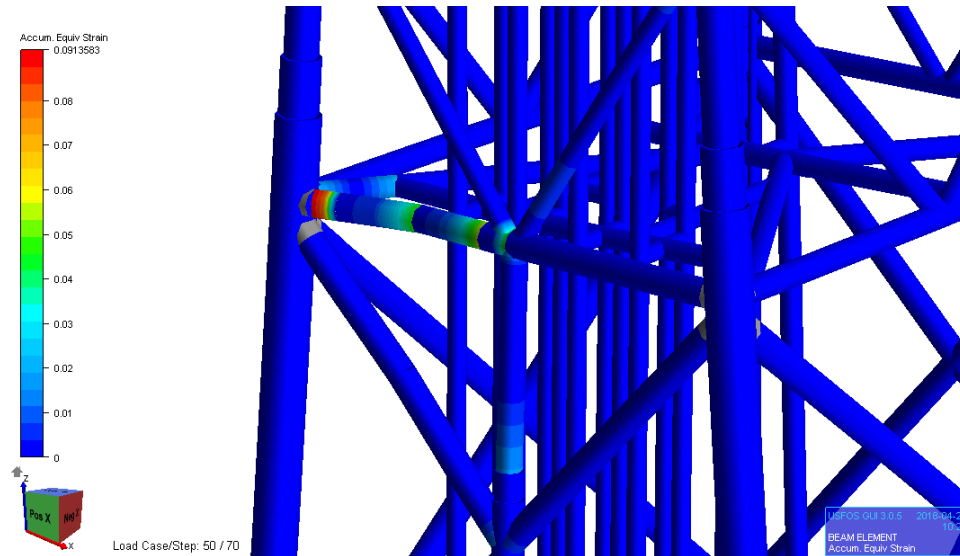


Figure 6-77: Dent against the impact force for horizontal brace without grout, impacted at the joint- Platform B

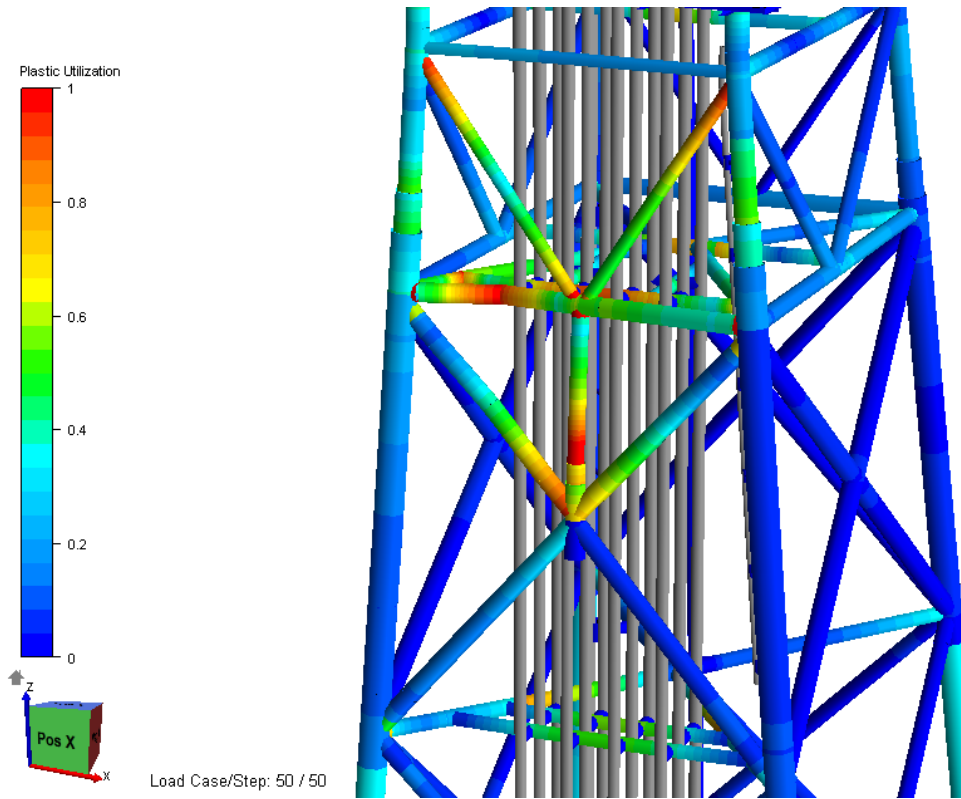


(a) Plastic Utilization

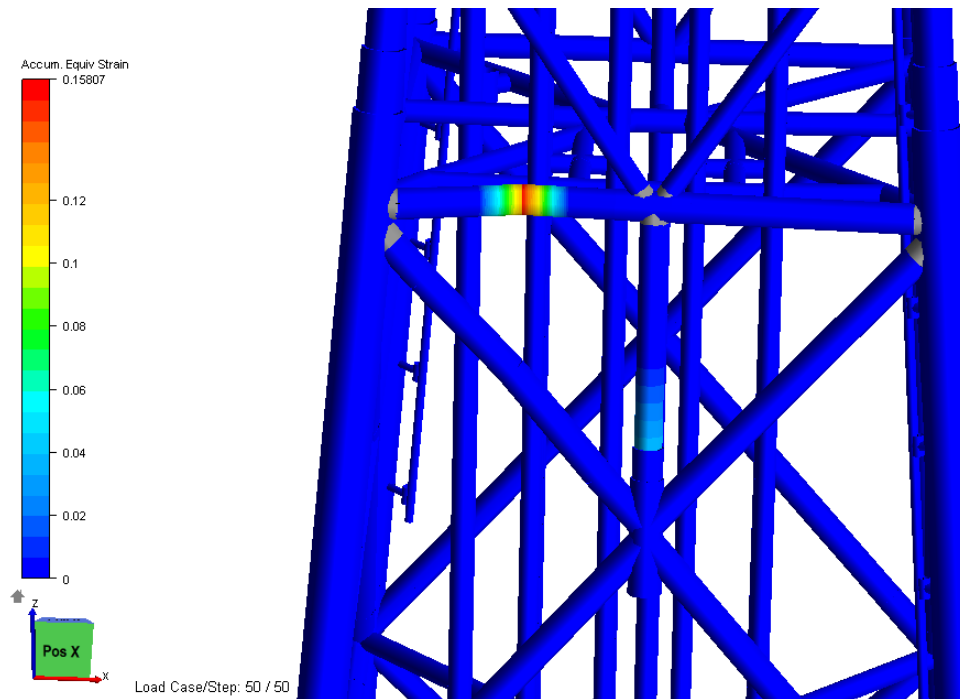


(b) Beam Strain

Figure 6-78: Utilization factor and strain distribution of the horizontal brace impacted at the midspan- Platform B

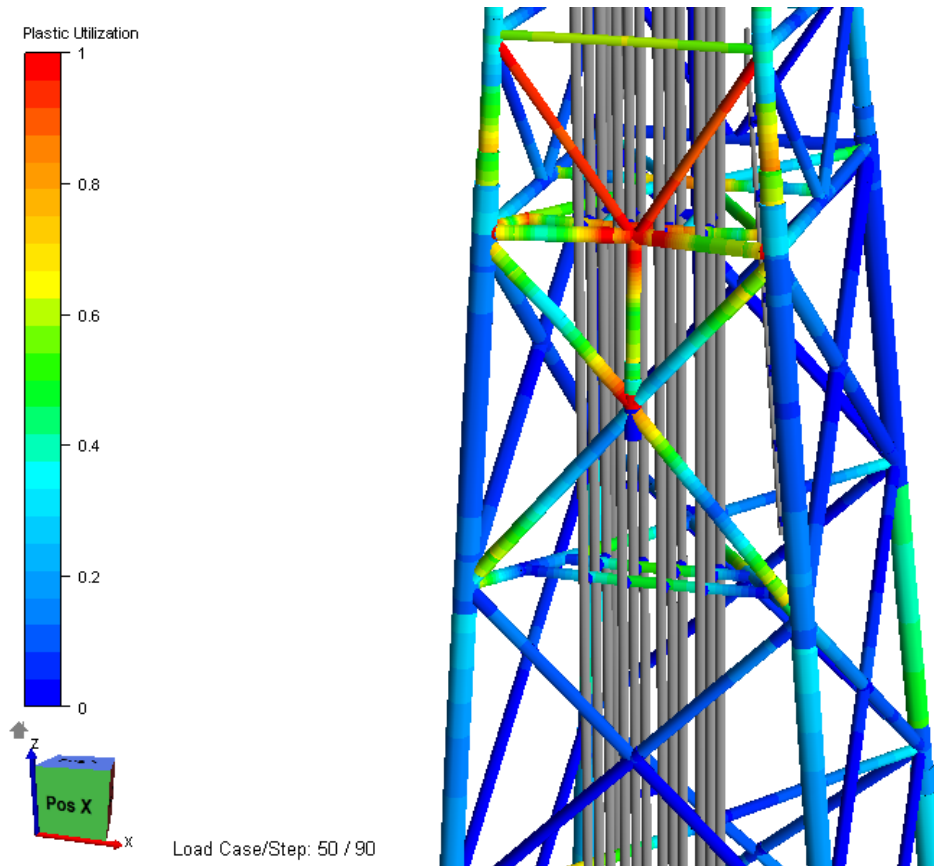


(a) Plastic Utilization

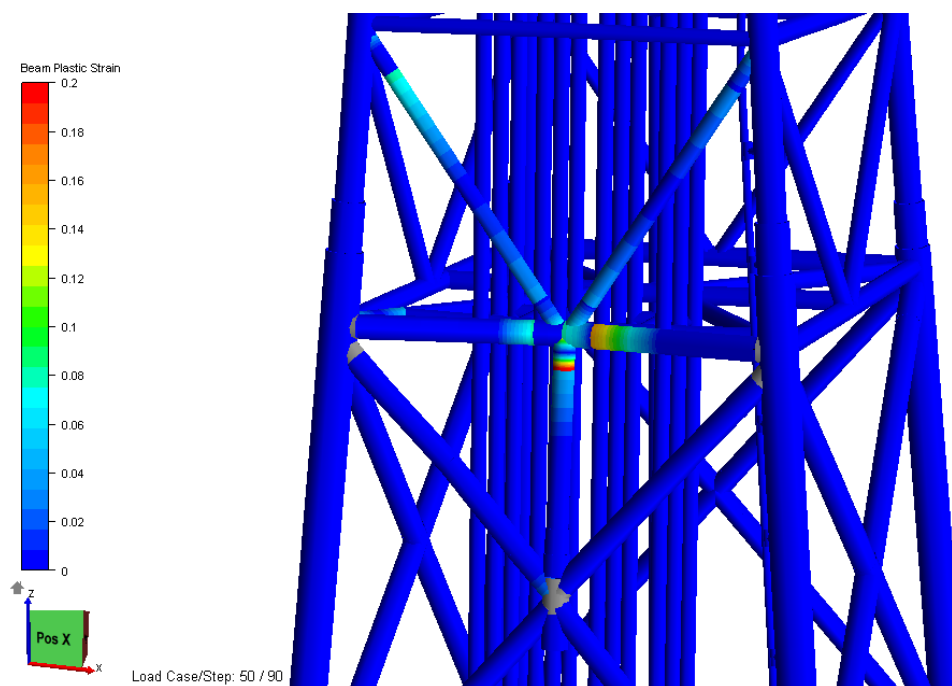


(b) Beam Strain

Figure 6-79: Utilization factor and strain distribution of the grouted horizontal brace impacted at the midspan- Platform B

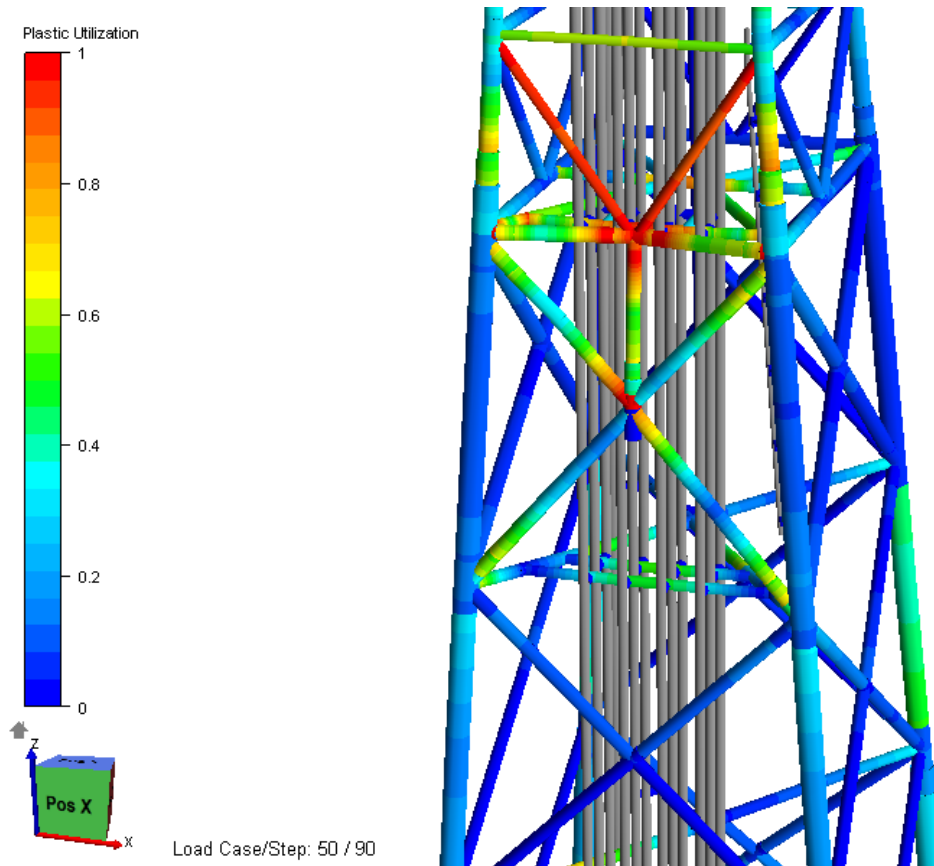


(a) Plastic Utilization

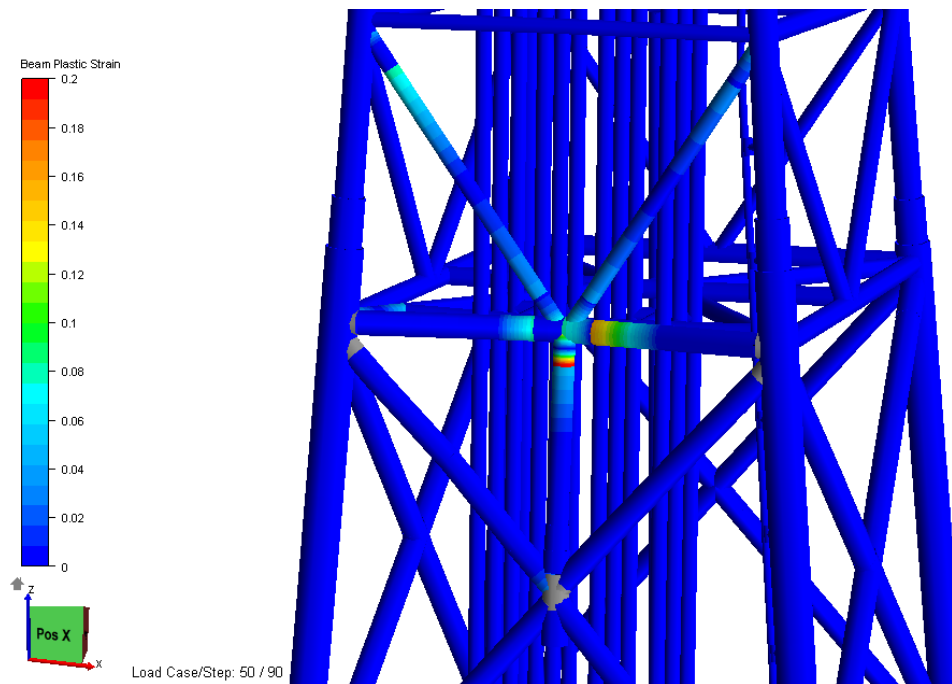


(b) Beam Strain

Figure 6-80: Utilization factor and strain distribution of the horizontal brace impacted at the joint- Platform B



(a) Plastic Utilization



(b) Beam Strain

Figure 6-81: Utilization factor and strain distribution of the grouted horizontal brace impacted at the joint- Platform B

7 Effect of the Vessel Velocity in the Ship Impact Analysis: Parametric Study

The forces than arise from a ship-jacket collision are normally handled by a quasi-static approach. However, dynamic analyses are very useful, specially for jacket-foundations interactions. In this section, a simple dynamic analysis is performed in Platform B to determine the speed effect, and the impact location effect in two parameters: The Base Shear Force (BS) and the Over-turning Moment (OM).

The impact energy is fixed to 50 MJ and the ship's mass and velocity are adjusted accordingly. Two impact positions have been chosen: at the mid-span of the leg (soft point) and at the joint leg (hard point). Table **7-19** presents the parameters used under the parametric study. Here, a structural damping ratio of 0.02 has been used at the first eigenperiod of the platform. This means 2% damping at frequency of 0.1, afterwards the damping is kept constant at 2% in the time domain. Moreover, the hydrodynamic damping is omitted in the analysis, this is a very simple approach, which does not have a significant influence in the large values produced at the moment of impact, and which are the focus of this study; instead of concentrating on how the forces are dissipated in the structure during time.

The USFOS program uses a HHT- α method, *"this method employs some sort of time averaging of the damping, stiffness and load term expressed by the α parameter. A beneficial feature of the method is that introduces artificial damping of higher frequency modes without degrading the accuracy"*, User's manual (USFOS, 2014).

The static and dynamic loads are imposed in the structure in two steps:

1. Static load is applied, this includes gravity and functional loads.
2. The impact energy is imposed as an impulse, by using a triangular load.

Characteristic	Value/Description
Velocity, v_s [m/s]	3.0, 3.5, 4.0
Ship Mass, m_s [Tonnes]	10000, 7500, 6250
Impact Energy E_k [MJ]	50
Impact Position	leg mid-span, leg joint
Damp ratio [unit-less]	0.02

Table 7-19: Parameters used in dynamic analysis for Platform B

Furthermore, the results are compared to the static analysis to characterize the dynamic factor for the base shear force and over-turning moment. Table **7-20** summaries the results obtained in the dynamic analysis (only the maximum values in the time domain are reported).

Impact Position	Dynamic Analysis						Static Analysis	
	Base Shear Force [MN]			Over-turning Moment [MN*m]			Base Shear Force [MN]	Over-turning Moment [MN*m]
	3.0m/s	3.5m/s	4.0m/s	3.0m/s	3.5m/s	4.0m/s		
Mid-span leg	41.45	42.35	43.90	3077.7	3157.2	3192.5	30.00	2100
Joint leg	62.66	75.57	76.74	5382.5	5080	4152.2	54.12	4298

Table 7-20: Base shear force and over-turning moment results for dynamic analysis

The forces and moments in the time domain are presented in Figures 7-82 to 7-85, here, only the firsts three seconds of the numerical simulation are plotted, as the large values are found at the moment of impact.

The results shown that BS and OM from ship impacts to hard points (joint legs) are larger than impacts to soft points (mid-span of a leg). Consequently, joint impacts are more relevant in terms of base shear force and over-turning moments. Furthermore, it is possible to see that for impacts in soft points, a larger velocity and increment in the base shear force and over-turning moment is expected. However, the difference is not large enough to consider it of importance.

In contrast, for impact at joints, a larger BS is registered for 4m/s, and it is equal to 76.74 MN and it also corresponds to 20% more than the value for the impact at 3m/s. On the other hand, the over-turning moment seems to reduce in value for larger velocities, this is due to the change in the topside inertia, where the weight of the topside is more relevant, and it acts as a "support" for the impact forces.

When the dynamic analysis is compared to the quasi-static analysis, the values obtained are larger in both parameters, the BS and OM. Being the dynamic factor expressed as the ratio between the dynamic response to the static response ($f_{dyn} = Dyn_{res}/Sta_{res}$). The maximum f_{dyn} for BS is 1.42 and 1.25 for the OM.

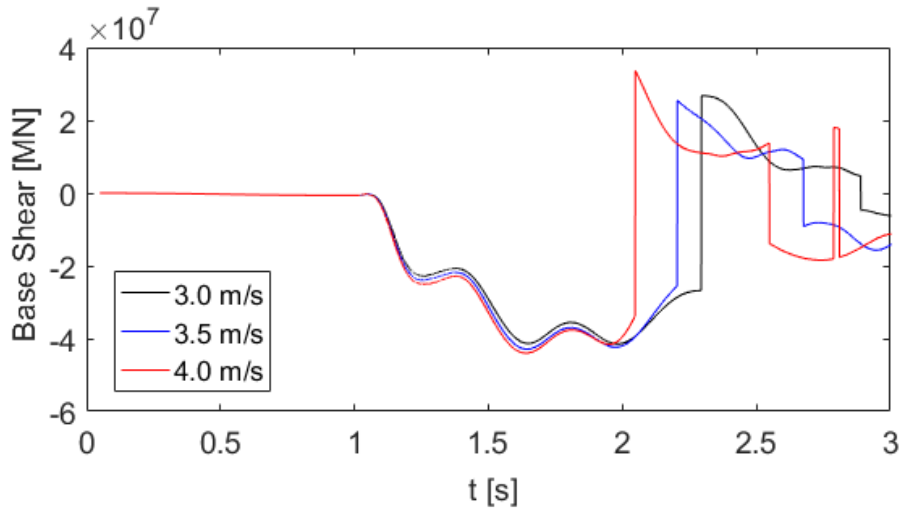


Figure 7-82: Vessel speed effect in the base shear force for the leg impacted at mid-span

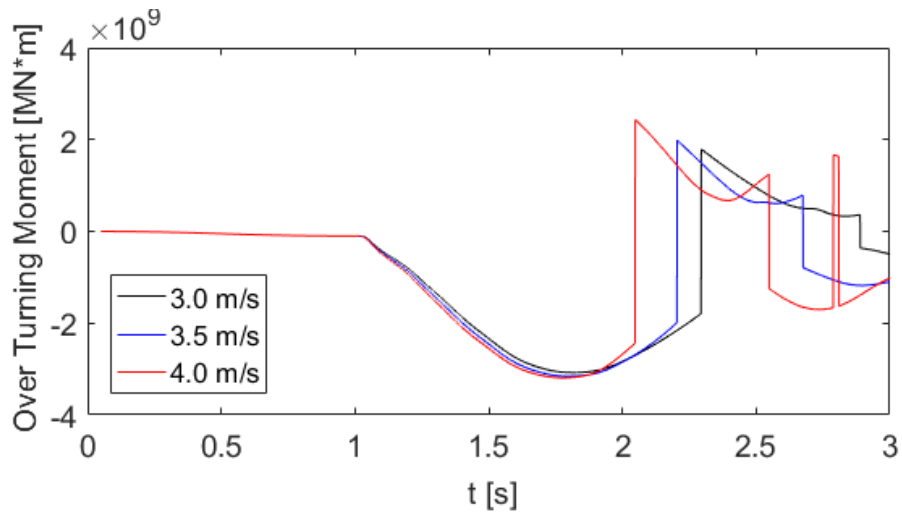


Figure 7-83: Vessel speed effect in the over-turning moment for the leg impacted at mid-span

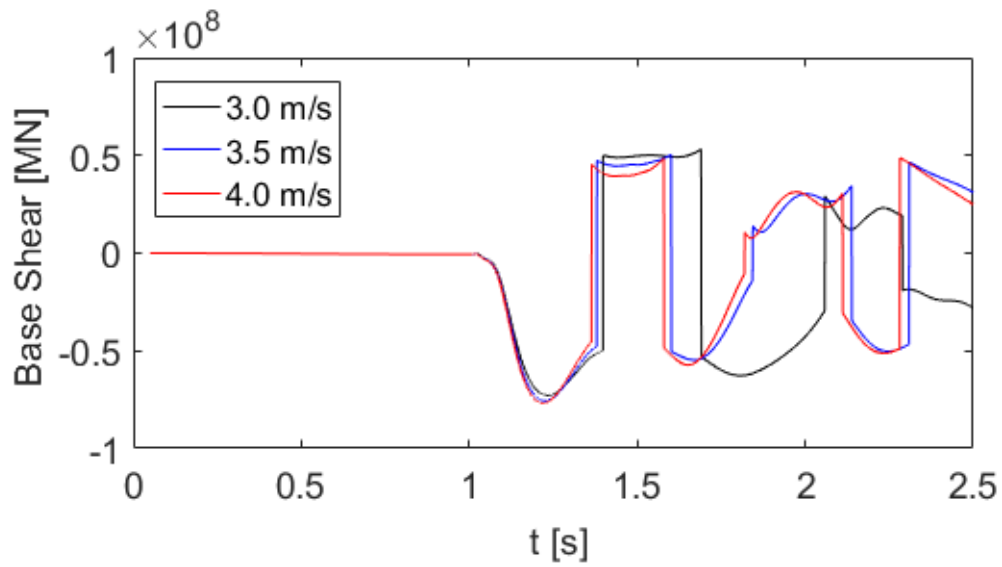


Figure 7-84: Vessel speed effect in the base shear force for the leg impacted at the joint

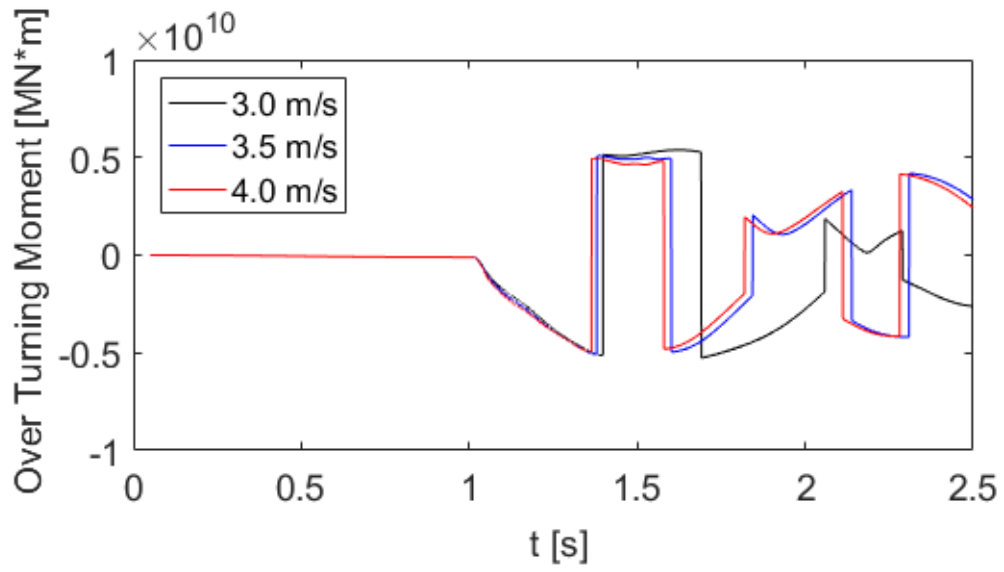


Figure 7-85: Vessel speed effect in the over-turning moment for the leg impacted at the joint

8 Denting Effect in the Axial Capacity of Steel Tubes: Parametric Study

The purpose of this section is to determine the axial capacity of steel members impacted at mid-span. Numerical tests have been performed in axially free steel tubes that are restricted to bending; the reason for this, is to allow the tube to take bending moment and axial force afterwards. The impact load is calculated in order to achieve 50%, 55% and 60% denting of the diameter. Larger denting was desired, but as the tube needs to be axially-free, the plastic moment capacity is reduced; thereby, it is very difficult to dent the legs further without making the pipe collapse in bending. The procedure for applying the loads can be summarized in 3 steps (see Figure 8-86):

1. Gravity load is applied.
2. The impact load is applied at mid-span as a point load.
3. Compressive load is applied until fracture is produced or when the leg cannot take more load.

Table 8-21 presents a summary of the parameters of the model, and Table 8-22 summarizes the results from the numerical tests.

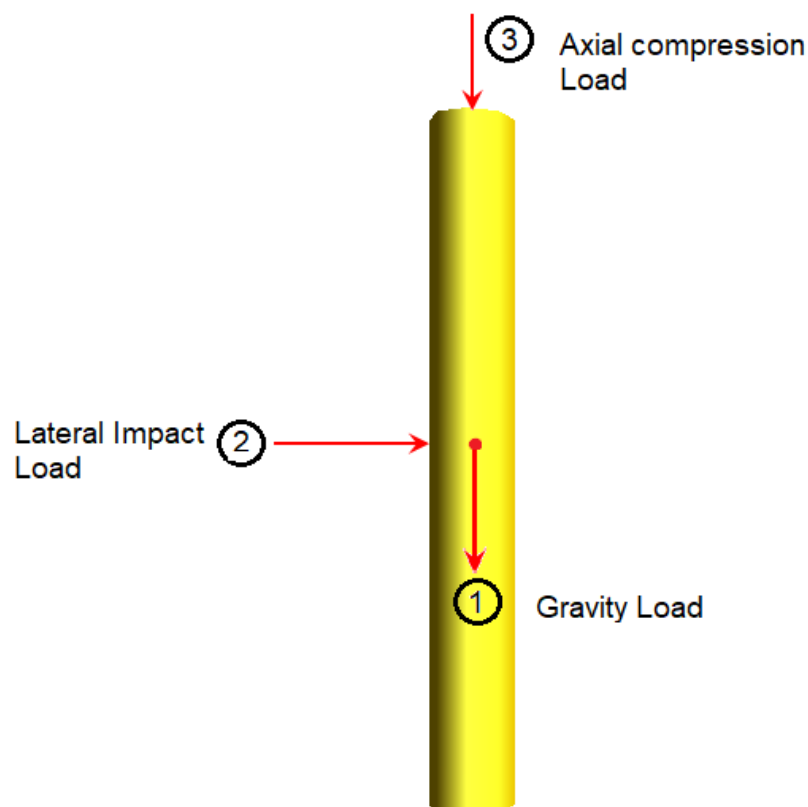


Figure 8-86: Loading procedure in the dented tubes.

Characteristic	Value/Description
Ratio L/D, [m]	8
Diameter, D[m]	1.3, 1.5, 1.8, 2.0
Thickness. t[mm]	40
Boundary conditions	Axially free on top and fixed at bottom
Denting w_d [%]	50,55,60
Yield strength f_y [MPa]	355

Table 8-21: Parameters used in numerical test for axial capacity of dented tubes

Section	Axial load in dented tubes (N_{max})				Axial compressive capacity (N_{Rd})
	0.5D	0.55D	0.60D		
D1300x40	42.6MN	38.14MN	-		54.74MN
D1500x40	51.36MN	47.34MN	38.56MN		63.86MN
D1800x40	74.00MN	64.10MN	60.20MN		77.11MN
D2000x40	81.00MN	65.20MN	62.00MN		85.00MN

Table 8-22: Results of numerical test for axial capacity of dented tubes

Figure 8-87 depicts the non-dimensional capacity of the members under axial compression against the non-dimensional denting of the wall. From the figure, it is possible to see that results for diameters 1.3m and 1.5m are very similar. Further, after denting 50% and 55% of the member, the steel tube still can take 70-75% of the axial capacity N_{Rd} of the undamaged member. As a result, section D1500x40 is the most affected, after denting 60% only 58% of the axial capacity remains.

Moreover, the findings for 1.8m and 2.0m diameters are also found closer to each other. After a 50% dent, a 96% of the axial capacity still remains in the leg, whilst a 55% dent and 60% of axial capacity is found between 73-83%. It is important to clarify that the numerical tests were done without axial-preloading on the member for simplicity, and due to time constrain. However, steel legs will be subjected to axial load previous to lateral impact, given that they hold the permanent and functional loads of the platform. Therefore, from the results obtained, it can be suggested that it is reasonable, the guidelines have as failure criteria the 50% denting of the section member; this, with the aim of assuring that the member is still capable of taking the compressive loads from the weight of the topside. Additionally, compressive loads will make the legs less resistant to dent. This is more relevant for 4-legs jacket platforms than for 8-leg jacket platforms, where the failure of one leg is less critical, as there is more redundancy in the structure.

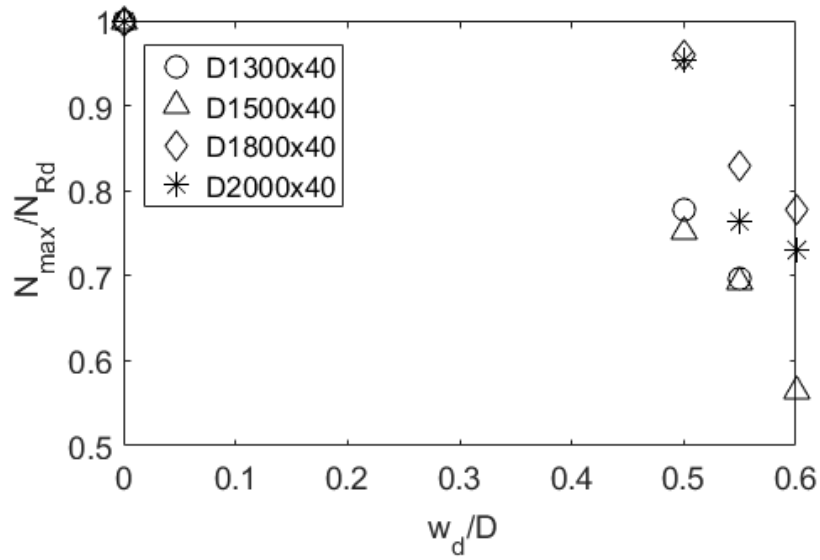


Figure 8-87: Non-dimensional axial capacity of steel tubes against non-dimensional denting.

Figure 8-88 presents the plastic utilization of the deformed member with section D1300x40 at the different three different stages (gravity load, lateral impact load and axial load). Furthermore, the strain distribution is also illustrated in Figure 8-89.

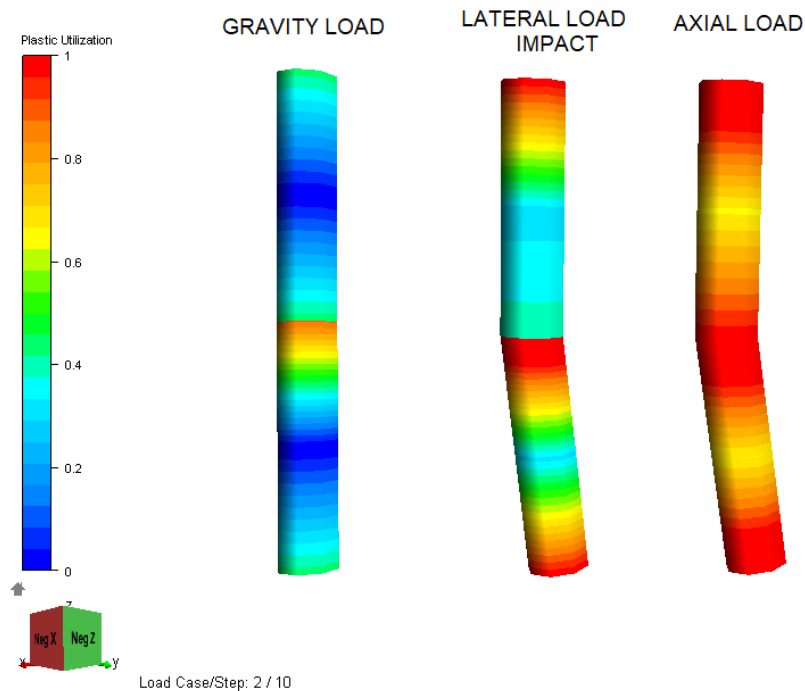


Figure 8-88: Plastic Utilization of the dented steel tube under axial load.

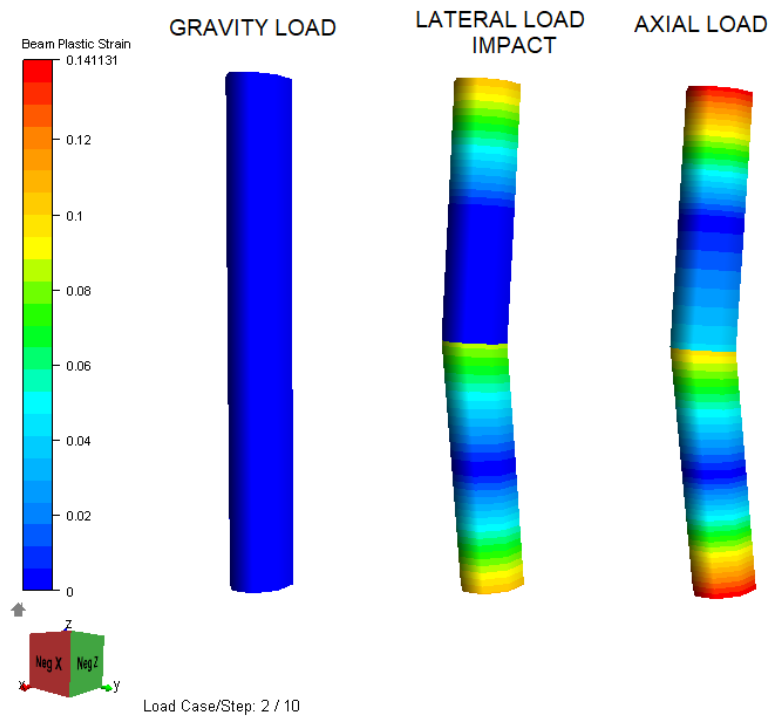


Figure 8-89: Strain distribution in the dented steel tube under axial load.

9 Conclusions and Recommendations for Further Work

The capacity of steel tubes and grouted steel tubes have been studied by means of USFOS program. The fixed steel members have been impacted at middle of the span until the strain reaches its critical value of 0.15. The results from the parametric study have been compared to the Simplified Method provided by the Veritas DNV-RP-C204 and Norsok Standard N-004. Good agreement in the prediction of the impact force, and overall energy absorption has been found between the two approaches. The impact force deviates in a range of 0-5% among all the diameters studied. The total energy absorption is in a range between 1-9% for small 1.3m and 1.5m diameters and 10-48% for 1.8m and 2.0m diameters. The total energy is the addition between the energy dissipated bending and the energy absorbed by denting. Large difference has been registered between the results from USFOS, and the simplified method in terms of denting and denting energy, the main reason is that the non-linear approach capture the effect of the membrane forces in the leg. Hence, these forces make the steel member more resistant to dent that is reflected in less local denting and less energy absorption by denting. Furthermore, the results are also compared to experimental tests from Jones et al. (1992), good resemblance for the ratios $D/t=21, 30$ and 40 , the force-deformation relationships from the guidelines and the USFOS program was found. The effect of the diameter and thickness in the energy absorption for the steel members were discovered to be proportionally. In other words, as the diameter and thickness are increased the capacity of the leg also increases, being the growth in the diameter the parameter that produces larger impact in the energy absorption compared to the same diameter with different thicknesses.

The presence of concrete in the steel tubes represents an enlargement in the overall capacity of the member. The energy absorption shows a growth of 63%, 83%, 92% and 51% for 1.3m, 1.5m, 1.8m and 2.0m diameters respectively. This is possible due to the increase in the stiffness and the additional capacity of concrete to take compression forces in the compressive side of the member. However, little influence was observed in the impact forces, energies absorptions and global displacements, when the grout specification was increased from 10 MPa to 50 MPa. Additionally, the numerical tests have been compared to different experiments from Han et al., Deng et al., Wang et al. and Shakir et al.. The USFOS program is shown to be able to predict the behavior of grouted members, as very satisfactory results were found in the impact energy and the global deformation relationships, between the numerical and experimental tests.

The ship impact analyses were performed in USFOS for two jacket platforms, denominated as Platform A and Platform B, legs and braces were impacted at mid-span and joints, to investigate the capacity of the members to dissipate an impact energy of 50 MJ. The ship was considered as a rigid body, and the Platforms were expected to dissipate all the energy from the impact.

Platform A with grouted members can dissipate 28 MJ and 50 MJ for mid-span leg and joint leg impact, respectively. Braces are observed between 13-22 MJ, meanwhile

brace joint can absorb an energy of 32.50 MJ. Moreover, for the ungrouted members little capacity was registered in general. This given that, the members without grout have little resistant to dent, therefore, they were highly sensitive to show large denting under low impact energies. Making the dent criteria of 0.50D, the most common failure condition in the leg/brace. The platform was also considered without the joint check command in USFOS, this shows an increase in the capacity of the impacted members. Thereby, further analyses are necessary to investigate how conservative is this command, and its applicability under ALS conditions.

Additionally, a fairly good agreement between the force-deformation relationship for dent and global displacement were found between the numerical model and the simplified method provided by the guidelines. However, some limitations were noticed in the simplified approach, as the inability of the force-dent relationships to account for the development of membrane forces in the members. Nevertheless, the guidelines have proven to be useful for self-checking, and pre-design activities for the ship impact analysis.

The platform B is the most robust from the two platforms, with its original sections it is capable of dissipating 50 MJ in the middle of the span and joint of the leg. The diagonal brace can absorb 21 MJ at mid-span and 23.15 MJ in the X-joint. Furthermore, the horizontal brace can take 17.30 MJ and 21.69 MJ for mid-span and joint, respectively. Here, the capacity of the horizontal brace is limited by the presence of the risers behind, being the risers 1.45m away, the failure is taken when the global deflection reaches the value of 1.4m. When Platform B is reduce in sections and filled with concrete, same capacity of energy is observed at mid-span and at the joint of the leg. However, the horizontal brace capacity is reduced to 11 MJ and 15 MJ for mid-span and joint, correspondingly. This, due to grouted members are not allowed to dent in USFOS, which represents a reduction in energy dissipation.

Moreover, a very simple dynamic analysis was performed in platform B, in order, to determine the effect of the velocity of the ship, in the base shear force and over-turning moment values. Findings suggest that impacts in hard points, as joint legs are more relevant in both parameters than impacts in soft points, as mid-span legs. Likewise, the base shear force reports and increase of 20% when the speed in the ship is increased from 3m/s to 4m/s. When the dynamic results are compared to the quasi-static model, growths of 42% and 25.2% were reported for the base shear and over-turning moment, respectively.

Finally, a parametric study in dented tubes was carried out to determine the remaining axial capacity in the damaged steel tubes. Small diameters as 1.3 and 1.5m registered a reduction to 58-75% of the axial capacity, and for large diameters as 1.8m and 2.0m the members were capable to take between 73-83% of the axial capacity of the undamaged member. The obtained results confirm then, as a good conservative practice, to consider the steel member failed when the denting reaches 50% of the diameter, given that the legs will be axially pre-loaded, and its axial capacity is crucial for taking the permanent loads from the topside structure.

Recommendations for further work

- Considering the ship as a rigid body, it represents a simplification but at the same time, it can be seen as disadvantage of capturing the real dynamics of the impact forces and energy distribution between the interacting structures. More sophisticated numerical models may be used to account for different non-linearities during the ship impacts.
- Multi-impact analyses were not considered in this thesis. However, the possibility of ship impacting more than one element and position is possible and should be taken into account.
- New ways of increasing the resistance capacity of steel members subjected to ship impact are needed. Present regulations may result in very thick members, thereby, approaches as grouting, vertical stiffeners and ring stiffeners can be beneficial in terms of cost, but further evaluation must be done.
- More local analyses are needed to assess the gains and limitations provided by the joint check command in USFOS.
- The parametric studies, ship velocity effect and axial capacity of the dented members were done with very simple approaches using USFOS program. Thus, more sophisticated experimental and numerical analyses will be needed to validate the findings in this thesis.

10 Annex

10.1 simplified Method

SIMPLIFIED METHOD: SHIP COLLISION

References

/1/ N-004 2013 Annex A
/2/ EN-1993-1-1 2005

Input Parameters:**Section Profile**

Outer diameter	$D := 1.1m$
Wall thickness	$t := 0.045m$
Length of the leg	$L_{ww} := 18m$
Clamped ends $C_1=2$	$C_{1ww} := 2$
Pinned ends $C_1=1$ (ref /1/ section A.3.10.2)	
Young's Modulus of elasticity	$E := 210000MPa$
Yield strength	$f_y := 340MPa$
Cross section area	$A_{ww} := \frac{\pi[D^2 - (D - 2 \cdot t)^2]}{4} = 0.149m^2$
Second moment of area	$I_x := \frac{\pi}{64} \cdot [D^4 - (D - 2t)^4] = 0.021m^4$

For the node stiffness the member is removed in the model and unit loads are applied in member axis direction. Here the node stiffness have been replaced for high number so $1/K_{node}$ tends to zero

Adjacent Node stiffness K_1	$K_{1ww} := 31250 \frac{MN}{m}$
Adjacent Node stiffness K_2	$K_2 := 13888 \frac{MN}{m}$
Equivalent axial stiffness on the nodes	$K_{node} := \left(\frac{1}{K_1} + \frac{1}{K_2} \right)^{-1} \cdot 2 = 1.923 \times 10^4 \cdot \frac{MN}{m}$
Axial Stiffness of the member	$K := \left(\frac{1}{K_{node}} + \frac{L}{2E \cdot A} \right)^{-1} = 2.947 \times 10^3 \cdot \frac{MN}{m}$
Critical strain (ref /1/ section A.3.10.5 Table A.3-4)	$\epsilon_{cr} := 0.15 = 0.15$
Non-dimensional plastic stiffness (ref /1/ section A.3.10.5 Table A.3-4)	
Cross Section properties	$H_{ww} := 0.0034$

Elastic Section modulus

$$W_w := \left(\frac{\pi}{32D} \right) \cdot [D^4 - (D - 2 \cdot t)^4] = 0.038 \cdot m^3$$

Plastic Section Modulus

$$W_p := \frac{[D^3 - (D - 2 \cdot t)^3]}{6} = 0.05 \cdot m^3$$

Yield strain

$$\epsilon_y := \frac{f_y}{E} = 1.619 \times 10^{-3}$$

Cross section type
(ref /2/ EN 1993-1-1-2005 Table 5.2)

$$\epsilon_w := \sqrt{\frac{235MPa}{f_y}}$$

$$Type := \begin{cases} \text{"Type1"} & \text{if } \frac{D}{t} \leq 50\epsilon^2 \\ \text{"Type2"} & \text{if } 50\epsilon^2 \leq \frac{D}{t} < 70\epsilon^2 \\ \text{"Type3"} & \text{if } 70\epsilon^2 \leq \frac{D}{t} < 90\epsilon^2 \end{cases}$$

$$Type = \text{"Type1"}$$

Collapse Resistance

Plastic Moment capacity

$$M_p := f_y \cdot W_p = 1.704 \times 10^7 \cdot N \cdot m$$

Plastic collapse resistance

$$R_o := \frac{4 \cdot C_1 \cdot M_p}{L} = 7.573 \times 10^6 N$$

Plastic force-deformation relationships including elastic, axial flexibility
(ref /1/ section A.3.7.2)Characteristic deformation for
tubular beams

$$W_c := \frac{D}{2} = 0.55m$$

Non-dimensional spring stiffness

$$\epsilon_w := \frac{4 \cdot C_1 \cdot K \cdot W_c^2}{f_y \cdot A \cdot L} = 7.813$$

Local Buckling

(ref /1/ section A.3.10.2)

Local buckling does not need to be considered for a beam with axial restrains if the following condition is fulfilled

Beta factor

$$\beta := \frac{\frac{D}{t}}{\frac{235MPa}{f_y}} = 35.366$$

Axial flexibility factor

$$C_f := \left(\frac{\sqrt{c}}{1 + \sqrt{c}} \right)^2 = 0.542$$

Smaller distance from location of collision to adjacent joint

$$kl := 0.5 \cdot L = 9 \text{ m}$$

Characteristic dimension for circular cross sections

$$dc := D = 1.1 \text{ m}$$

$$Wb := \begin{cases} 0 & \text{if } \beta \leq \left[\left(\frac{14 \cdot Cf \cdot fy}{C_1 \cdot MPa} \right) \cdot \left(\frac{kl}{dc} \right)^2 \right]^{\frac{1}{3}} \\ \frac{dc}{2 \cdot Cf} \cdot \left[1 - \sqrt{1 - \frac{14 \cdot Cf \cdot fy}{C_1 \cdot \beta^3} \cdot \left(\frac{kl}{dc} \right)^2} \right] & \text{otherwise} \end{cases} \quad Wb = 0 \text{ m}$$

Tensile fracture in yield hinges

(ref/1/ section A.3.10.5)

If local buckling does not take place, fracture is assumed to occur when the tensile strain takes place.

Plastic zone length factor

$$Clp := \frac{\left(\frac{\epsilon cr}{\epsilon y} - 1 \right) \cdot \frac{W \cdot H}{Wp}}{\left(\frac{\epsilon cr}{\epsilon y} - 1 \right) \cdot \frac{W \cdot H}{Wp} + 1} = 0.19$$

Displacement factor

$$Cw := \frac{1}{C_1} \cdot \left[Clp \cdot \left(1 - \frac{Clp}{3} \right) + 4 \cdot \left(1 - \frac{W}{Wp} \right) \cdot \frac{\epsilon y}{\epsilon cr} \right] \cdot \left(\frac{kl}{dc} \right)^2$$

Lateral displacement due to tensile strain

$$Cw = 6.32$$

$$Wts := \frac{dc \cdot C_1}{2Cf} \cdot \left(\sqrt{1 + \frac{4Cw \cdot Cf \cdot \epsilon cr}{C_1}} - 1 \right) = 0.86 \text{ m}$$

Selection of lateral displacement

$$Wl := \begin{cases} Wb & \text{if } Wb \neq 0 \wedge Wb < Wts \\ Wts & \text{otherwise} \end{cases}$$

$$Wl = 0.86 \text{ m}$$

Non-dimensional deformation

$$Wbar := \frac{Wl}{C_1 \cdot Wc} = 0.782$$

Finally with \bar{w} and c , the value R/R_0 is found from figure A.3-8 for bending and membrane if tensile strain..

$$\underline{R}_{\bar{w}} := 1.45 \cdot R_0 = 10.981 \cdot MN$$

The total energy absorbed can be approximate to:

$$E_{leg} := R \cdot W_{ts} = 9.448 \times 10^6 \cdot J$$

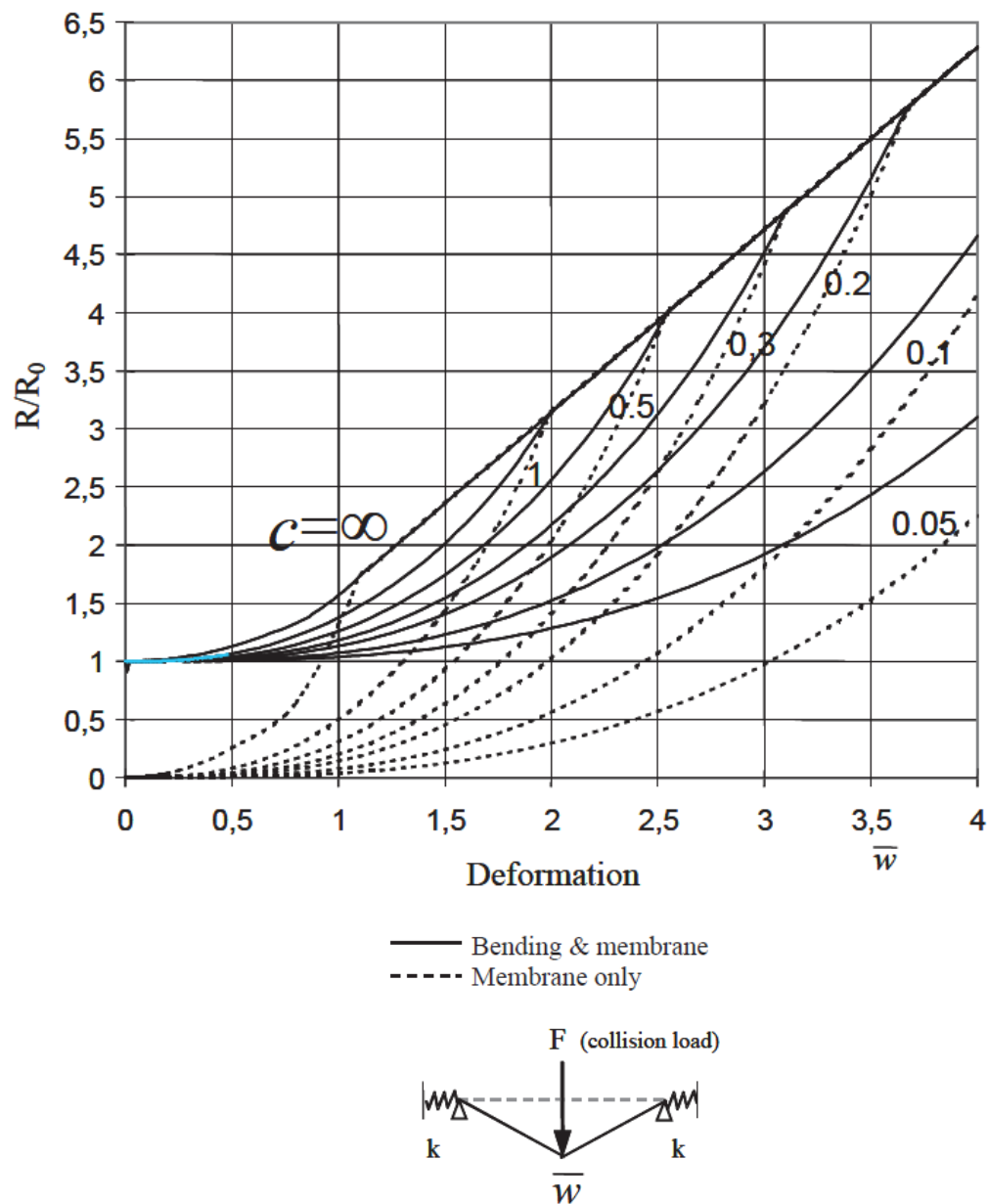


Figure A.3-8 Force-deformation relationship for tubular beam with axial flexibility

Local denting of the leg
ref/1/A.3.6

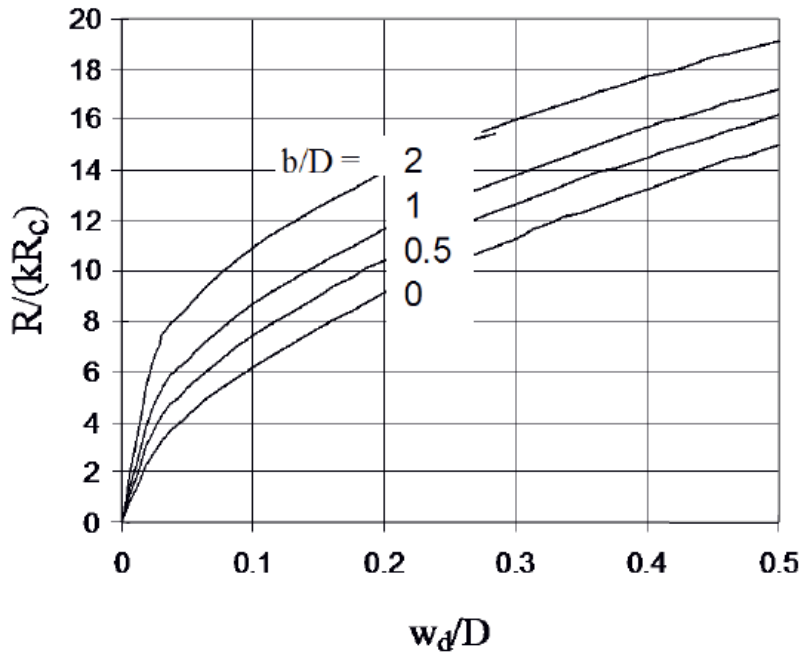


Figure A.3-6 Resistance Force for local denting

Contact extension

$$B := 1.3m$$

Parameter C_{1d}

$$C_{1d} := 22 + \frac{1.2B}{D} = 23.418$$

Parameter C_2

$$C_2 := \frac{1.925}{3.5 + \frac{B}{D}} = 0.411$$

Characteristic resistance to denting

$$R_c := f_y \cdot \frac{t^2}{4} \cdot \sqrt{\frac{D}{t}} = 8.51 \times 10^5 N$$

Effective length factor

1 for legs, and 0.7 for braces

$$k_l := 0.7$$

Axial compression resistance is made according to N-004 6.3.3

Design Axial force (compression positive)

$$N_{sd} := -2MN$$

Critical elastic buckling coefficient $C_e := 0.3$

Characteristic elastic local buckling strength $f_{cle} := 2 \cdot C_e \cdot E \cdot \frac{t}{D} = 5.155 \times 10^3 \cdot MPa$

Characteristic local buckling strength

$$f_{cl} := \begin{cases} f_y & \text{if } \frac{f_y}{f_{cle}} \leq 0.17 \\ \left(1.047 - \frac{0.274 \cdot f_y}{f_{cle}}\right) \cdot f_y & \text{if } 0.17 < \frac{f_y}{f_{cle}} < 1.911 \\ f_{cle} & \text{if } \frac{f_y}{f_{cle}} > 1.911 \end{cases}$$

$$f_{cl} = 340 \cdot MPa$$

Radius of gyration

$$A_{ww} := \frac{\pi [D^2 - (D - 2t)^2]}{4} = 0.149 m^2 \quad I_{xx} := \frac{\pi}{64} [D^4 - (D - 2t)^4] = 0.021 m^4$$

$$i := \sqrt{\frac{I_x}{A}} = 0.373 m$$

Column slenderness parameter

$$\lambda := \frac{k \cdot L}{\pi \cdot i} \cdot \sqrt{\frac{f_{cl}}{E}} = 0.432$$

Characteristic axial compressive strength

$$f_c := \begin{cases} [(1 - 0.28 \cdot \lambda^2) \cdot f_{cl}] & \text{if } \lambda \leq 1.34 \\ \left(\frac{0.9}{\lambda^2} \cdot f_{cl}\right) & \text{otherwise} \end{cases}$$

$$f_c = 322.212 \cdot MPa$$

Material factor

$$\gamma_M := 1$$

Axial design resistance

$$NRd := A \cdot \frac{f_c}{\gamma_M} = 48.057 \cdot MN$$

k factor accounting for axial loading

$$k := \begin{cases} 1 & \text{if } \frac{N_{sd}}{NRd} \leq 0.2 \\ \left[1 - 2 \left(\frac{N_{sd}}{NRd} - 0.2\right)\right] & \text{if } 0.2 < \frac{N_{sd}}{NRd} < 0.6 \\ 0 & \text{otherwise} \end{cases}$$

$$k = 1$$

Denting of the wall

$$Wd := \left(\frac{R}{k \cdot Rc \cdot C1d} \right)^{\frac{1}{C2}} \cdot D = 0.258 m$$

Energy due to denting N-004

$$Ed := \left[\frac{\left(\frac{Wd}{m} \right)^{(C2+1)}}{C2 + 1} \right] \cdot \left[\frac{k \cdot C1d \cdot Rc}{\left(\frac{D}{m} \right)^{C2}} \right] \cdot m = 2.009 \times 10^6 J$$

Total energy N-004

$$Et := Eleg + Ed = 1.146 \times 10^7 J$$

References

- Aghdamy, S., Thambiratnam, D. P., Dhanasekar, M., & Saiedi, S. (2015). Computer analysis of impact behavior of concrete filled steel tube columns. *Advances in Engineering Software*, 89, 52–63.
- Aldilana, D. (2014). *Effects of impacts from large supply vessels on jacket structures* (Unpublished master's thesis). University of Stavanger, Norway.
- Amdahl, J., & Eberg, E. (1993). Ship collision with offshore structures. In *Proceedings of the 2nd european conference on structural dynamics (eurodyn'93), trondheim, norway, june* (pp. 21–23).
- Amdahl, J., Johansen, A., et al. (2001). High-energy ship collision with jacket legs. In *The eleventh international offshore and polar engineering conference*.
- Amdahl, J., Watan, R., Hu, Z., & Holmås, T. (2012). Broad side ship collision with jacket legs: examination of norsok n-004 analysis procedure. *OMAE Proceedings*.
- Boresi, A. P., Schmidt, R. J., & Sidebottom, O. M. (1993). *Advanced mechanics of materials* (Vol. 6). Wiley New York.
- Calle, M. A., Verleysen, P., & Alves, M. (2017). Benchmark study of failure criteria for ship collision modeling using purpose-designed tensile specimen geometries. *Marine Structures*, 53, 68–85.
- Codecogs.com. (2014). *Plastic theory of bending*. <http://www.codecogs.com/library/engineering/materials/plastic-theory-of-bending.php>.
- Deng, Y., Tuan, C. Y., & Xiao, Y. (2011). Flexural behavior of concrete-filled circular steel tubes under high-strain rate impact loading. *Journal of Structural Engineering*, 138(3), 449–456.
- Ellinas, C., & Valsgard, S. (1985). Collisions and damage of offshore structures: a state-of-the-art. *Journal of energy resources technology*, 107(3), 297–314.
- Han, L.-H. (2004). Flexural behaviour of concrete-filled steel tubes. *Journal of Constructional Steel Research*, 60(2), 313–337.
- Han, L.-H., Hou, C.-C., Zhao, X.-L., & Rasmussen, K. J. (2014). Behaviour of high-strength concrete filled steel tubes under transverse impact loading. *Journal of Constructional Steel Research*, 92, 25–39.
- Jin, W.-l., Song, J., Gong, S.-f., & Lu, Y. (2005). Evaluation of damage to offshore platform structures due to collision of large barge. *Engineering structures*, 27(9), 1317–1326.
- Jones, N., Birch, S., Birch, R., Zhu, L., & Brown, M. (1992). An experimental study on the lateral impact of fully clamped mild steel pipes. *Proceedings of the Institution of Mechanical Engineers, Part E: Journal of Process Mechanical Engineering*, 206(2), 111–127.
- Kristiansen, L. (2013). *Analysis and design of columns in offshore structures subjected to supply vessel beam collisions* (Unpublished master's thesis). NTNU.
- Kvitrud, A. (2011). Collisions between platforms and ships in norway in the period 2001–2010. In *Proceedings of the 30th international conference on ocean, offshore and arctic engineering, rotterdam, the netherlands*.

- Learneasy.info. (2014). *Properties of materials*.
<http://www.learneasy.info/MDME/MEMmods/MEM30007A/properties/Properties.html>.
- Li, L., Hu, Z., & Jiang, Z. (2013). Plastic and elastic responses of a jacket platform subjected to ship impacts. *Mathematical Problems in Engineering*, 2013.
- Moan, T., Amdahl, J., & Ersdal, G. (2017). Assessment of ship impact risk to offshore structures-new norsok n-003 guidelines. *Marine Structures*.
- Norsok Standard N-003, N. (2017). N-003. *Actions and Action Effects, Edition 2*.
- Norsok Standard N-004, N. (2013). N-004. *Design of steel structures, Rev. 4*.
- Petroleum Safety Authority, N. (2016). *Trends in risk level in the petroleum activity. summary report* (Tech. Rep.). Petroleum Safety Authority. Retrieved from <http://www.ptil.no/summary-report-2016/category1264.html>
- Shakir, A., Guan, Z., & Jones, S. (2016). Lateral impact response of the concrete filled steel tube columns with and without cfrp strengthening. *Engineering structures*, 116, 148–162.
- Skallerud, B., & Amdahl, J. (2002). *Nonlinear analysis of offshore structures*. Research Studies Press Baldock, Hertfordshire, England.
- Søreide, T. H. (1981). *Ultimate load analysis of marine structures*. Tapir.
- Storheim, M. (2016). *Structural response in ship-platform and ship-ice collisions* (Unpublished doctoral dissertation). NTNU.
- Storheim, M., Amdahl, J., & Martens, I. (2015). On the accuracy of fracture estimation in collision analysis of ship and offshore structures. *Marine Structures*, 44, 254–287.
- Travanca, J., & Hao, H. (2014a). Dynamics of steel offshore platforms under ship impact. *Applied Ocean Research*, 47, 352–372.
- Travanca, J., & Hao, H. (2014b). Numerical analysis of steel tubular member response to ship bow impacts. *International Journal of Impact Engineering*, 64, 101–121.
- Travanca, J., & Hao, H. (2015). Energy dissipation in high-energy ship-offshore jacket platform collisions. *Marine Structures*, 40, 1–37.
- USFOS, A. (2014). Usfos 8.7 user’s manual. *Bergen, Norway*.
- Veritas DNV-RP-C204, D. N. (2017). Design against accidental loads. *Recommended Practice DNV-RP-C204*.
- Wang, R., Han, L.-H., & Hou, C.-C. (2013). Behavior of concrete filled steel tubular (cfst) members under lateral impact: Experiment and fea model. *Journal of Constructional Steel Research*, 80, 188–201.
- Zeinoddini, M., Parke, G., & Harding, J. (2002). Axially pre-loaded steel tubes subjected to lateral impacts: an experimental study. *International Journal of Impact Engineering*, 27(6), 669–690.